```
:           ,

                    (2/3)
```

NSC94-2113-M009-002-
94 08 01   95 07 31
(   )

95   5   11

Progress Report (2004~2006) for the Research Project Supported by NSC

Studies of Complex Fluid Systems:

Interplay of Computer Simulation, Theory and Experiment (1/3, 2/3)

複雜流體系統之研究:電腦模擬,理論及實驗之互補互成(1/3, 2/3)

(NSC 93-2113-M-009-015; NSC 94-2113-M-009-002)

主持人: 林銀潢 教授, 國立交通大學應化系

Professor Yn-Hwang Lin,

Department of Applied Chemistry,

National Chiao Tung University

This progress report will be expressed in terms of the major accomplishments made from the NSC-supported research, as summarized below in two parts: A and B (five preprints submitted to or to be submitted to the Journal of Physical Chemistry B for publication are attached).

Part A: A series of five papers on the thermorheological complexity related to glass transition in polystyrene have been published in or submitted to the Journal of Physical Chemistry B(listed at the end of this report), reporting the following important contributions:

(1) Demonstrate the validity and accuracy in practice of using the successful description of the entropic region (long-time region) in terms of the extended reptation theory (ERT) for the entangled system or in terms of the Rouse theory for the entanglement-free system as the reference frame for analyzing the whole range of viscoelastic response: creep compliance $J(t)$ line shapes and viscoelastic spectra $G'(\omega)$ & $G''(\omega)$, yielding important dynamic and structural information related to the glass transition of polystyrene (see Figures 1 and 2 of paper 1; Figure 1 of paper 3; and Figures 1–3 and Table 1 of paper 5).

(2) First quantitative analyses of the creep compliance $J(t)$ line shapes of nearly monodisperse polystyrene samples over 5 decades of dynamic range (or as wide as 9 decades in time; as far as I know, this is a record-breaking span of time), yielding the frictional-factor value in close agreement with the values obtained previously from other types of measurements: relaxation modulus, viscosity and diffusion. (see Figure 1, Figure 2 and Table 1 of paper 1; and Figure 1 of

paper 3).

(3) From the results obtained from analyzing the $J(t)$ line shapes, it is shown that the thermorheological complexity in polystyrene behaves in a universal way, entangled or not. (see Figures 4, 5 and 6 of paper 3).

(4) The basic mechanism for the thermorheological complexity (TRC) in polystyrene is analyzed and shown to be also responsible for the breakdown of the Stokes‒Einstein relation (BSE) in fragile glass-forming liquids, such as OTP and TNB. The equivalent quantities in the two effects are shown to behave in a similar way. (see Figure 1 of paper 4). The importance of this study can be reflected by the comments of the two reviewers of paper 4, who support the publication of the paper with recommendations for minor changes: "*TRC and BSE is an important issue for polymer scientists and physical chemist.*" and "*…the manuscript addresses an important issue in glass forming liquid.*"

(5) It is shown how the length-scales associated with the Rouse‒Moody normal modes (for the entangled system) or the Rouse normal modes (for the entanglement-free system) may be used as the internal yardstick for estimating the characteristic length-scale of relaxation at the glass transition temperature, giving ~3 nm consistently for three different polystyrene systems, two entangled and one entanglement-free, which is also in agreement with the value obtained by other studies. (see Figures 8 of paper 3). The importance of this result can be reflected by the comment of a reviewer of paper 3, who would like to support the publication of the paper after it is properly shortened: "*To my opinion a highlight is the possibility to determine the length scale of relaxation around T_g which, in agreement with different experiments, turns out to be around 3nm.*"

(6) The comparison of dynamic quantities as reported in paper 2 clearly differentiates for the first time the motion associated with a single Rouse segment from the α-relaxation‒ due to the lack of clear definition in the past and the proximity of one to the other in the time scale, the two modes could be easily confused.

The research accomplishments as listed above have resulted from analyzing or benefited from the

published data of the following laboratories: D. J. Plazek at the University of Pittsburg; M. D. Ediger at the University of Wisconsin and T. Inoue et al at the University of Kyoto.

Part B: A series of two papers studying the stress relaxations, linear and nonlinear, of entanglement-free Fraenkel chains will soon be submitted to the Journal of Physical Chemistry B for publication. The important contributions in these two papers are highlighted as in the following:

(1) The characteristic viscoelastic behavior of the Fraenkel chain is revealed, including (a) distinctive two modes of dynamics; (b) the holding of the Lodge–Meissner relation over the whole time of relaxation; (c) nonzero second normal-stress difference.

(2) It is shown through analysis that the fast mode arises from the segment-tension fluctuations or reflects the relaxation of the segment-tension arising from segments being stretched by the applied step strain—an energetic interactions-derived dynamic process; while the slow mode arises from the fluctuating segmental-orientation anisotropy or represents the randomization of the induced segmental-orientation anisotropy—an entropy-derived dynamic process. The physical basis for the distinctive coexistence of the energetic interactions-derived dynamics and the entropy-derived dynamics, as observed in experiment, is fully revealed.

(3) Very significantly the slow mode is well described by the Rouse theory in all aspects: the magnitude of modulus, the line shape and the number-of-beads dependence of the relaxation time. In other words, with one Fraenkel segment substituting for one Rouse segment, it has been shown that the entropic-force constant on each segment is not a required element to give rise to the Rouse modes of motion, which have been typically observed in the long-time region of the linear viscoelastic response of an entanglement-free polymer.   This conclusion provides an explanation resolving a long-standing fundamental paradox in the success of modern molecular theories of polymer viscoelasticity based on the Rouse segment as the most basic structural unit—namely, the paradox between the Rouse segment size being of the same order of magnitude as that of the Kuhn segment and the meaning of the Rouse segment as defined in the Rouse chain model.

(4) The holding of the Lodge‒Meissner relation—which was originally proposed based on a phenomenological argument—over the whole time of relaxation as observed in the simulation is proven analytically.

(5) The workings of the fluctuations‒dissipation theorem and virial theorem are, respectively, illustrated by the simulation, which are valuable examples in the teaching of statistical mechanics.

Reports from **Part A**:

(1) Lin, Y.-H. "**Whole Range of Chain Dynamics in Entangled Polystyrene Melts Revealed from Creep Compliance: Thermorheological Complexity between Glassy-Relaxation Region and Rubber-Fluid Region. 1**" *J. Phys. Chem. B* **2005**, *109*, 17654.

(2) Lin, Y.-H. "**Motion Associated with a Single Rouse Segment versus the α Relaxation. 2**" *J. Phys. Chem. B* **2005**, *109*, 17670.

(3) Lin, Y.-H. "**Universality in Thermorheological Complexity Related to Glass Transition in Polystyrene Melts. 3**" *J. Phys. Chem. B*, revised and resubmitted.

(4) Lin, Y.-H. "**Thermorheological Complexity in Polystyrene Melts and Breakdown of the Stokes‒Einstein Relation in *o*-Terphenyl. 4**" *J. Phys. Chem. B*, revised and resubmitted.

(5) Lin, Y.-H. "**Range of Universality Regarding the T_g-Related Thermorheological Complexity in Polystyrene Melts. 5**" *J. Phys. Chem. B*, submitted.

Reports from **Part B**:

(1) Lin, Y.-H.; Das, A. K. "**Monte Carlo Simulations of Stress Relaxations of Entanglement-Free Fraenkel Chains. 1: Linear Polymer Viscoelasticity**" *J. Phys. Chem. B*, to be submitted.

(2) Lin, Y.-H.; Das, A. K. "**Monte Carlo Simulations of Stress Relaxations of Entanglement-Free Fraenkel Chains. 2: Non-Linear Polymer Viscoelasticity**" *J. Phys. Chem. B*, to be submitted

Universality in Thermorheological Complexity Related to

Glass Transition in Polystyrene Melts. 3

Y.-H. Lin[1]

Department of Applied Chemistry

National Chiao Tung University

Hsinchu, Taiwan

Abstract

In paper 1, using the successful description of the entropic region (long-time region) in terms of the extended reptation theory (ERT) as the reference frame, the creep compliance $J(t)$ curves over the whole range of two *entangled* nearly monodisperse polystyrene melts: samples A and B, were quantitatively analyzed, characterizing the energetic interactions-derived glassy-relaxation process occurring in the short-time region in a perspective way. In this report, the $J(t)$ curves and steady-state compliance J_e^0 of an *entanglement-free* nearly monodisperse polystyrene melt, sample C, are equally quantitatively analyzed in terms of an equivalent scheme using the Rouse theory instead of ERT as the reference frame. These studies show that the uneven thermorheological complexity in $J(t)$ arises from the temperature dependence of the glassy relaxation being stronger in a simple way than that of the entropy-derived dynamics, as carried by the frictional factor K. The structural-relaxation times τ_S of samples A, B and C extracted from the glassy-relaxation process are equally well separated into two decoupled quantities: one, *s'*, determined entirely by the *line shape* of $J(t)$ and the other, *K'*, converted by the predetermined molecular weight-dependent parameter $R_K(M)$ from the frictional factor K calculated from the time-scale *shifting factor* ($K' = R_K(M)K$ and $\tau_S = 18s'K'$). With decreasing temperature, the

---
[1] E-mail:yhlin@mail.nctu.edu.tw

increase in *s'* represents the structural growth and characterizes the thermorheological complexity while the increase in *K'* represents the frictional slowdown. The effect due to the T_g difference among samples on τ_S, *s'* and *K'* can be accounted for by expressing them as a function $\Delta T = T - T_g$ where T_g is defined as the temperature at which the structural-relaxation time $\tau_S = 1000$ sec. From this it is shown that the glass transition together with the thermorheological complexity behaves in a *universal* way within the polystyrene system, *entangled or not*. The observed universality supports the previously obtained result that the frictional factor K in ERT is in quantitative agreement with that in the Rouse theory indicating the same footing at the Rouse-segmental level for both theories. Representing important physical features of the universality, it is shown that vitrification at the Rouse-segmental level occurs gradually in the same way as ΔT diminishes and the length-scale at T_g (or $\Delta T = 0$) has nearly the same value ~ 3 nm for all the three studied samples.

Universality in Thermorheological Complexity Related to

Glass Transition in Polystyrene Melts. 3

Y.-H. Lin

Department of Applied Chemistry

National Chiao Tung University

Hsinchu, Taiwan

1. Introduction

About forty years ago thermorheological complexity in polystyrene melts was first observed by Plazek as the temperature approaches the glass transition temperature.[2,3]   The effect is directly observed as the change with temperature in the creep-compliance $J(t)$ line shapes of entangled polystyrene samples. As entanglement gives rise to distinct features in the observed $J(t)$ curve—three bending regions along the course of time, the difference in temperature dependence between different zones of the $J(t)$ curve can be discerned easily.   As reported in papers 1 and 2,[4,5] the $J(t)$ curves over the whole range of two entangled nearly monodisperse polystyrene samples A and B (or s-A and s-B as in Table 1) have been quantitatively analyzed using the successful description of the rubber(like)-to-fluid region[6] (or, simply but less accurately or specifically, the entropic region or the long-time/large-compliance region) by the extended reptation theory (ERT)[7,8,9,10,11] as the reference frame. With respect to the reference frame, the

---

[2] Plazek, D. J. *J. Phys. Chem.* **1965**, *69*, 3480.

[3] Plazek, D. J. *J. Polym. Sci., Part A*-2: *Polym. Phys.* **1968**, *6*, 621.

[4] Lin, Y.-H. *J. Phys. Chem. B* **2005**, *109*, 17654.

[5] Lin, Y.-H. *J. Phys. Chem. B* **2005**, *109*, 17670.

[6] See the note at ref. 9 of ref 3 for the definition of the term "rubber(like)-to-fluid."

[7] Lin, Y.-H. *Macromolecules* **1984**, *17*, 2846.

glassy-relaxation process occurring in the short-time region of $J(t)$ at different temperatures was analyzed in a perspective way. The relaxation times of the various dynamic modes in ERT are expressed as the products of the frictional factor K and a structural factor; thus, the time-scale of the large-compliance region of $J(t)$ is characterized by the frictional factor K. In ERT[6-10] as well as in the Rouse theory[8,10,12,13] the frictional factor K is defined by

$$K = \frac{\zeta \langle b^2 \rangle}{kT\pi^2 m^2} \tag{1}$$

where ζ, $\langle b^2 \rangle$ and m are the frictional constant, mean square bond length and mass of the Rouse segment, respectively. As obtained from the analyses of relaxation modulus $G(t)$ line shapes of a series of nearly monodisperse polystyrene samples of different molecular weights and calculated from the viscosity and diffusion data in terms of ERT, it has been shown that the frictional factor K is independent of molecular weight as expected from the theory.[3,6-10] As the logical consequence of K being independent of molecular weight, ERT explains the molecular-weight dependences of the zero-shear viscosity and steady-state compliance; and their respective transition points, M_c and M_c'.[6-10] The proven validity of ERT serves as the foundation for the quantitative description of $J(t)$ over the whole range. With the $G(t)$ functional

[8] Lin, Y.-H. *Macromolecules* **1986**, *19*, 159.

[9] Lin, Y.-H. *Macromolecules* **1986**, *19*, 168.

[10] Lin, Y.-H. *Macromolecules* **1987**, *20*, 885.

[11] Lin, Y.-H. *Polymer Viscoelasticity: Basics, Molecular Theories, and Experiments*;
World Scientific: Singapore, 2003.

[12] Rouse, P. E. Jr. *J. Chem. Phys.* **1953**, *21*, 1271.

[13] Bird, R. B.; Curtiss, C. F.; Armstrong, R. C.; Hassager, O. *Dynamics of Polymeric Liquids, Vol.* 2, *Kinetic Theory,* 2nd ed.; Wiley: New York, 1987.

form known (see section 2), the line shape of $J(t)$ can be calculated from the $G(t)$ with K fixed at a certain value through the basic equation of linear viscoelasticity:

$$t = \int_0^t J(t')G(t-t')dt' \tag{2}$$

The calculation can be accurately done numerically using the Hopkins–Hamming[3,14,15] method (see Appendix A of ref. 3).   Then the frictional factor K can be determined from the shifting factor obtained in the superposition of the calculated and measured $J(t)$ line shapes; the K value (Table 1) obtained from analyzing the $J(t)$ result of sample A is in close agreement with the previously obtained values ($4.9 \times 10^{-9} \pm 10\%$ at 127.5°C),[3] confirming the unique importance of K and the validity of ERT.   While being independent of molecular weight, K carries the temperature dependence—often described by the Fulcher and Tammann–Hesse (FTH) equation or the Williams–Landel–Ferry (WLF) equation[16,17,18]—of all the relaxation times of the processes in the rubber-to-fluid region.[3,6–10]   As opposed to the entropic nature of the dynamics in this region, the glassy-relaxation process that occurs in the short-time region is derived from the energetic interactions among segments. It has been shown that the thermorheological complexity with temporal unevenness in $J(t)$ arises from the temperature dependence of the energetic

[14] Hopkins, I. L.;   Hamming, R. W. *J. Appl. Phys.* **1957**, *28,* 906; *J. Appl. Phys.* **1958**, *29,* 742.

[15] Tschoegl, N. W. *The Phenomenological Theory of Linear Viscoelastic Behavior*; Springer-Verlag: Berlin, 1989.

[16] Ferry, J. D.   *Viscoelastic Properties of Polymers*, 3rd ed.; Wiley: New York, 1980.

[17] Fulcher, G. S. *J. Am. Chem. Soc.*, **1925**, *8,* 339, 789; Tammann, G. and Hesse, G., Z. *Anorg. Allg. Chem.* **1926**, *156*, 245.

[18] Williams, M. L.; Landel, R. F.; Ferry, J. D. *J. Am. Chem. Soc.* **1955**, *77*, 3701.

interactions-derived process being stronger than that of the entropy-derived dynamics in a simple way,[3,4] as characterized by the parameter *s* defined by

$$s = \frac{\langle \tau \rangle_{\mathrm{G}}}{K} \qquad (3)$$

where $\langle \tau \rangle_{\mathrm{G}}$ is the average glassy-relaxation time. *s* increases about an order of magnitude with decreasing temperature over the range studied just above T_{g} in s-A and s-B.

According to the analysis in terms of eq 3,[3,4] the thermorheological complexity should occur to a polystyrene melt as long as its molecular weight is greater than that of a Rouse segment, which has been estimated to be about 850 by various methods.[19,20,21,22,23,24,25,26,27] Below the entanglement molecular weight, the viscoelastic response of polystyrene in the long-time/low-frequency region (or the entropic region) is described by the Rouse theory.[8,10,28]

[19] Ballard, D. G. H.; Rayner, M. G.; Schelten, J. *Polymer* **1976**, *17*, 349.

[20] Norisuye, T.; Fujita, H. *Polymer J.* **1982**, *14*, 143.

[21] Inoue T.; Okamoto, H.; Osaki, K. *Macromolecules* **1991**, *24*, 5670.

[22] Inoue, T.; Hayashihara,H.; Okamoto, H.; Osaki, K. *J. Polym. Sci. Polym. Phys. Ed.* **1992**, *30*, 409.

[23] Inoue, T.; Osaki, K. *Macromolecules* **1996**, *29*, 1595; Inoue, T.; Uematsu, T.; Osaki, K. *Macromolecules* **2002**, *35*, 820.

[24] Lin,Y.-H. *J. Polym. Res.* **1994**, *1*, 51.

[25] Lin, Y.-H.; Lai, C. S. *Macromolecules* **1996**, *29,* 5200.

[26] Lai, C. S.; Juang, J.-H.; Lin, Y.-H. *J. Chem. Phys.* **1999**, *110*, 9310.

[27] Lin, Y.-H.; Luo, Z.-H. *J. Chem. Phys.* **2000**, *112*, 7219; Lin, Y.-H. *J. Chin. Chem. Soc.***2002**, *49*, 629.

[28] Lin, Y.-H.; Juang, J.-H. *Macromolecules* **1999**, *32*, 181: Note: blend solutions as studied in this reference denote blends consisting of two polystyrene components: one

In an entanglement-free case, the time/frequency range covered by the viscoelastic response is not as wide as in an entangled case and the line shape is much more monotonous. As a result, it is not as obvious to identify a region in the viscoelastic response where the time–(frequency–)temperature superposition principle can be applied, reflecting that another region does not follow the same temperature dependence—i.e. the manifestation of the thermorheological complexity.   Instead, the viscoelastic response changes its line shape over the whole range greatly with a change in temperature.   We shall show in this report that the same thermorheological complexity occurs in an entanglement-free sample and is reflected by the decrease in its steady-state compliance J_e^0 with temperature decreasing towards T_g as observed by Plazek.[29]

A scheme of analysis in terms of eq 3 equivalent to that for analyzing s-A and s-B is used for analyzing the J_e^0 and $J(t)$ results reported by Plazek[28] of a low-molecular-weight polystyrene sample, as denoted by s-C in Table 1, by replacing ERT with the Rouse theory—because the molecular-weight distribution of s-C is not that narrow, the Rouse theory becomes applicable here even thought its M_w value is slightly greater than M_e=13500 as will be explained in section 3.

T_g is defined by the temperature at which the structural relaxation time τ_S reaches 1000 sec for all the samples.   Using the thus defined T_g as the common reference point, the dynamic and

---

with molecular weight M_2 (weight fraction denoted by W_2) much greater than entanglement molecular weight M_e=13500 and the other with molecular weight M_1 slightly below $M_{e,}$ serving as the "solvent" for the high molecular-weight component as far as the "dilution" of entanglement is concerned; and the entanglement molecular weight in the blend solution is given by $M_e^{'} = M_e / W_2$. With the increase in W_2 the system transits from entanglement-free region to entangled region as M_2 becomes greater than $M_e^{'}$.

[29] Plazek, D. J.; O'Rourke, V. M. J. *Polym. Sci. A-2: Polym. Phys.* **1971**, *9,* 209.

structural quantities as obtained from analyzing the $J(t)$ results of s-A, -B and -C are compared, revealing the fundamental universal relationships between viscoelasticity–particularly the glassy relaxation–and the glass transition.

2. $G(t)$ Functional Forms in the Entanglement and Entanglement-Free Regions

Incorporating the glassy-relaxation process into ERT, the stress relaxation modulus $G(t)$ for a nearly monodisperse entangled sample is expressed[3,6–10] as

$$G(t) = \frac{4\rho RT}{5M_e} F(t) \int f(M) G_E(M,t) dM \qquad (4)$$

with

$$G_E(M,t) = \left[1 + \frac{1}{4}\mu_X(t/\tau_X(M))\right]\left[\sqrt{M_e/M}\,\mu_B(t/\tau_B(M)) + \left(1 - \sqrt{M_e/M}\right)\mu_C(t/\tau_C(M))\right] \qquad (5)$$

and

$$F(t) = 1 + \mu_A(t/\tau_A) + A_G \mu_G(t/\tau_G) \qquad (6)$$

where $f(M)$ is the molecular-weight distribution of the sample under study, $\mu_G(t)$ represents the glassy-relaxation process and A_G is its relaxation strength; $\mu_A(t)$ represents the Rouse–Mooney normal modes of motion[10,30,31] of an entanglement strand with both ends fixed; $\mu_X(t)$, the chain slippage through entanglement links to equilibrate the uneven tension along the primitive chain; $\mu_B(t)$, the primitive-chain contour-length fluctuation; and $\mu_C(t)$, the reptation motion corrected for

---

[30] Mooney, M. *J. Polym. Sci.* **1959**, *34*, 599.

[31] Doi, M. *J. Polym. Sci., Polym. Phys. Ed*. **1980**, *18,* 1005.

the chain length-fluctuation effect. The relaxation times of these different processes are each expressed as a product of the frictional factor K and a structural factor—a functional form containing M_e and/or M.   We refer the functional forms of the four processes and their respective characteristic (relaxation) times to the previous publications[6-10] but point out that, normalizing (dividing) all the relaxation times by the relaxation time of the first mode of $\mu_A(t)$, τ_A^1, the whole $G(t)$ can be expressed as a universal function of the normalized molecular weight M/M_e—the topological universality in polymer viscoelasticity.   It has been found that the glassy-relaxation process is well described by the Kohlrausch, Williams and Watts (KWW) equation:

$$\mu_G(t/\tau_G) = \exp\left(-(t/\tau_G)^\beta\right); \quad 0 < \beta \leq 1 \qquad (7)$$

For a relaxation process as given by eq 7, the average relaxation time is defined by

$$\langle \tau \rangle_G = \int_0^\infty \mu_G(t/\tau_G)dt = \frac{\tau_G}{\beta}\Gamma(1/\beta) \qquad (8)$$

where Γ is the gamma function.   Eq 3 has been used to characterize the relative position of the glassy-relaxation times with respect to those in the $\mu_A(t)$-$\mu_X(t)$-$\mu_B(t)$-$\mu_C(t)$ region, which are all proportional to the frictional factor K (note: the relaxation times in $\mu_A(t)$ are proportional to $K'=R_K(M)K$; see section 4).[6-10] The combination of eqs 3 and 4-8 has been used to analyze the $J(t)$ results of s-A and -B at different temperatures consistently and quantitatively, revealing the basic mechanism for the thermorheological complexity.[3]

It has been shown that in an *entanglement-free* melt[8] or blend solution[27] (see the note at ref 27), the viscoelastic spectrum over the entropic region is well described by the Rouse theory.   The

13

onset molecular weight of entanglement as observed by monitoring the initial deviation

from the Rouse theory as the molecular weight or concentration (weight fraction W_2 of

the high-molecular-weight component) increases is shown to be in close agreement

with the entanglement molecular weight, M_e or $M_e^{'}$ (as defined by eq 17) as calculated

from the plateau modulus ($G_N = 4\rho RT/5M_e$ or $G_N^{'} = 4W_2\rho RT/5M_e^{'}$).   As reported

in ref 9,[9,10] the $G(t)$ and $G'(\omega)$ line shapes of a series of *entangled* blend solutions have

been analyzed in terms of the linear combination of ERT and the Rouse theory weighed

by the weight fractions of the two components in the blend solution (see refs 9 and 10

for details).   From the extensive line-shape analysis, it has been shown that the

frictional factor K in ERT is the same as that in the Rouse theory within a small

possible experimental error ($< 20\%$); in other words, the two theories have the same

footing at the Rouse-segmental level.   Furthermore, as mentioned above, the

thermorheological complexity should occur to a polystyrene melt as long as its

molecular weight is greater than that of a Rouse segment.   Thus, corresponding to eqs

4–6 for an entangled polymer melt, the relaxation modulus for an entanglement-free

melt is expressed by

$$G(t) = A_G^f \mu_G(t) + \rho RT \int \frac{f(M)}{M} \mu_R(t, M) dM \tag{9}$$

where A_G^f is the full relaxation strength of the glassy-relaxation process and is related

to A_G of eq 6 by $A_G^f = A_G \rho RT / M_e = (5/4) A_G G_N$ (see the note at ref 31)[32] and $\mu_R(t,M)$ represents the Rouse relaxation for the component with molecular weight M as given by[8,10-12]

$$\mu_R(t,M) = \sum_{p=1}^{N-1} \exp\left(-\frac{t}{\tau_p}\right) \qquad (10)$$

with

$$N = \mathrm{c\,int}(M/m) + 1 \qquad (11)$$

and

$$\tau_p = \frac{\zeta \langle b^2 \rangle}{24kT \sin^2(p\pi/2N)} = \frac{K\pi^2 M^2}{24N^2 \sin^2(p\pi/2N)} \qquad (12)$$

---

[32] Because the relaxation times of the $\mu_X(t)$, $\mu_B(t)$ and $\mu_C(t)$ processes are much greater than the slowest relaxation time in $\mu_G(t)$, it makes no difference for a practical purpose to express the glassy relaxation either as the $A_G \mu_G(t)$ term inside $F(t)$ (eq 6) or as a separate term $A_G^f \mu_G(t)$ as used in eq 9; note that incorporating $A_G \mu_G(t)$ into ERT or $A_G^f \mu_G(t)$ into the Rouse theory is intended to be only a phenomenological description.

where the function cint(x) converts a number x to an integer by rounding the fractional part of x. N as defined by eq 11 leads to the numerically calculated rubbery modulus at zero time closest to the value $\rho RT/m=3.75\times10^7$ dynes/cm^2 with $\rho=1.0286$ at $T=373$K.

3. Analysis of the η, J_e^0 and $J(t)$ Results

The polydispersity of a nearly monodisperse polymer sample is often given in terms of the M_w/M_n ratio, which as can be easily affected by a small tail in the molecular-weight distribution of the sample, is in general difficult to determine accurately by GPC. Thus, the M_w/M_n data coming with any standard sample in general can only be used as a reference rather than be taken as rigorous. Under such a situation, $f(M)$ for a nearly monodisperse polystyrene sample as appearing in eqs 4 and 9 is assumed to be well described by the Schulz distribution[33] characterized by the polydispersity parameter Z, giving $M_w/M_n=(Z+1)/Z$. And the Z value of a studied system is determined as an adjustable parameter giving the best fitting to the line shape of the measured stress-relaxation modulus or viscoelastic spectrum. The justification for such an approach is that the obtained Z values are well-behaving, all giving $M_w/M_n \leq 1.03$ in the series of the samples studied in ref 7, well within the range expected for a nearly monodisperse distribution.

The viscoelastic properties of s-A, -B and -C as analyzed using ERT or the Rouse

---

[33] Schulz, G. V. *Z. Physik. Chem., Abst. B* **1943**, *43*, 25; Tung, L. H. *Polymer Fractionation*; Cantow, M. J. R Ed.; Academic: New York, 1967.

theory as the reference will be compared in this study; their values of M_w, $Z(M_w/M_n)$, K (at127.5°C), $A_G^f \times 10^{-9}$ and β as well as the reference theory used in the analysis are listed in Table 1 for easy reference below.   The studies of s-A and s-B have been reported in detail in papers 1 and 2; mainly s-C will be studied in the following. In Table 1, the results of sample E167 from a previous study is also listed for a latter comparison.

To achieve quantitative agreements between the calculated and measured in both J_e^0 and $J(t)$ of s-C, the proper choice of the functional form—i.e. either eq 4 or 9, and the Z parameter for the molecular weight distribution $f(M)$ as well as the A_G (or A_G^f) and β values for the glassy relaxation matter. They can be best found by a trial-and-error process until consistently quantitative agreements are obtained.   The functional form chosen must be well justified and consistent with other studies and the obtained parameters must be within the expected range.   A full discussion of the uniqueness and significance of the involved fitting parameters and their determinations can be found in section 3.4 of paper 1.[3] For s-C, we have found that the combination of eq 9 and $Z \approx 20$ gives the best result—the analysis does not have the resolution to differentiate, say, between $Z=20$ and $Z=21$, while a slight improvement of $Z=20$ over $Z=25$ can be noticed.   In fact, the uses of eq 9 and $Z=20$ are closely related.   In view of s-C's M_w value being slightly above M_e (=13500),[8,10,27] eq 4 instead of eq 9 should be used.   However, s-C's molecular-weight distribution, though nearly monodisperse, is broad enough to have a sufficiently large amount of components with molecular weights below M_e, significantly diluting the entanglement.

At $Z=20$, s-C has 21 wt% of the distribution below M_e. The dilution increases the entanglement molecular weight from M_e to $M_e^{'}=17090$ based on [9,10]

$$M_e^{'} = \frac{M_e}{W_2} \qquad\qquad (13)$$

As $M_e^{'} > M_w$, s-C immerses in an entanglement-free state. As opposed to this, the stress-relaxation modulus and storage-modulus spectrum over the entropic region of E167 with a similar molecular weight (see Table 1), were successfully analyzed in terms of ERT with $Z=120$ corresponding to $M_w/M_n<1.01$ but could not be described by the Rouse theory.[7,8,10] See the Appendix for additional discussion of the viscoelastic difference between s-C and E167.

With the explanation as given above, we shall use eq 9 as the chosen functional form in discussing the analysis of the J_e^0 and $J(t)$ results of s-C below. With $\langle \tau \rangle_G$ being related to K by eq 3, an increase in s will lead to a decrease in J_e^0. Thus, a computer program can be set up to scan through a wide range of s to calculate a large set of J_e^0 values, from which the best matching with the values measured at different temperatures can be identified. In an entangled system, because of the broad relaxation-time distribution in the rubber-to-fluid region, the J_e^0 value is not sensitive to the change in s when the temperature is not close to T_g–here s is relatively small; on the other hand, the J_e^0 value is difficult to measure when the temperature is close to T_g. Thus, s for an entangled system can mainly be obtained from analyzing the line

shape of $J(t)$.   For s-C, s can be extracted from both the analyses of $J(t)$ and J_e^0.

The A_G^f and β values listed in Table 1 for s-C allow consistent and quantitative

matching of the calculated with the $J(t)$ line shapes from 93 to 119.4^{o}C and

the J_e^0 values from 93 to 134.1^{o}C as obtained by Plazek.   The A_G^f and β values are

very much uniquely dictated by the compliance values and line shapes, respectively,

of $J(t)$ at 93 and 96°C—namely, the short-time region of $J(t)$.   Similarly as shown in

paper 1 for s-A and s-B, the time range covered by the available $J(t)$ results of s-C at

higher temperatures is only affected by the product of A_G^f and $\langle \tau \rangle_G$ (or s with K

being fixed) and is virtually independent of β.   As shown in Table 1, the β value of

s-C is basically consistent with those obtained for s-A and s-B.   And the A_G^f value for

s-C is between those for s-A (corresponding to A_G=5482) and s-B (corresponding to

A_G=4119). As explained in paper 1, the A_G^f value of s-B being smaller is due to the

contamination by residual plasticizers in the sample (see ref 2 about the residual

plasticizers).   That the A_G^f value of s-C is smaller than that of s-A should be due to its

smaller molecular weight.

We use 100°C as the reference temperature at which the calculated and

measured J_e^0 values are matched; the same will be used for the compliance

coordinate in the comparison of the calculated and measured $J(t)$ line shapes.   Thus,

the J_e^0 values listed in Table II of ref. 28 are first adjusted by the multiplication with

the factor $\rho T / \rho_0 T_0$ where ρ_0 is the density at T_0=373K; the adjusted J_e^0 will be

denoted by J_{ep}^0.   With the A_G^f and β values as chosen, from matching the

calculated J_{ep}^0 values with the adjusted experimental values the s values at different

temperatures are obtained.   These s values are then used to calculate the $J(t)$ line

shapes for comparison with the measured ones. In general, the agreement between the

thus calculated $J(t)$ and the measured is quite close.

The s values obtained from matching the calculated with the measured J_{ep}^0 values

have been modified somewhat in some cases to obtain a better agreement between the

calculated and measured $J(t)$ line shapes as shown in Figure 1. The experimental $J(t)$

results shown in Figure 1 are those shown in Figure 1 of ref. 28, which have all been

reduced to using 100°C as the reference temperature for the compliance–i.e.,

multiplied by $\rho T / \rho_0 T_0$. Accordingly, all the theoretical $J(t)$ curves are calculated

at $\rho T / \rho_0 T_0$ =1; following Plazek's notation,[28] the thus calculated $J(t)$ is denoted by

$J_p(t)$–as used above and will be used below, the corresponding viscoelastic quantities

$G(t)$, J_e^0 and η will be denoted by $G_p(t)$, J_{ep}^0 and η_p, respectively.   In this study, each

of the theoretical $J_p(t)$ curves is first calculated with $K=10^{-4}$.   In superposing the

calculated on the measured $J_p(t)$ at a certain temperature, *only* shifting along the time

axis is allowed.   From each superposition, a time-scale shifting factor, SF, is

obtained, which, when multiplied by 10^{-4}, gives the K value at the corresponding

temperature. s values obtained from fitting to the $J_p(t)$ line shapes and the

corresponding SF and K values at different temperatures are listed in Table 2.   Using

the obtained s values, the viscosity values with K set at 0.0001 are also calculated, as

listed under the $\eta_p(K=10^{-4})$ column in Table 2.   Because the glassy relaxation

occurs in the short-time region, its contribution to the zero-shear viscosity, η_p, often

referred to as the internal viscosity,[12] is in general negligible if the molecular weight of the sample is sufficiently large. The contribution of the internal viscosity to η_p in s-C is in general significant because of its relatively low molecular weight. The comparative importance of the contributions of the internal viscosity to η_p at different temperatures and the associated changes in the $J_p(t)$ line shape of s-C are clearly illustrated in Figure 2, with all the curves calculated with $K=10^{-4}$ corresponding to those shown in real time in Figure 1. Numerically the contributions of the internal viscosity can be obtained by comparing the $\eta_p(K=10^{-4})$ values calculated without (i.e., setting $A_G^f=0$; see the first row of Table 2) and with the glassy-relaxation process using the s values determined at different temperatures. The enhancement by the internal viscosity is expressed as the ratio, $\eta_p(K=10^{-4})\diagup\eta_p(K=10^{-4}; A_G^f=0)$, as also listed in Table 2. The contribution of the internal viscosity is about 11% at 134.1^{o}C and increases with decreasing temperature, enhancing the viscosity by a factor of 4.6 at 93°C. As shown in Figure 2, the large enhancement by the internal viscosity at a low temperature is reflected by the large shift of the flow region in $J_p(t)$ to the longer normalized time from one at a high temperature—the term "normalized time" is used because the time-scales of all the curves are on the same basis of $K=10^{-4}$. While the inclusion of the glassy relaxation process allows us to adjust the s values so that the calculated $J_p(t)$ line shapes are in close agreement with the measured at different temperatures, whether the glassy-relaxation process contributes to the viscosity in the right amount at different temperatures need be checked. Multiplying the $\eta_p(K=10^{-4})$ values by SF and the ratio $\rho T/\rho_0 T_0$ gives the theoretical viscosity values at the

corresponding temperatures, as listed under the η(calcd) column in Table 2. The

obtained η(calcd) values are in close agreement with the measured as also listed under

the η(exp) column in Table 2, further confirming the validity of the present analysis.

This is also illustrated by the agreement between the calculated and measured $J_p(t)$

long-time limit lines, t/η_p, at different temperatures as also shown in Figure 1.

As the $J_p(t)$ result of 134.1^{o}C is not available, its SF and K values cannot be

obtained from the $J_p(t)$ line shape analysis. However, with its s value obtained from

matching the calculated J_{ep}^0 with the measured, the K value of 134.1^{o}C can be

calculated from the K values at other temperatures by using the

temperature-dependence information of K that can be extracted from the viscosity

data. Dividing a measured viscosity value by both $\rho T/\rho_0 T_0$ and the viscosity

enhancement factor $\eta_p(K=10^{-4})/\eta_p(K=10^{-4}; A_G^f=0)$, a viscosity value, denoted by η_R,

is obtained, which is free from the contribution of the internal viscosity and, thus, is

only proportional to K. Then, the K value at 134.1^{o}C can be calculated from

multiplying the K values at other temperatures by the ratios $\eta_R(134.1^oC)/\eta_R(t^oC)$.

In this way, the average K value at 134.1^{o}C obtained from the K values at other seven

temperatures is 1.06×10^{-9} with a standard deviation of only 3.5%. As any

substantial error in s—especially at low temperatures—can cause a large error in the

calculated η_R value, the small standard deviation supports that the s values are

correctly obtained from the $J_p(t)$ line-shape analysis.

The two set of s values as a function of temperature: one obtained from the

analysis of J_{ep}^0 and the other from that of $J_p(t)$, are in good agreement as shown in

Figure 2, indicating the consistency of the data analyses. The consistency is also indicated by the close agreement of the measured J_e^0 values and those calculated based on the s values obtained from the $J_p(t)$ line-shape analysis, as listed in Table 2.

The K values shown in Table 2 can be well fitted to an equation of FTH form. Using the FTH equation obtained from the fitting, the K values at 127.5 and $93.7_{56}{}^{o}C$ are calculated and also listed in Table 2, with the former also listed in Table 1; the K values of s-C at different temperatures will be compared with those of s-A in the discussion section and the result of K (and τ_S) at $93.7_{56}{}^{o}C$ will be used in sections 5 and 7 studying the molecular-weight dependence of T_g and the length-scale at T_g.

4. Dynamic Anisotropy in Entangled Systems

The K values obtained from analyzing the viscoelastic results at $127.5{}^{o}C$ of 11 nearly monodisperse samples of different molecular weights ranging from 3.4×10^4 to 6×10^5 (see Appendix B of ref 3)[3,7,10] in terms of ERT are independent of molecular weight, giving an average value of $4.9 \times 10^{-9} \pm 10\%$. As listed in Table 1 the K value of E167 at $M_w = 1.24 M_e$ is only about 20% below the average value. While these results of entangled systems indicate the molecular-weight independence of K extending to a molecular weight virtually as low as just above M_e, T_g starts to decrease with decreasing molecular weight at around $10 M_e$. From the view point of the conventional concept of the relation between viscoelastic dynamics and T_g as related to free volume,[15,34,35,36] this contrast represents a paradox. The paradox has

---

[34] Doolittle, A. K. *J. Appl. Phys.* **1951**, *22*, 1471; **1952**, *23*, 236; **1952**, *23*, 418.

been explained by the physical picture[7-10,37,38] that the free volume at both chain ends is always available to the modes of motion along the primitive path (of the tube model), whose relaxation times are all proportional to K. Such a mechanism may allow K to be disengaged from a dependence on the free volume in the bulk and become independent of molecular weight. Thus, as proposed previously,[7-10,36,37] the decrease in T_g with decreasing molecular weight in the entangled region should be related to the molecular-weight dependence of the K'/K ratio as described by the empirical equation:

$$\frac{K'}{K} = R_K(M) = \frac{2.525}{\exp\left[-0.643\left((M/M_e) - 4.567\right)\right] + 1} + 0.769 \tag{14}$$

where K' is the frictional factor in the Rouse–Mooney process $\mu_A(t/\tau_A)$ (eq 9.B.20 of ref 10 or eq 20 of ref 6 with K replaced by K'). $R_K(M)$ as given by eq 14 has been obtained from fitting the empirical form of equation to the obtained K'/K values at different molecular weights.[7,9,10] $K'/K > 1$ indicates the dynamics in an entangled system is anisotropic in respect of the frictional factor. As the $\mu_A(t/\tau_A)$ process is the motion of an entanglement strand with both ends fixed, unlike K being for the modes of motion along the primitive path that are always facilitated by the free volume at

[35] Cohen, M. H.; Turnbull, D. *J. Chem. Phys.* **1959**, *31*, 1164; Turnbull, D.; Cohen, M. H. *J. Chem. Phys.* **1961**, *34*, 120.

[36] Berry, G. C.; Fox, T. G. *Adv. Polym. Sci.* **1968**, *5*, 261 and references therein.

[37] Lin, Y.-H. *Macromolecules* **1990**, *25*, 5292.

[38] Lin, Y.-H. *Macromolecules* **1991**, *24*, 5346.

both chain ends, K' should be like T_g sensitive to the free volume *in the bulk*. The free volume increases with increasing number of chain ends per unit volume, and thus increases with decreasing molecular weight. $R_K(M)$ has a plateau value 3.3 in the high-molecular-weight region and starts to decline with decreasing molecular weight at around $10M_e$–where T_g also starts to decrease–to the limiting value 1 as $M/M_e \rightarrow 1$. These results indicate that because of the tube (of the reptation model), the K value in the entanglement region is not affected by the decline in T_g with decreasing molecular weight.   The tube is very much intact to a molecular weight as low as just above M_e as K has been rigorously shown independent of molecular weight to this point at and above 127.5^oC[39].   The molecular-weight independence of K is subjected to a correction caused by the strong structural formation when the temperature is significantly closer to T_g than 127.5^oC as will be discussed in section 8.3.

The variations in s with temperature for s-A, -B, and -C are shown together in Figure 3.   The results of both the entangled (s-A and s-B) and entanglement-free (s-C) systems are obtained through an equivalent analysis scheme, involving ERT as the reference frame in the former and the Rouse theory in the latter.   In the case of s-A and s-B, the s values are obtained entirely from the $J_p(t)$ line-shape analysis, while in the case of s-C, the s values are obtained from both the analyses of the J_{ep}^0 values and $J_p(t)$ line shapes. The s values for both the entangled and entanglement-free systems

---

[39] As shown in Table 1 of ref 3, K is independent of molecular weight at 127.5 and

174^oC. As pointed out in ref 4, it is also true that the temperature dependence of

viscosity at different molecular weights can be superposed on one another over the

temperature range covered by viscosity measurements as reported in ref 28.

change in a similar way in a similar range of temperature above their individual T_g's. This similarity between the entangled and entanglement-free systems is significant, considering that different molecular theories are involved. Yet, this similarity and the consistency and relationships among them as will be further revealed from the analysis given in section 6 should not be surprising, considering the two basic conclusions derived from previous studies and listed below, on which the extraction of s values is based:

(1) ERT and the Rouse theory have the same footing at the Rouse-segmental level—the frictional factor K in both theories has been shown to be the same within a small experimental error.[9,10]

(2) The thermorheological complexity should occur as long as the molecular weight is greater than the Rouse segment size.[3,4]

Neglecting the small difference in T_g between s-A and s-B, it was pointed out[3] that their s values at the same temperature follows the molecular-weight dependence of K'/K, namely, $R_K(M)$ given by eq 14. This molecular-weight dependence of s is also borne out by the analysis (including s-C's results) taking the T_g difference into account, which will be given in section 6. s and K'/K having the same molecular-weight dependence should be closely related to the fact that the $\mu_G(t)$ and $\mu_A(t)$ processes are next to each other in time-scale.[3,4]

To eliminate this molecular-weight dependence in s, we define

$$s' = \frac{s}{(K'/K)} = \frac{\langle \tau \rangle_G}{K'} \tag{15}$$

in which eq 3 has been used for the second equality.   Although the s values of s-C

have been obtained from analyzing its $J_p(t)$ and J_e^0 results by involving the Rouse

theory rather than ERT, we may regard its s to be the same as that of a sample at the

same molecular weight, but with a molecular-weight distribution sufficiently narrow

for ERT to be applicable.   From the analyses of the relaxation modulus and

viscoelastic spectrum of E167 in terms of ERT as reported previously[7,8,10] and

mentioned above, $K'/K=1$ was obtained within a small experimental error ($<$10%)

indicating, as eq 14 does, $K'/K=1$ as $M_w \rightarrow M_e$.   When the tube (of the reptation model)

is disappearing and the Rouse theory becoming applicable at M_e, $K'=K$ is meaningful

physically as it indicates that the dynamics in the system becomes isotropic as it

should.[8-10] As the molecular weights of both s-C and E167 are so close to M_e, we may

regard the s values of s-C as corresponding to $K'/K=1$.   In other words, $s'=s$ for s-C.

Furthermore, in the entanglement-free region of molecular weight, there is only one

frictional factor K as the dynamics is isotropic; $s'=s$ should always be applicable.

5. T_g Defined by Structural Relaxation Time τ_S=1000 sec.

In paper 1, the structural-relaxation or α-relaxation time τ_S was defined by the

time when the ratio between the contribution of the glassy-relaxation process (G) to

the relaxation modulus and that from all the entropic processes (R), G/R, reaches 3.[3]

The structural relaxation time defined this way is basically equivalent physically to

that defined by[3,4]

$$\tau_S = 18\langle\tau\rangle_G \qquad\qquad (16)$$

which was shown, in the case of s-A, to be in close agreement with one of the two traditional ways of defining the α-relaxation time: the time at which the relaxation modulus reaches 10^8 dynes/cm^2 (see Figures 8 and 9).[15] The detailed physical meanings of the structural relaxation time as defined by these different but basically equivalent criterions are referred to papers 1 and 2. As explained previously, the structural relaxation time defined by eq 16, besides reflecting the effect of the glassy relaxation on the bulk mechanical properties, has the virtue of following exactly the temperature dependence of the involved dynamic process, unlike the other definitions which are affected by the change in the line shape with temperature.

Using eq 15, the structural relaxation time given by eq 16 may be rewritten as

$$\tau_S = 18sK = 18s'K' \qquad\qquad (17)$$

From the $J(t)$ line-shape analysis at the calorimetric T_g (97°C) of s-A, it was shown[3,4] that the structural-relaxation time τ_S as defined by eq 17 reaches 1000sec and that the length scale is about 3nm, which is of the same order of magnitude as estimated by other methods.[40,41,42,43,44] In the literature,[45,46,47] τ_S reaching 100~1000 sec with

[40] Sillescu, H. *J. Non-Crystal. Solids* **1999**, *243*, 81; and references therein.

[41] Hempel, E.; Hempel, G.; Hensei, A.; Schick, C.; Donth, E. *J. Phys. Chem. B* **2000**, *104*, 2460.

decreasing temperature has been used as the criterion for defining T_g. In view of the τ_S

value for s-A at its calorimetric T_g, we shall use $\tau_S=1000$ sec for defining the T_g's of

s-B and s-C as well in the analysis below; such a criterion will allow us to have a

common reference point equivalent for all the three samples.   It will be shown that

the thus defined T_g's are consistent with values expected from calorimetric

measurements. The dynamic and structural quantities: K, K', s and τ_S obtained at the

thus defined T_g and different temperatures from analyzing the creep results of s-A are

listed in Table 3.

By interpolation—using the FTH equation obtained from the least-squares fitting

to the τ_S values listed in Table 2, we obtained $\tau_S=1000$ sec at $93.7_{56}\,^{\circ}C$, which is then

regarded as T_g of s-C.   Then, as also listed in Table 2, K and s values of s-C at this

temperature can be obtained from their values at different temperatures by

interpolation—using the FTH equation for K obtained from the least-squares fitting as

explained above and a modified FTH equation (the form as given by eq 19) for s.

s-B is contaminated by residual plasticizers;[2] it has been shown that its frictional

factor K is smaller than that of a normal sample as expected.[3]   Because of the

---

[42] Tracht, U.; Wilhelm, M.; Heuer, A.; Feng, H.; Schmidt-Rohr, K.; Spiess, H. W. *Phys. Rev. Lett.* **1998**, *81*, 2727.

[43]   Cicerone, M. T.; Blackburn, F. R.; Ediger, M. D. *J. Chem. Phys.* **1995**, *102*, 471.

[44] Arndt,M.; Stannarius, R.;   Groothues, E.; Hempel,   E.;   Kremer, F. *Phys. Rev. Lett.* **1997**, *79*, 2077.

[45] Angell, C. A. Science **1995**, *267*, 1924; and references therein.

[46] Sillescu, H. *J. Non-Crystal. Solids* **1999**, *243*, 81; and references therein.

[47] Angell, C. A. *J. Non-Cryst. Solids* **1991**, *131-133*, 13.

contamination, the T_g value of s-B is also somewhat smaller than that of a normal sample at the same molecular weight.[2]   The T_g of s-C is smaller than that of s-A because of its smaller molecular weight.   Here we shall treat in a similar way the contamination by residual plasticizers in s-B causing its T_g to become smaller.   In other words, we shall also use τ_S=1000 sec to define the T_g of s-B as it is.   From the s and K values extracted from the $J_p(t)$ of s-B available at the lowest temperature (98.3^{o}C), τ_S=779 sec is obtained, which is somewhat smaller than the criterion τ_S=1000 sec.   Because the difference is not large, we may calculate the temperature at which τ_S=1000 sec by extrapolation using the FTH equation that has been obtained from fitting the τ_S values at different temperatures.   The T_g determined this way for s-B is 98.0$_{25}$^{o}C.   Then from the FTH equation best describing the K values of s-B at different temperatures, the K at this temperature is obtained as listed in Table 3. The s or s' value at T_g is then calculated from thus obtained τ_S and K values, using eq 17.   The K, K', s and τ_S values of s-B at different temperatures including those at T_g as determined above are listed in Table 3.

As it is well-known and commonly observed that the structural-relaxation time τ_S increases sharply as the temperature approaches T_g from above.   The temperature dependence of s of s-A and s-B has been obtained in paper 1 and that of s-C above; as shown in Figure 2, the s values of the three samples increase in a similar way as the temperature decreasing toward T_g.   The T_g as defined above allows us to have a common reference point equivalent for the different samples, with respect to which we may compare the obtained τ_S and s or s' in a perspective way.

6. Dependences of τ_S, s' and K' on $\Delta T = T - T_g$

The results obtained from the $J_p(t)$ line-shape analyses of s-A, -B and -C strongly suggest that the τ_S and s' values of the three samples depend in a universal way within the polystyrene system on how far the temperature is away from each individual T_g. Using the above defined T_g individually for each sample, we display the τ_S values of s-A, -B and -C as a function of the temperature difference from T_g: $\Delta T = T - T_g$, as shown in Figure 4. In spite of the facts that s-C has a significantly smaller T_g due to its smaller molecular weight and that s-B is contaminated by residual plasticizers, the τ_S values of the three samples fall closely on the same line. Clearly, because the contamination in s-B by plasticizers is so low that s-B keeps the T_g-related basic nature of polystyrene.   And the residual plasticizers in s-B function in a similar way as a low-molecular-weight polystyrene component would lower the T_g of the host slightly. The close agreement among the three samples strongly supports the way of using ΔT to account for the T_g difference. The τ_S values can be collectively well fitted by the FTH equation of the form:

$$\log(\tau_S) = a_\tau + \frac{b_\tau}{(\Delta T + t_\tau)} \qquad (18)$$

as shown by the calculated curve in Figure 4 with $a_\tau = -11.5045$, $b_\tau = 539.3497$ and $t_\tau = 37.1827$.   The τ_S values as shown in Figure 4 has the exactly same temperature dependence as that of $\langle \tau \rangle_G$, purely reflecting that of the glassy-relaxation process itself; in other words, free from the effect of the change in line shape of the

viscoelastic spectrum.   The consistency of the ΔT dependence of τ_S among the three

samples should make one prefer using eq 16 or 17 to define the structural-relaxation

time.

In Figure 5, the *s'* values of s-A, -B and -C are shown together as a function of

ΔT.   The consistency as revealed in the comparison indicates that the three sets of *s'*

values basically follow a universal curve for polystyrene; the thermorheological

complexity as analyzed in this study—i.e. expressed in terms of *s'*—is a general

phenomenon whether the system is *entangled or not*.   This consistency supports the

validity of the two previously derived conclusions listed in section 4, upon which all

the analyses of s-A, -B and -C have been based.   The ΔT dependence of *s'* of the

three samples can be collectively well fitted by a modified FTH form:

$$\log(s') = c_1 + c_2(\Delta T + t_s) + \frac{c_3}{\Delta T + t_s} \tag{19}$$

The curve shown in Figure 5 has been calculated with $c_1 = -4.2189$, $c_2 = 0.0364$,

$c_3 = 375.6136$ and $t_s = 55.0922$.

The consistency of the ΔT dependences of *s'* and τ_S among the three samples

implies that the same consistency should occur to *K'* according to eq 17; indeed so as

illustrated in Figure 6.   In s-C, the dynamics is isotropic; there is only one frictional

factor indicating $K' = K$ in effect.   Furthermore, $K'/K \rightarrow 1$ when the molecular weight

approaches M_e, as observed in E167.   Indeed, when the dynamics is isotropic, it is *K*

itself that is sensitive to the free volume in the bulk, and thus related to T_g.   Thus,

whenever K' of s-C is indicated below, automatically its K is meant or used, just as s and s' are the same in the case of s-C as explained in section 4. The ΔT dependence of K' of s-A, -B and -C can be collectively fitted by the FTH equation of the form given by eq 18 with the notations τ_S, a_τ, b_τ and t_τ replaced by K', a_K, b_K, and t_K, respectively. Shown in Figure 6 is the curve calculated with $a_K = -15.3931$, $b_K = 536.9037$ and $t_K = 42.8976$. As the molecular-weight dependence of T_g has been accounted for by expressing the dynamic quantity in terms of ΔT, the fact that the K' values of s-A, -B and -C as a function of ΔT fall on the same curve supports that the molecular-weight dependence of T_g is directly related to the molecular-weight dependence of K' as proposed previously[7-10,36,37] and pointed out above. In the meanwhile, K is independent of molecular weight at and above 127.5°C; therefore, as opposed to the consistency in the ΔT dependence of K' among s-A, -B and -C, their K values are not expected to have a common ΔT dependence, as shown in Figure 7. Further discussion of K at temperatures very close to T_g will be made in section 8.3.

It is interesting to point out that the obtained best values $t_\tau = 37.1827$, $t_s = 55.0922$ and $t_K = 42.8976$ imply that the τ_S, s' and K' values become infinitely large each at a temperature in the range 35~60 degrees below T_g. The combination of $t_\tau = 37.1827 < t_K = 42.8976$ and $b_\tau = 539.3497 > b_K = 536.9037$ is consistent with the fact that τ_S has a stronger temperature dependence than K'. For τ_S being the product of s' and K' (eq 17), as inherent in the procedure of analysis, an error in s' tends to be canceled by an opposing one in K'. Because of such a mutual cancellation, the ΔT dependence of τ_S has smaller fluctuations of data than that of either s' and K'. In spite of some fluctuations in the data points, the consistency of the ΔT dependences of

s' and *K'* among the three samples as well as the implied universality is very clear. Such a consistency is particularly significant considering the fact that *s'* values are determined entirely by the *line shapes* of $J(t)$ while *K'* values are converted from *K* values which are determined from the *shifting factors* SF (see section 3). These results indicate that the ΔT dependence of *K'* serves as an intermediate between this universality in thermorheological complexity occurring in the short-time region and another universality of topological nature occurring in the long-time region: On the one hand, just as for *s'*, it requires a T_g correction to show the consistency in *K'*; on the other hand by the predetermined parameter $R_K(M)$ it is converted from *K*, which is independent of molecular weight at and above 127.5°C.[37] The importance of $R_K(M)$ cannot be overemphasized; without it, the universal ΔT dependences of *s'* and *K'* cannot be obtained.

7. Information in $G(t)$ as Extracted from the Analysis

7.1. Length-Scale at T_g

With the *s* (or *s'*) and *K* (or *K'*) values at T_g for s-A, -B and -C as determined in section 5, the $G_p(t)$ curves of the three samples at their individual T_g points may be calculated, using eqs 4–8 for s-A and s-B and eqs 7–12 for s-C. The three calculated $G_p(t)$ curves are shown together in Figure 8 for a comparison that would be revealing. In the figure, the curves calculated by setting A_G (or A_G^f)=0 are also shown; in each set of curves, the area between the full curve and the curve with A_G (or A_G^f)=0 represents the contribution of the glassy-relaxation process to the relaxation modulus. For s-A

and s-B, the curves calculated without both the glassy-relaxation and Rouse‒Mooney normal modes are also shown; the area between a thus calculated curve and that with A_G=0 represents the contribution of the Rouse‒Mooney normal modes to $G_p(t)$. Also indicated in the figure are the positions in time corresponding to the relaxation times of the Rouse normal modes in s-C (calculated from its K value) and the relaxation times of the Rouse‒Mooney normal modes in s-A and s-B (calculated from their K' values; K'=1.61K in s-A and K'=3.16K in s-B[3]).

It has been proposed in paper 1 that the positions of the relaxation times of the normal modes may be used as "graduations" of a yardstick for estimating the extent of the influence of the glassy-relaxation process. The relaxation time of the p-th normal mode, τ_A^p (in the Rouse‒Mooney process of s-A and s-B) or τ_p (in the Rouse process of s-C), is associated with a length-scale given by[10,48]

$$\lambda_p \approx (a^2 / p)^{0.5} \qquad (20)$$

with a standing for the entanglement distance in the entangled case (s-A and s-B) or standing for the end-to-end distance in the entanglement-free case (s-C). The value a may be calculated from the characteristic ratio C_∞ or equivalently K_∞

---

[48] Doi, M.; Edwards, S. F. *The Theory of Polymer Dynamics*; Oxford Univ. Press: New

York, 1986.

$(=0.43 \times 10^{-2} \text{nm}^2/\text{Da}$ for polystyrene);[10,49,50] one obtains $a^2 = K_\infty M_e = 58.1$ nm^2 for

s-A and s-B, and $a^2 = K_\infty M_w = 70.5$nm^2 for s-C. One sees in Figure 8 that the

vertical dotted line at the time 1000 sec representing the structural-relaxation time τ_S

at T_g passes through between the relaxation times of the seventh and the eighth normal

modes in all three cases. Using the relative position of $\tau_S = 1000$ with respect to

τ_A^7 and τ_A^8 (in s-A and s-B) or to τ_7 and τ_8 (in s-C), we may calculate from the values

of λ_7 and λ_8 (eq 20) the length-scale λ at T_g by interpolation. The λ values so

obtained are 2.76, 2.87 and 3.0nm for s-A, -B and -C, respectively. These values are

consistent with one another, indicating the universality of the characteristic

length-scale at $\Delta T \to 0$; at the same time, they are nearly the same as that estimated by

the calorimetric method.[39,40]

7.2. Change in Length-Scale with ΔT

For illustrating the change in length-scale with ΔT occurring in all the studied

samples in perspective, shown in Figure 9 is the comparison of the $G_p(t)$ curves of the

three samples calculated at $\Delta T = 9.7^\circ$, where $\tau_S = 1$ sec is expected according to the

calculated curve shown in Figure 4. The parameters: s' and K' (or s and K) used to

calculate the $G_p(t)$ curve for each of the samples are obtained from the values

determined at different temperatures by interpolation through least-squares fitting. It

is shown in the figure that the vertical dotted line at 1 sec representing the

[49] Lin, Y.-H. *Macromolecules* **1987**, *20*, 3080.

[50] Fetters, L. J.; Lohse, D. J.; Richter, D.; Witten, T. A.; Zirkel, A. *Macromolecules* **1994**, *27*, 4639.

structural-relaxation time occurs before the relaxation time of the highest Rouse or Rouse–Mooney mode by about an equal "distance" in all three cases—equivalent to log1.9, log2.0 and log1.6 for s-C, -A and -B, respectively—indicating a universal effect. τ_S=1 sec being shorter than the motional time of a single Rouse segment means that the length-scale associated with the structural-relaxation process is shorter than the Rouse-segmental length, ~ 2nm, and indicates a rubbery state, as opposed to vitrification at the Rouse-segmental level at T_g or ΔT=0 as indicated by what is shown in Figure 8.

Heuer and Okun[51] have simulated the dynamics of entanglement-free chains using the bond fluctuation model which contains the effect of intermolecular interactions; based on the study, they have presented a sketch (Figure 12 of ref 50) showing the encroaching of the heterogeneous dynamic mode on the homogeneous dynamic modes at larger length-scales with decreasing temperature. As discussed in paper 1,[3] dynamic heterogeneity is enhanced as s' increases with temperature decreasing towards T_g. Thus, with the homogeneous modes as corresponding to the Rouse modes and a one-to-one correspondence between length-scale and time-scale, the sketch given by Heuer and Okun may represent a rough picture of the actual results of entanglement-free case shown in Figures 8 and 9.

8. Discussion

8.1. Structural Factor and Frictional Factor of Viscosity

---

[51] Heuer A.; Okun, K *J. Chem. Phys*. **1997**, *106*, 6176.

The free-volume theory together with the molecular-weight dependence of T_g led to the notion that the friction constant decreases with decreasing molecular weight below a certain point.[15,33-35] Traditionally the viscosity η data are corrected to a state with presumably the same friction constant for studying the structural factor of η; after the correction, it is generally observed that $\eta \propto M$ below M_c, which is about $2.4M_e$, and $\eta \propto M^{3.4}$ above M_c.[35] To isolate the information of the structural factor, the viscosity values at different molecular weights may be compared at equal distance from individual T_g's rather than at the same temperature. As viscosity is dominated by the slow modes of motion, the correction for the T_g difference implies that the correction is mainly made to the modes of motion whose relaxation times are proportional to K. This conventional notion of the relation between viscoelasticity and T_g contradicts directly what have been revealed in our previous studies:[6-10] K is independent of molecular weight at and above 127.5^{o}C to as low as just above M_e; and K' starts to decline from a plateau value of $3.3K$ around $10M_e$ with decreasing molecular weight to become identical to K when the molecular weight approaches M_e. Although, the conventional way of T_g correction for viscosity doesn't contain an element equivalent to the dynamic anisotropy (i.e., $K'/K=R_K(M)\geq 1$), it was proposed[8,37] that the conventional way of correction may be equivalent in a practical sense approximately to correcting for the molecular-weight dependence of K'/K. Indeed, if the viscosity is calculated with K'/K fixed at its plateau value in the high-molecular-weight region, 3.3, rather than following $R_K(M)$ given by eq 14, the viscosity curve numerically calculated from ERT has an apparent $\eta \propto M$ relation below M_c and is closely approximated by $\eta \propto M^{3.4}$ above M_c; and the transition point

M_c that can be identified in the calculated η curve is in close agreement with the experimental value, 33000 (see Figures 1 and 2 of ref. 8).   It has been shown that the difference between the conventional correction and the molecular theoretical correction is not great and may be easily buried in experimental errors.[37] In other words, the molecular theoretical correction has basically "explained" what has been obtained through the conventional phenomenological way.   Theoretically such a molecular correction is valid when the contribution of the glassy-relaxation process—i.e. the internal viscosity—is negligible as at temperatures sufficiently far above T_g ($\gtrsim T_g + 20^\circ$), where s is small.   Most likely due to the lack of viscosity data in the temperature range close to T_g, the conventional T_g correction for viscosity is typically done at a temperature quite far above T_g.[35]   More details are revealed and clarified as the faster and directly T_g-related glassy-relaxation process is analyzed in this study.

8.2. Frictional Slowdown and Structural Growth

The results shown in Figure 6 indicate that after the T_g correction is made directly to the K' values of the three different samples, they fall on the same line; thus, the molecular-weight dependence of K' and that of T_g are directly related as proposed previously.[7-10,36,37] The consistency of the ΔT dependence of s' among the three samples indicates that the molecular-weight dependence of K' extends into the time domain of the glassy-relaxation process—see eqs 16 and 17.   After the T_g correction is made to both the $\mu_A(t)$ (or $\mu_R(t)$) and $\mu_G(t)$ processes by expressing K' and s' in terms of ΔT, they both become independent of molecular weight.   This also means that the molecular-weight dependence of T_g in the entanglement region is directly

related to the fast dynamic processes: $\mu_A(t)$ and $\mu_G(t)$, both following the same molecular-weight dependence.

While K' is a frictional factor, s' should be regarded as a *structural factor*; indeed, s' has the unit of Da^2. Thus the ΔT dependence of s' shown in Figure 5 and the ΔT dependence of K' shown in Figure 6 are of different physical nature; with decreasing ΔT, the former reflects the growth of structure, while the latter represents purely the frictional slowdown. The structural relaxation, with relaxation time defined by eq 17, contains the effects of both the frictional slowdown and structural growth while the $\mu_A(t)$ process is only affected by the frictional slowdown. As a result, the relative positions of τ_S with respect to $\{\tau_A^p\}$ or $\{\tau_p\}$ in time-scale change with ΔT as can be observed by comparing Figures 8 and 9 (also see Figures 6 and 7 of ref 3). This effect is further illustrated in Figure 10 by the comparison of τ_S and the Rouse-segmental motional time τ_v over a wide ΔT range. τ_v is defined by

$$\tau_v = \frac{K\pi^2 m^2}{24} \qquad (21a)$$

for an entanglement-free case, or

$$\tau_v = \frac{K'\pi^2 m^2}{24} \qquad (21b)$$

for an entangled case, where $m=850$ is used for the mass of a Rouse segment. When $N=M/m$ or $N_e=M_e/m$ is sufficiently large for $(N-1)/N \approx 1$ or $(N_e-1)/N_e \approx 1$ to be

valid as in the present study, eq 21 is a close approximation to the relaxation time of the highest Rouse or Rouse–Mooney normal mode as given by eq 12 (K in eq 12 is replaced by K' for the Rouse–Mooney modes).   In Figure 10 one sees the crossing of τ_S over τ_v as ΔT decreases near zero, indicating vitrification at the Rouse-segmental level.   What is shown in Figure 10 is equivalent to that shown in Figure 5 of ref 4 for s-A; here the results are shown for s-A, -B and -C collectively, illustrating that the crossing-over is a universal behavior as the correction for T_g difference is made by expressing both τ_S and τ_v in terms of ΔT.   This universality and the consistency among the three samples as observed in each of and between Figures 8 and 9 are results logically expected from the universality of the ΔT dependences of τ_S, s' and K' as shown in Figures 4–6, respectively.

In addition to the illustrations of universality as discussed above, it can be observed that the T_g correction to the $\mu_A(t)$ (or $\mu_R(t)$) and $\mu_G(t)$ processes *as a whole* is a nonlinear   one. This is also clear from eq 17: τ_S is proportional to the product s' and K', both changing with ΔT.   In other words, the glass transition together with the closely related thermorheological complexity as a general phenomenon is a nonlinear effect.   The fact that both s' and K' individually change with ΔT in a universal way indicates that we have succeeded in separating the general nonlinear effect into two decoupled effects: structural growth and frictional slowdown.   The decoupling is fundamentally a clean-cut process, as s' is first determined *entirely* by the line shape of $J(t)$ and then the time-scale shifting factor is obtained from which $K'(=R_K(M)K)$ is calculated.   In terms of the two decoupled quantities, important features associated with the glass transition and thermorheological complexity are revealed or explained.

A severe test of the scheme of analysis is of course the quantitative explanation of the $J(t)$ line shapes as a function of temperature—including explaining naturally in a precise way the temporal unevenness in the thermorheological complexity of $J(t)$ and in the case of a low-molecular-weight polystyrene melt the dramatic decrease in J_e^0 with temperature approaching T_g from above. Representing important features revealed in this study are the physical picture of vitrification at the Rouse-segmental level and the length-scale at T_g for all the three studied samples.

Because of the validity of the molecular theories used as the reference frame and the precise physical picture they contain, the time-scale and length-scale of the glassy-relaxation process can be characterized in detail as they increase with temperature decreasing towards T_g. The universality covering both the *entangled* and *entanglement-free* cases as revealed in this study signifies two important points: (1) It supports the conclusion derived from the study of the blend-solution systems that ERT and the Rouse theory share the same frictional factor K within a small experimental error and thus have the same footing at the Rouse-segmental level. Putting it in another way, if the previously derived conclusion weren't true and thus couldn't be a valid premise, the universality as obtained in this study couldn't have occurred at all. (2) It strongly indicates the importance of the roles which the obtained time-scale and length-scale may play. An example of such importance is the outcome that the basic mechanism of the thermorheological complexity as analyzed and detailed in refs 3 and 51[52] should be also responsible for the breakdown of the Stokes‒Einstein

---

[52] Lin, Y.-H. *J. Phys. Chem. B* (submitted).

equation in relating the translational diffusion constant with the shear viscosity, which has been observed for glass-forming liquids, such as OTP (*o*-terphenyl)[53,54,55] and TNB[56] (*tris*-napthylbenzene), when T_g is approached from above.

8.3. *K* Values in the Close Neighborhood of *T_g*

As pointed out above, the common length-scale at τ_S=1000 or 1sec (at ΔT=0 or 9.7) as shown in Figures 8 and 9, respectively, and the same relative position of τ_S with respect to the Rouse-segmental motional time τ_v as shown in Figure 10 for the three samples are direct results of the universal behavior of *s'* and *K'* as a function of ΔT. As Figures 8–10 are all displayed in real time, the positions or magnitudes of the relaxation times are ultimately determined by the *K* values.   Thus, although, as expected, the *K* values as a function of ΔT for the three samples as shown in Figure 7 do not fall on a universal line, the *K* value of a sample at a certain ΔT does not occur without following a certain "rule" as the somewhat "chaotic" look of the collective display may suggest.   As the temperature is approaching T_g ($\Delta T \lesssim 20$; in this temperature region $\tau_S \gtrsim 1^{-2}$), because *K'*=*KR$_K$(M)* (*K'*=1.61*K* for s-A; *K'*=3.16*K* for s-B; and *K'*=*K* for s-C) *K* has to change with ΔT in such a way that the corresponding

[53] Fujara, F.; Geil, B.; Sillescu, H.; Fleischer, G.   *Z. Phys. B: Condens. Matter* **1992**, *88*, 195.

[54] Cicerone, M. T.; Ediger, M. D. *J. Phys. Chem.* **1993**, *97*, 10489.

[55] Kind, R.; Liechti, N.; Korner, N.; Hulliger, J. *Phys. Rev. B* **1992**, *45*, 7697.

[56] Swallen, S. F.; Bonvallet, P. A.; McMahon, R. J.; Ediger, M. D. *Phys. Rev. Lett.* **2003,** *90*, 015901.

K' values will behave in the universal way as shown in Figure 6.   As the temperature

is very close to T_g, this effect becomes dominant; *K* becomes influenced through *K'*

by the T_g value, which declines with decreasing molecular weight below $\sim 10 M_e$ for

polystyrene.   This has to be reconciled with the fact that *K* is independent of

molecular weight at and above 127.5°C. As shown in Figure 11, the comparison of the

K values as a function of temperature between s-A, -B and -C illustrates such a

transition.

As s-C and E167 have very similar M_w values, their *K* values as a function of

temperature should not be very different.   The physical difference in *K* between s-C

and E167 should be quite small even though the viscoelastic response in the entropic

region of the former is described by the Rouse theory while that of the latter by ERT.

See the Appendix for a detailed discussion of the viscoelastic difference between s-C

and E167.   As described by the Rouse theory, the dynamics in s-C has only one

frictional factor *K*—dynamically isotropic.   In the case of E167, because its molecular

weight is so close to M_e, it has been found that *K=K'* within a small experimental

error—virtually isotropic dynamically.   Thus, as far as the frictional factor *K* is

concerned, it is basically the same in both samples. The pattern that the *K* values of

s-A and s-C diverge as the temperature approaching T_g and merge at high

temperatures, $\geqslant 130$°C, as shown in Figure 11, should similarly occur between s-A and

E167.   The divergence in approaching T_g in the latter case should be smaller as E167

has a slightly higher M_w value and a much narrower molecular-weight

distribution—factors favoring a higher T_g.   At 127.5°C the *K* values (Table 1) for s-C

and for E167 are both about $17 \sim 20\%$ smaller than the average value *K*=4.9×

$10^{-9} \pm 10\%$ over the molecular weight range from 3.4×10^4 to 6.0×10^5. [3,7,10] The 17% smaller in K for s-C may be due to the effect of a substantial T_g difference, while the 20% smaller in K for E167 is at least partly due to the likely effect that very small amounts of components with molecular weight below M_e in the sample system—as its M_w is only $1.24M_e$—will reduce the obtained K value somewhat. In any case, as these differences in K are so small, these results actually confirm that K at 127.5$^\mathrm{o}$C is independent of molecular weight to a molecular weight virtually as low as M_e and that the Rouse theory and ERT have the same footing at the Rouse-segmental level.

Because s-B is contaminated by residual plasticizers, the K values of s-B cannot be directly compared with those of s-A.[2,3] To illustrate the point made above, we show the curve calculated from the FTH equation that has been obtained from least-squares fitting to the K values of s-B and shifted to the higher temperature side by 1.5$^\mathrm{o}$. The temperature shift is to account for the decrease in T_g by the contamination of residual plasticizers; after the shift, the curve superposes on the FTH curve of s-A over the region of 118~140$^\mathrm{o}$C very closely, including at 127.5$^\mathrm{o}$C, where the K values of s-A and the "uncontaminated s-B" are expected to be in close agreement. After such a shift, the FTH curve of s-B begins to rise above that of s-A below~115$^\mathrm{o}$C, illustrating the divergence similar to, but smaller than, that between s-A and s-C. If we use the value $K'=1.35 \times 10^{-3}$ expected at $\Delta T=0$ (see Figure 6), the K value ($=K'/3.16$) at T_g should be around 4.3×10^{-4}, which occurs at 99.55$^\mathrm{o}$C on the shifted FTH curve of s-B. In other words, from such a "restoration" of s-B to its uncontaminated state, its T_g is estimated to be about 99.5$^\mathrm{o}$C. Thus, we have the T_g values for s-A, hypothetically uncontaminated s-B, and s-C to be 97, 99.5 and 93.8$^\mathrm{o}$C,

respectively; these values are consistent with what may be expected from calorimetric measurements (see the note at ref 56).[57]

The above discussion of the results shown in Figure 11 suggests that the glass transition is a nonlinear effect not only in form as expressed by the product of s' and K' (eq 17) but also in the interplay between the two variables: an increase in s' can enhance a further increase in K' and vice versa. The sharper rise in both s' and K' as the temperature is getting closer to T_g may be the manifestation of such an effect. Such an effect is imposed through K' on the frictional factor K; consequently, as the temperature decreases below $\sim 120^oC$, K gradually deviates from its purely topologically controlled behavior—namely, being independent of T_g and molecular weight—which holds at higher temperatures. Below $\sim 120^oC$, K becoming dependent on molecular weight does not mean ERT ceases to be valid in describing the topological effect on viscoelasticity; as shown in paper 1 (ref 3), in this low-temperature range the line shapes of $J(t)$ in the rubber(like)-to-fluid region remains quantitatively described by ERT. Clearly, only the value of the frictional factor K is affected; the functional forms of the entropy-derived dynamic modes and the structural factors of their relaxation times as given in ERT are not affected. Thus, using ERT as the reference frame in analyzing the $J(t)$ line shapes remains valid below $\sim 120^oC$. On such a basis, it is no accident that the ΔT dependences of s' and K' are found to be universal; the result of analysis represents a real advancement in

[57] Note: From Figure 3 of ref 36, one may obtain T_g=93.4, 97 and 100^oC at M_w=16400, 46900 and 122000, respectively.

understanding the glass transition of polystyrene, which may be generalized to polymers in general.

9. Summary

The quantitative success of the Rouse theory and ERT in describing the entropic region of relaxation modulus $G(t)$ or creep compliance $J(t)$ allows them to be used as a reference frame—the former for an entanglement-free system (s-C) and the latter for an entangled system (s-A and s-B)—with respect to which the glassy-relaxation process that occurs in the short-time region can be studied in a perspective way. From the analyses of the $J(t)$ results of three polystyrene samples: s-A, -B and -C, the structural-growth parameter s', the frictional factor K' for the Rouse–Mooney process $\mu_A(t)$ in the entangled case or the frictional factor K (equivalent to K'; and also treated as K' in notation as explained in section 6) for the Rouse process $\mu_R(t)$ in the entanglement-free case, and the structural-relaxation time $\tau_S = 18s'K'$ are extracted. It has been shown that the thermorheological complexity occurring in $J(t)$ of polystyrene is due to the temperature dependence of the glassy-relaxation process $\mu_G(t)$ being stronger than that of the entropy-derived ones. The uneven thermorheological complexity in $J(t)$ is fully characterized by a simple increase of the structural-growth parameter s' with decreasing temperature in both the entangled and entanglement-free systems.

For all the three studied samples, T_g is defined by the temperature at which the structural-relaxation time τ_S=1000 sec. Thus defined T_g provides a common reference point equivalent to all the samples, with respect to which the obtained τ_S, s' and K'

results may be compared in a proper perspective. When these values of s-A, -B and -C are displayed as a function of $\Delta T = T - T_g$, universal behavior related to T_g is revealed.

A significant point of this study is that the universal ΔT-dependence of τ_S is separated into two decoupled effects: structural-growth as represented by s' and frictional-slowdown as represented by K'—by a clean-cut process: s' being first determined entirely by the $J(t)$ line shape; then K' determined from the time-scale shifting factor—both changing with ΔT individually in a universal way. Because of the universality of s' and K' as a function of ΔT, the $\mu_G(t)$ process and the $\mu_A(t)$ or $\mu_R(t)$ process in both their absolute positions and positions relative to each other in time depend on ΔT in the same way for all the three studied samples. In other words, the thermorheological complexity is a universal effect within the polystyrene system, *entangled or not*. Ultimately this conclusion supports the result from the study of the blend-solution systems that ERT and the Rouse theory have the same footing at the Rouse-segmental level.[9,10] It also strongly indicates the importance of the roles which the obtained time-scale and length-scale may play.

It has been shown that the relaxation times of the Rouse–Mooney normal modes (for s-A and s-B) or the Rouse normal modes (for s-C) may be used as the "graduations" of an internal yardstick for estimating the extent of the influence of the glassy relaxation at T_g. As a logical consequence of s' and K' depending on ΔT in a universal way, the length-scales at T_g obtained this way for the three samples agree with each other closely—about 3nm for all the three samples. As pointed out previously,[3] this kind of analysis represents a new methodology for studying the length-scale at T_g. As the characteristic ratio and entanglement molecular weight of

various polymers have been well documented,[10,48,49] this method would be of wide application.

Key concepts: decoupling of the structural-growth and frictional-slowdown effects; universality in the thermorheological complexity; and the time-scale and length-scale in respect of the motion and size associated with the Rouse segment, as developed, revealed and obtained in the previous and present studies represent a new way to see and study the glass transition of a polymer.

Appendix: Viscoelasticity at Molecular Weights Just Above M_e: Comparison of Samples C and E167.

As explained in section 3, because the molecular-weight distribution of s-C is not that narrow, its viscoelastic results have to be analyzed in terms of the Rouse theory (eqs 9–12) even though its M_w is $1.22M_e$. As also pointed out, the viscoelastic results of E167, which with $M_w = 1.24M_e$ has an extremely narrow molecular-weight distribution, have been well analyzed in terms of ERT.[7,8,10] The analysis of E167's results gives the K value at 127.5^oC, very much the same as the value obtained for s-C, (see Table 1) both being smaller than the average K value $(4.9 \times 10^{-9} \pm 10\%)$[3,7,10] in the entanglement region of molecular weight by about $17\sim20\%$. The difference in

viscoelastic behavior between E167 and s-C is structural: entangled and described by ERT in the former; entanglement-free and described by the Rouse theory in the latter. This difference in the structural aspect of viscoelasticity between the two samples has already been indicated by the comparison of their viscosity results with the theoretical curves of ERT and the Rouse theory in a previous report[8]—though the author has not become aware of the subtlety involved until the present study of s-C: analysis of its $J(t)$ line shapes. As shown in Figure 3 of ref. 8, the viscosity of s-C is below the line of the Rouse theory by a small amount corresponding to its K value being about 17% smaller than the average value. As opposed to this and also shown in the same figure, the viscosity of E167 is above the Rouse line because its viscoelastic behavior is structurally described by ERT, even though its K value is also smaller than the average value by $\sim 20\%$. These discrepancies were displayed when the calculated molecular-weight dependence of η for *ideal monodispersity* was superposed on the experimental results of *nearly monodisperse* samples over a wide molecular-weight range—allowing the viscosity values over the whole range of molecular weights to shift vertically in the superposition as implied by "relative viscosity" used for the ordinate in Figure 3 of ref 8. Here, we take a closer examination by comparing the *absolute* values of viscosity for *ideal monodispersity* calculated with $K=4.9\times10^{-9}$ and the experimental values which have been corrected for the effect of molecular-weight distribution and the contribution of the glassy-relaxation process—the contribution of the internal viscosity is appreciable only in the low molecular-weight region, about 3 $\sim 10\%$ from M_c to M_e. It has been shown that the molecular-weight distribution of a nearly monodisperse sample can enhance the viscosity by about 20~30% depending

50

on the polydispersity, if the M_w value of the sample is used as equivalent to the molecular weight of a theoretically ideally monodisperse system in the comparison between experiment and theory.   As described in detail in ref 10[58] and in Appendix B of paper 1,[3] the molecular-weight distribution for each individual sample as described by the Schulz distribution can be extracted from matching the calculated J_e^0 with the measured value. Using the obtained polydispersity parameter Z, the bulk of correction for the molecular-weight-distribution effect on viscosity may be made, which should reduce the systematic error of 20~30% further to a basically negligible level.   As shown in Figure 12, the calculated absolute values of η for ideal monodispersity are in close agreement with the corrected values over the whole range, excluding s-C and E167.   The values of Z involved in the viscosity corrections for all the samples are in the range expected for nearly monodisperse samples.[59] In this

---

[58] See pages 190‒191 of ref. 10.

[59] Note: Because of the presence of a small tail in the molecular-weight distribution of s-A on the high side (see ref 1), whose contribution is included in $J(t)$ but has been eliminated by Plazek from the listed J_e^0 values,[1,28] the Z value involved in the viscosity correction is larger than that obtained from the $J(t)$ line-shape analysis as reported in paper 1.[3] The Z value from the $J(t)$ line-shape analysis is 20 (equivalent to M_w/M_n=1.05); that from matching the J_e^0 values is 60 (equivalent to $M_w/M_n \approx 1.02$).

more exact comparison, the relative positions of the data points of s-C and E167 to the

Rouse line and the ERT line (calculated with $K'/K = R_K(M)$ given by eq 18) confirm

what have been shown in Figure 3 of ref. 8.

Figure 1

Creep compliance $J_p(t)$ data of s-C measured at 119.4 ($\bigcirc$); 109.4 ($\bullet$); 105.1 ($\triangle$); 102.9

($\blacktriangle$); 100.6 ($\diamondsuit$); 96 ($\blacklozenge$); and 93 ($\square$) $^{\rm o}$C in comparison with the theoretical curves (——;

from left to right, respectively) calculated with the s and K values at different

temperatures as listed in Table 2; and the $A_{\rm G}^{\rm f}$ and β values as explained and given in

the text. Also shown is the comparison between the experimental ($- -$) and calculated

$(+ + +)$ long-time $J_p(t)$ limits, t/η_p, at each corresponding temperature.

Figure 2

Comparison of creep compliance $J_p(t)$ curves of s-C calculated with $K=10^{-4}$ and the s

values corresponding to the calculated curves shown in Figure 1; lines from left to

right corresponding to 119.4, 109.4, 105.1, 102.9, 100.6, 96 and 93 $^{\rm o}$C, respectively.

Figure 3

s values as a function of temperature of s-A ($\bigcirc$), s-B ($\diamondsuit$) and s-C ($\square$ determined from

$J_p(t)$ line-shape analysis; $\blacktriangle$ from the analysis of $J_{\rm ep}^0$).

Figure 4

The structural relaxation time, τ_S, of s-A ($\bigcirc$), s-B ($\diamondsuit$) and s-C ($\square$) as a function of the

temperature difference from each individual T_g, ΔT. The solid line is calculated

from the FTH equation which best fits the data of the three samples collectively.

Figure 5

s' values of s-A ($\bigcirc$), s-B ($\diamondsuit$) and s-C ($\square$ obtained from the $J_p(t)$ line-shape analysis; $\blacktriangle$ from the analysis of J_{ep}^0) as a function of the temperature difference from each individual T_g, ΔT. The solid line is calculated from the modified FTH equation (eq 19) which best fits the data of the three samples collectively.

Figure 6

K' values of s-A ($\bigcirc$), s-B ($\diamondsuit$) and s-C ($\square$) as a function of the temperature difference from each individual T_g, ΔT. The solid line is calculated from the FTH equation which best fits the data of the three samples collectively.

Figure 7

K values of s-A ($\bigcirc$), s-B ($\diamondsuit$) and s-C ($\square$) as a function of the temperature difference from each individual T_g, ΔT.

Figure 8

Comparison of the $G_p(t)$ figures of s-A (middle figure), s-B (bottom one) and s-C (top one) at individual T_g or $\Delta T=0$. In each figure, the relaxation times of the Rouse–Money normal modes (for s-A and s-B) or the Rouse normal modes (for s-C) are indicated by ($+$); the ($--$) line is calculated with A_G^f or $A_G=0$; and the ($--$) line is calculated with $A_G=0$ as well as setting the contribution of the Rouse–Mooney normal

modes to zero. The common vertical dotted line represents the structural-relaxation time τ_S=1000 sec. The points where the $G_p(t)$ curves cross the horizontal dotted lines at 10^8 dynes/cm^2 represent the traditionally defined structural- or α-relaxation times.[15]

Figure 9

Comparison of the $G_p(t)$ figures of s-A (middle figure), s-B (bottom one) and s-C (top one) at ΔT=9.7^o. In each figure, the relaxation times of the Rouse–Money normal modes (for s-A and s-B) or the Rouse normal modes (for s-C) are indicated by (+); the (- -) line is calculated with A_G^f or A_G=0; and the (— —) line is calculated with A_G=0 as well as setting the contribution of the Rouse–Mooney normal modes to zero. The common vertical dotted line represents the structural-relaxation time τ_S=1 sec. The points where the $G_p(t)$ curves cross the horizontal dotted lines at 10^8 dynes/cm^2 represent the traditionally defined structural- or α-relaxation times.[15]

Figure 10

Collective comparison of the τ_S and τ_v values as a function of ΔT of s-A, -B and -C (τ_S: ● for s-A, ◆ for s-B and ■ for s-C; τ_v: ○ for s-A, ◇ for s-B and □ for s-C). The lines are each calculated from the FTH equation which best fits the data of the three samples collectively (— for τ_S; – – for τ_v).

Figure 11

The comparison of K values as a function of temperature between s-A (○), s-C (●),

and the hypothetically uncontaminated s-B ($+$) (see the text).   The lines are calculated from the FTH equation best fitting the experimental data: (——) for s-A , (— —) for s-C, and (– –) for the hypothetically uncontaminated s-B.

Figure 12

Comparison of the theoretical viscosity curves of ERT (the upper solid line) and the free Rouse theory (the lower solid line) both calculated with $K=4.9 \times 10^{-9}$ (and with $K'/K=R_K(M)$ as given by eq 14 for the ERT curve) with the experimental values at 127.5$^{\text{o}}$C corrected for the effect of molecular weight distribution and the internal-viscosity contribution as explained in the Appendix ($\circ$ from ref. 8, with $\diamond$ specifically representing the data point of E167; $\bullet$ from ref. 28, with $\blacklozenge$ specifically representing the data point of s-C).

Table 1: Weight Average Molecular Weight of Samples A, B and C and E167; and the Reference Theories and Key Parameters: Z, M_e or M_e', K (at 127.5°C), A_G^f and β (see the text) Used in or Obtained from the Creep Compliance $J(t)$ Analyses (for s-A, -B and -C) or the Relaxation Modulus $G(t)$ Analysis (for E167)

Sample	M_w	Z (M_w / M_n)	Entanglement MW	Reference Theory	K (s/Da^2) (127.5°C)	$A_G^f \times 10^{-9}$ dynes/cm^2	β
s-A	46900	20(1.05)	M_e=13500	ERT	4.8×10^{-9}	12.95	0.41
s-B	122000	20(1.05)	M_e=13500	ERT	[60]	9.73	0.41
s-C	16400	20(1.05)	M_e'=17090	Rouse	4.15×10^{-9}	9.93	0.42
E167	16700	120(1.01)	M_e =13500	ERT	4.0×10^{-9}		

---

[60] Because s-B is contaminated by residual plasticizers, the K value in its pure state is not obtained.

Table 2: Structural and Dynamic Quantities Extracted from the $J(t)$ Line-Shape Analysis of Sample C

Temp ($^{\circ}$C)	s (Da^2)	SF	K (s/Da^2)	$\log \eta_p$ ($K=10^{-4}$)	$\eta_p / \eta_p(A_G{=}0)$ ($K=10^{-4}$)	$\rho T / \rho_0 T_0$	$\log \eta$ exp.	$\log \eta$ calcd	$\log J_e$ exp.	$\log J_e$ calcd	τ_S (s)
$A_G{=}0$				10.159	1						
134.1	1640		(1.06×10^{-9})	10.205	1.111	1.072	5.257	(5.261)	-6.75	-6.75	(3.13×10^{-5})
127.5			$[4.15 \times 10^{-9}]^a$								$[1.28 \times 10^{-4}]^a$
119.4	1800	3.09×10^{-4}	3.09×10^{-8}	10.210	1.125	1.042	6.730	6.717	-6.79	-6.75	1.00×10^{-3}
109.4	4400	6.89×10^{-3}	6.89×10^{-7}	10.275	1.306	1.021	8.116	8.122	-6.90	-6.87	5.46×10^{-2}
105.1	7000	3.6×10^{-2}	3.6×10^{-6}	10.331	1.486	1.012	8.882	8.893	-6.96	-6.98	4.54×10^{-1}
102.9	8990	8.33×10^{-2}	8.33×10^{-6}	10.370	1.626	1.008	9.270	9.294	-7.05	-7.05	1.35
100.6	13200	0.245	2.45×10^{-5}	10.442	1.919	1.003	9.820	9.832	-7.16	-7.19	5.82
96	28500	2.89	2.89×10^{-4}	10.633	2.979	0.993	11.088	11.090	-7.54	-7.57	1.48×10^{2}
$93.7_{56}^{\ 61}$	[43960]		$[1.19 \times 10^{-3}]^a$								$[1000]^a$
93	52300	20.8	2.08×10^{-3}	10.825	4.635	0.987	12.156	12.138	-7.94	-7.94	1.96×10^{3}

[a] Calculated from the equations obtained from least-squares fittings to the values determined at different temperatures (see the text)

**Table 3: Structural and Dynamic Quantities: *s*, *K*, *K'* and τ_S Extracted from the *J(t)* Line-Shape Analyses of Samples A and B**

Sample A					Sample B				
Temp	K	$K'(1.61K)$	s	τ_S	Temp	K	$K'(3.16K)$	s	τ_S
(°C)	(s/Da²)	(s/Da²)	(Da²)	(s)	(°C)	(s/Da²)	(s/Da²)	(Da²)	(s)
97	9.84×10^{-4}	1.58×10^{-3}	56500	1000	[98.0$_{25}$][62]	[$4.40_3\times10^{-4}$]	[1.39×10^{-3}]	[126190]	[1000]
100.6	9.7×10^{-5}	1.56×10^{-4}	28275	49.4	98.3	3.6×10^{-4}	1.14×10^{-3}	120258	779
104.5	1.2×10^{-5}	1.93×10^{-5}	16337	3.53	101	6.02×10^{-5}	1.9×10^{-4}	77426	83.9
109.6	1.2×10^{-6}	1.93×10^{-6}	10053	0.217	103.3	1.515×10^{-5}	4.79×10^{-5}	58900	16.06
114.5	1.96×10^{-7}	3.16×10^{-7}	6283	2.22×10^{-2}	105.5	5.43×10^{-6}	1.72×10^{-5}	41184	4.03
					113.8	1.49×10^{-7}	4.71×10^{-7}	17297	4.64×10^{-2}
					119.8	2.61×10^{-8}	8.25×10^{-8}	9060	4.26×10^{-3}

---

[62] Listed values at this temperature are calculated from the equations obtained from least-squares fittings to the values determined at different temperatures (see the text)
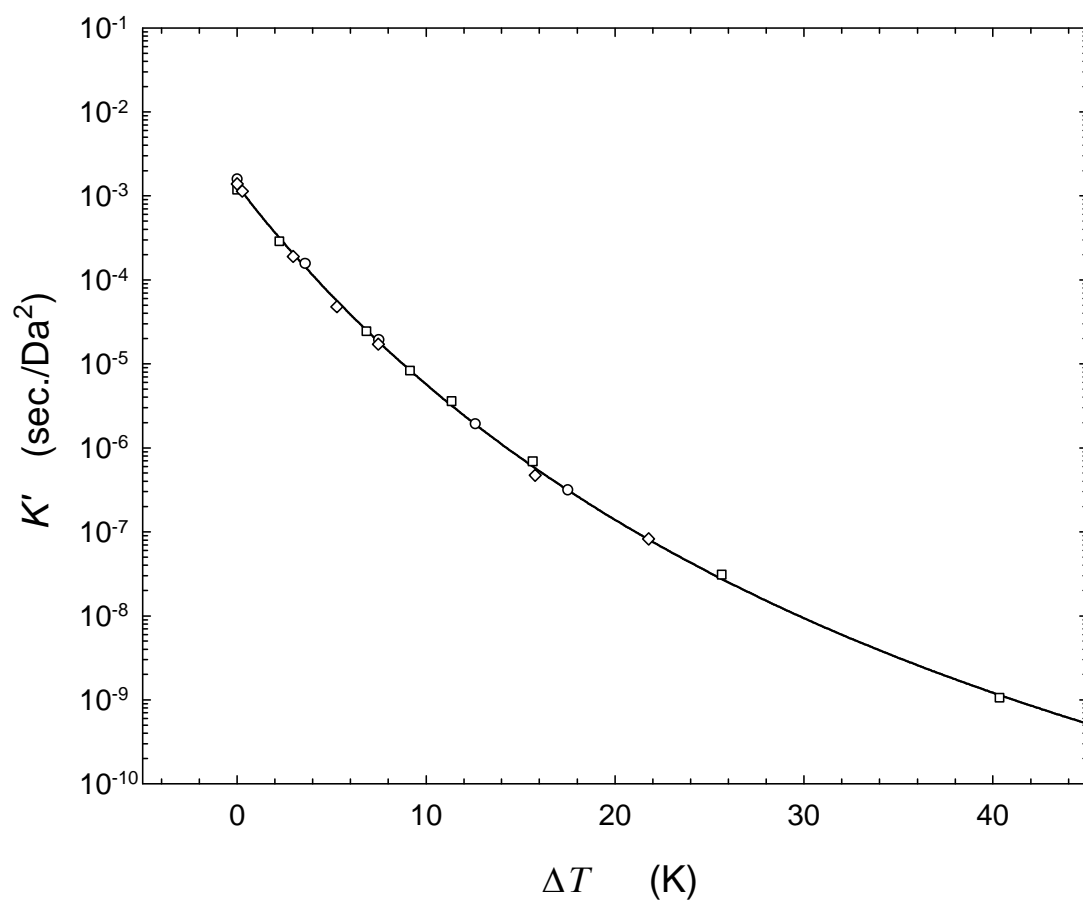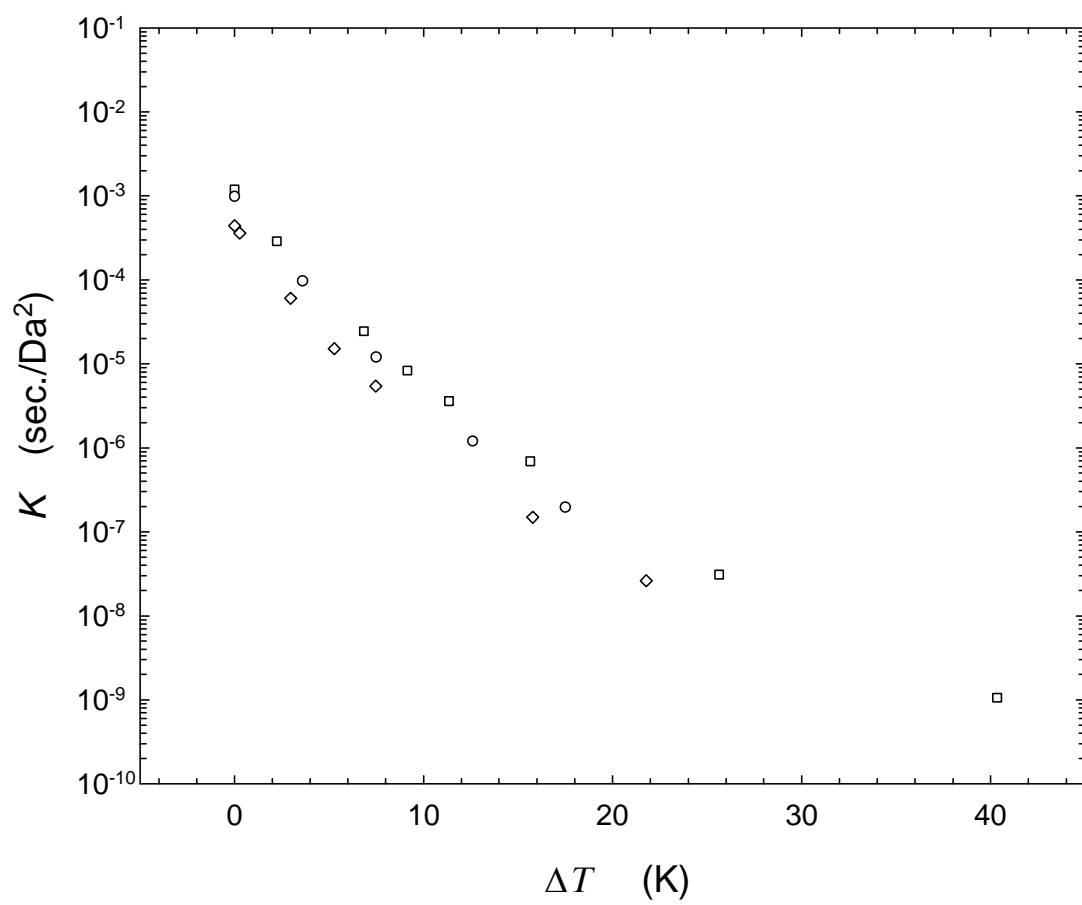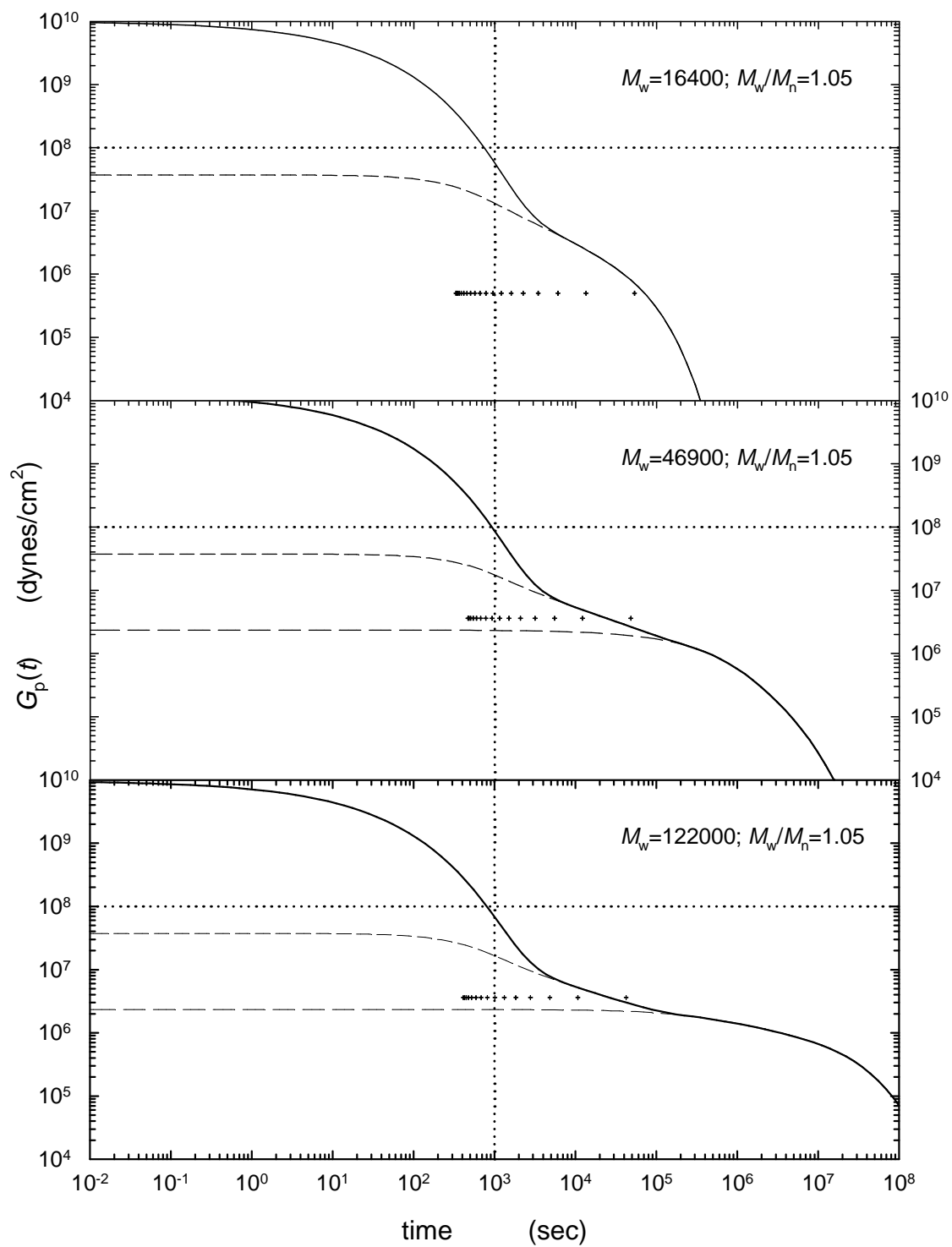
Figure 1
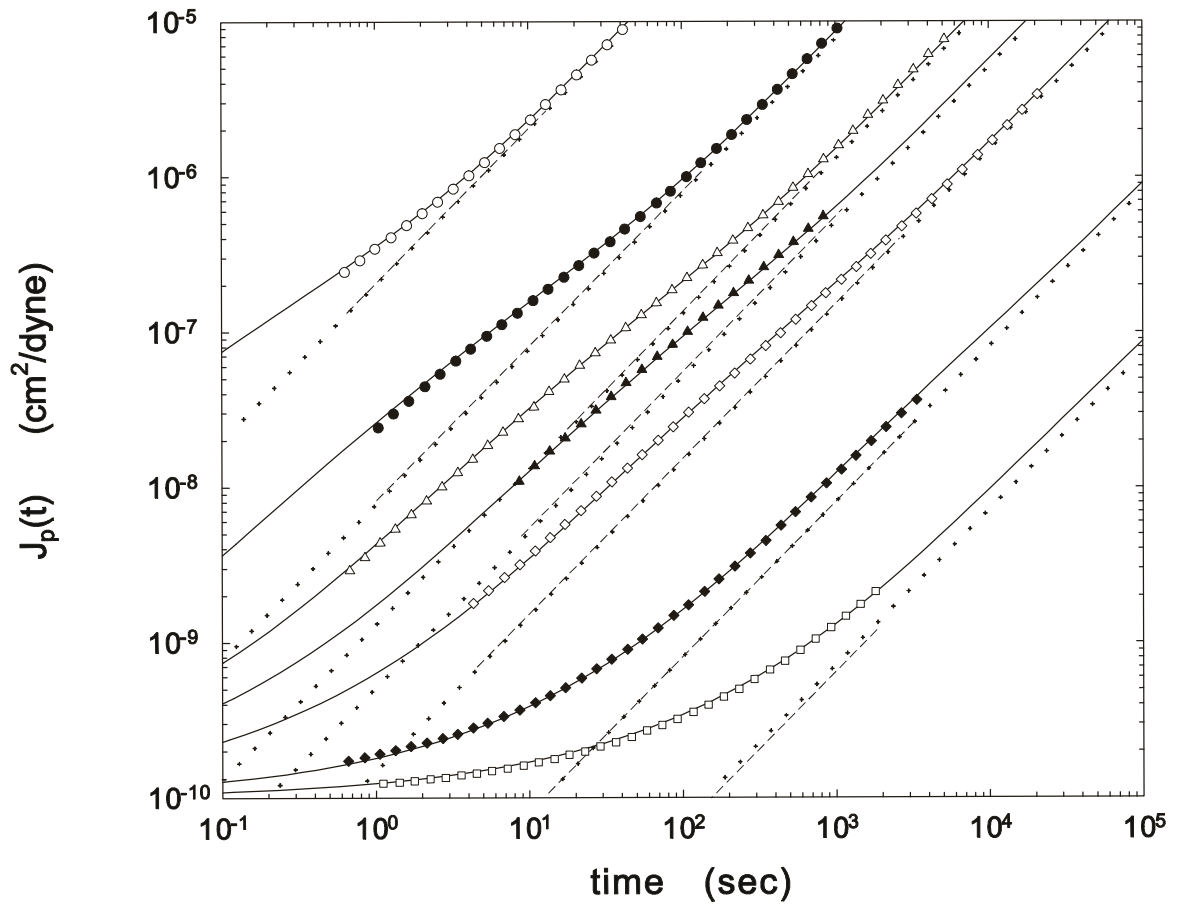
Figure 2

Figure 3

Figure 4

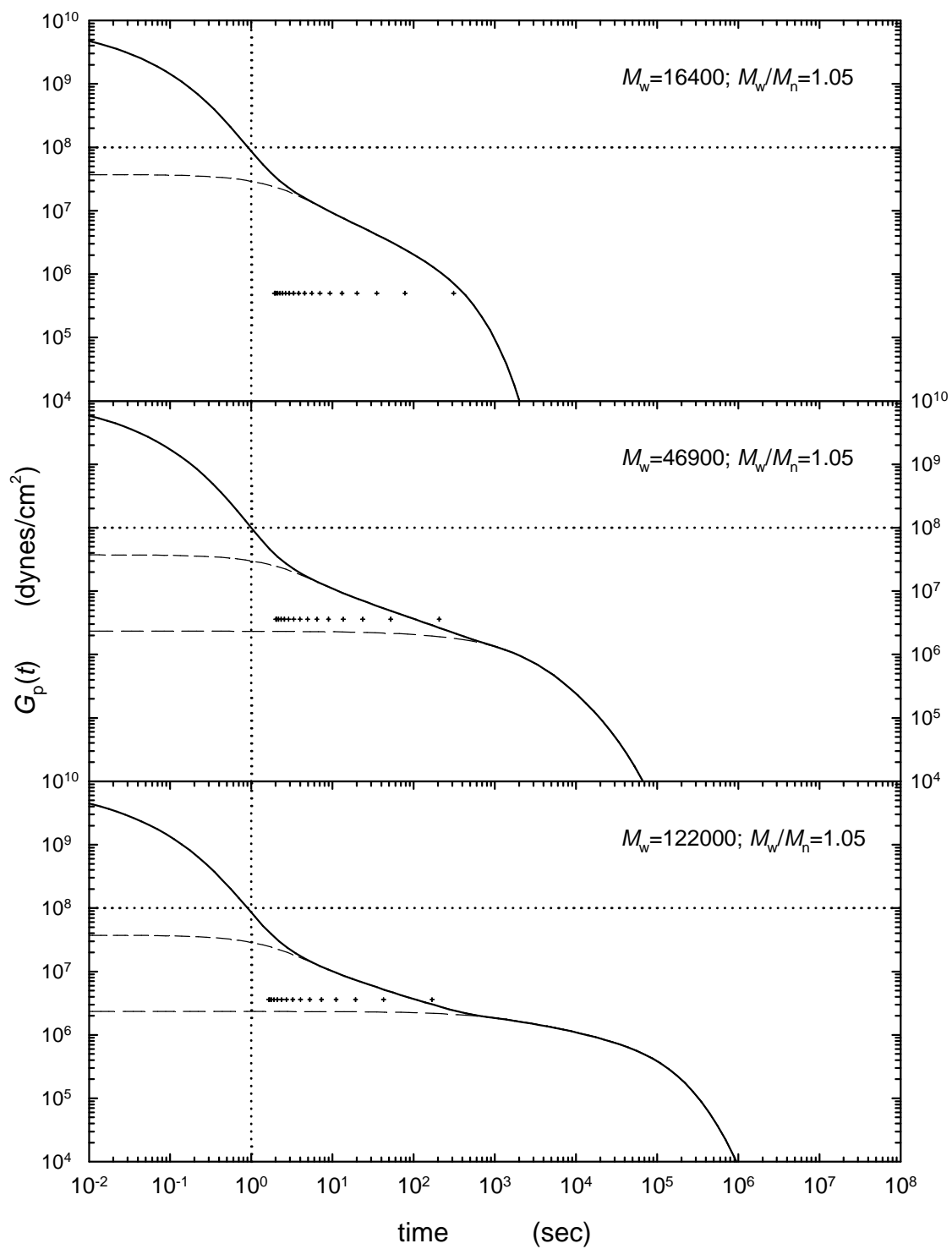Figure 5

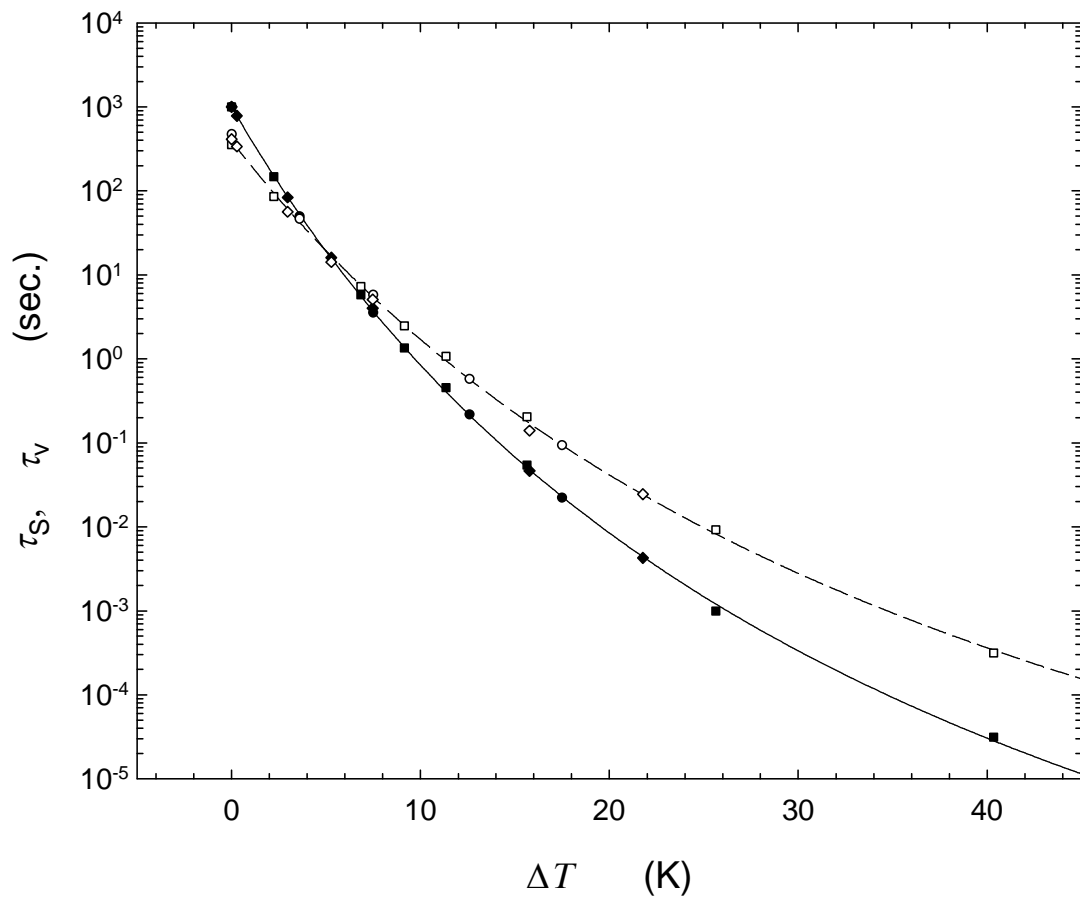Figure 6

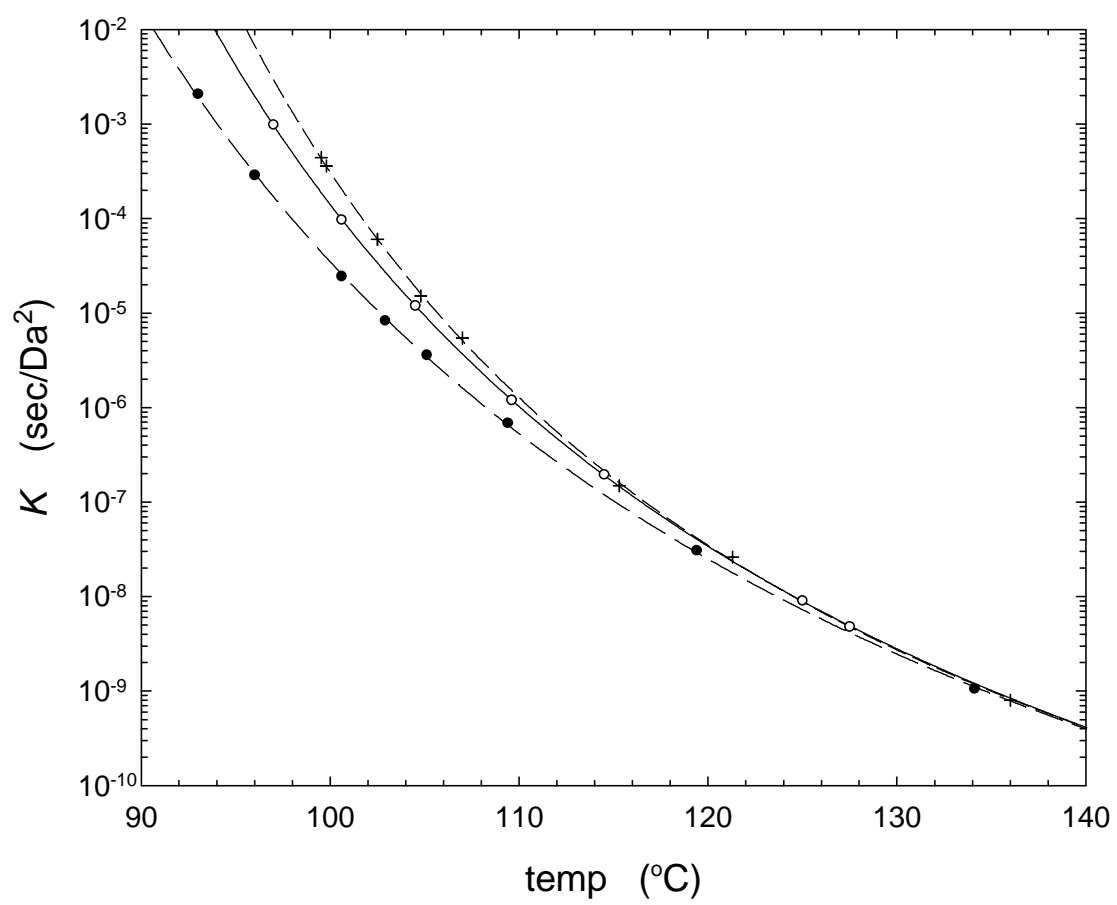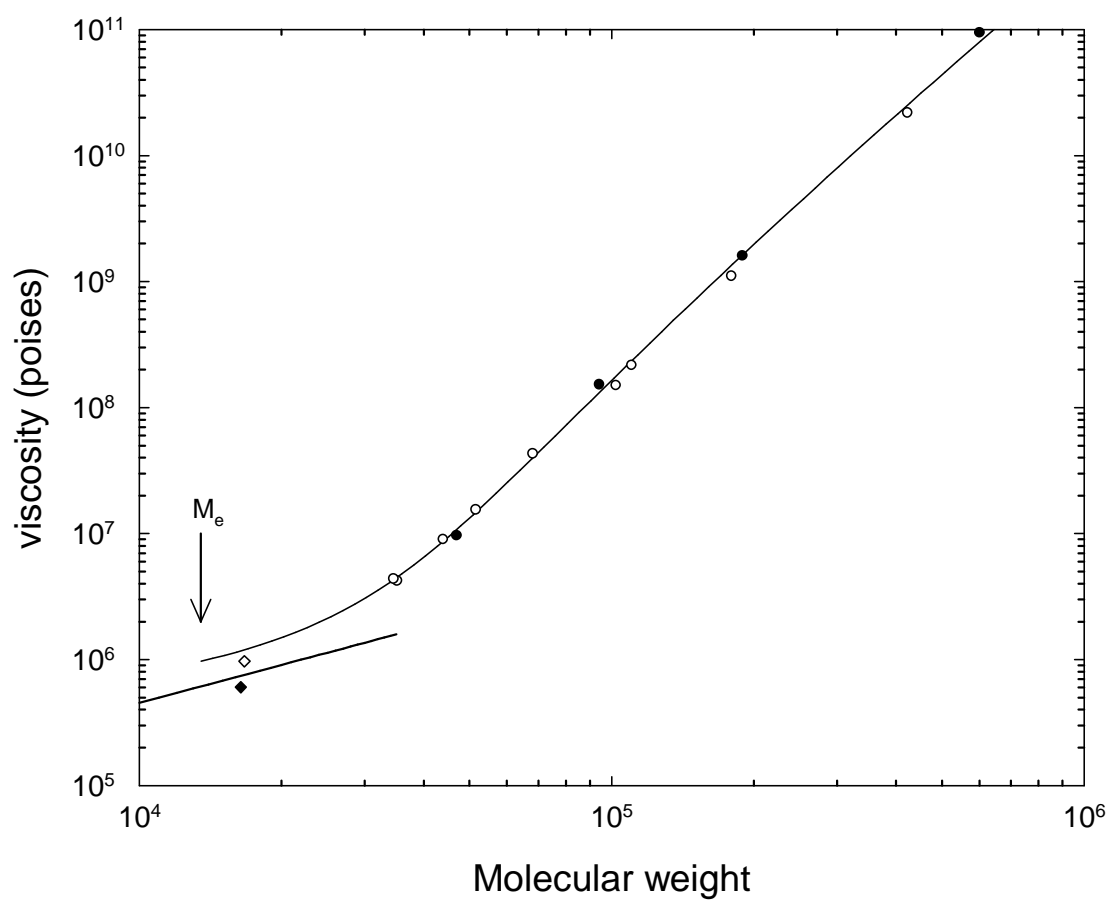Figure 7

Figure 8

Figure 9

68

Figure 10

69
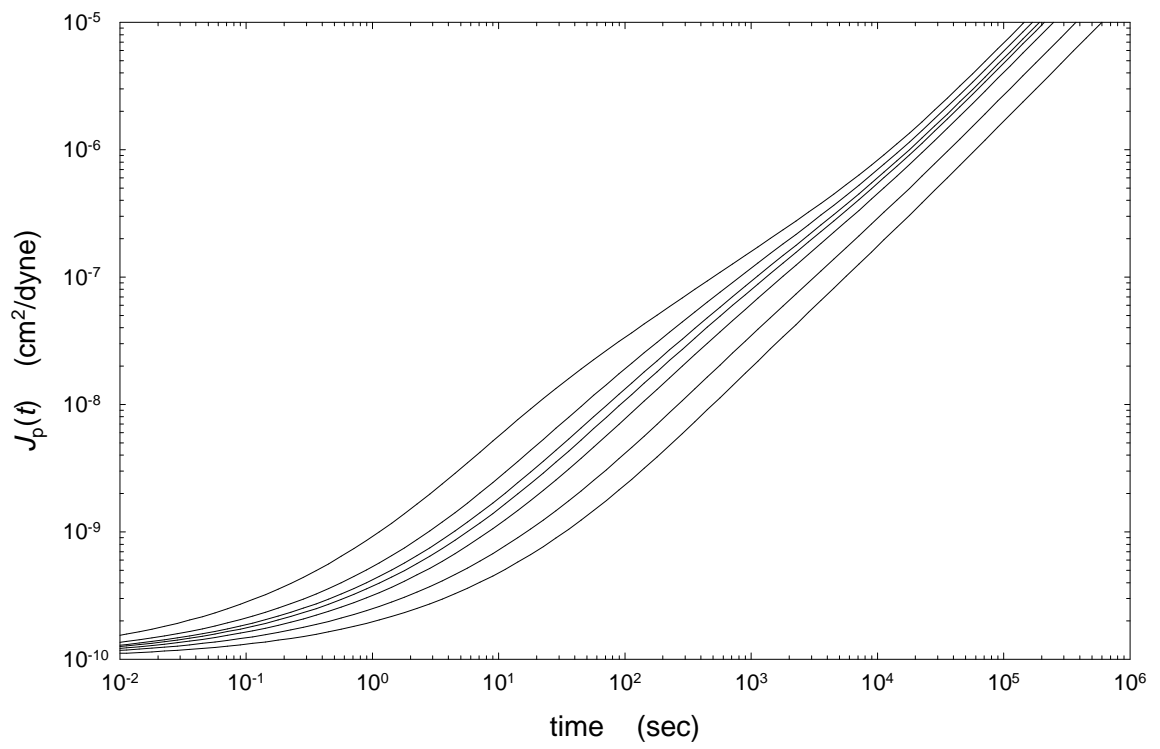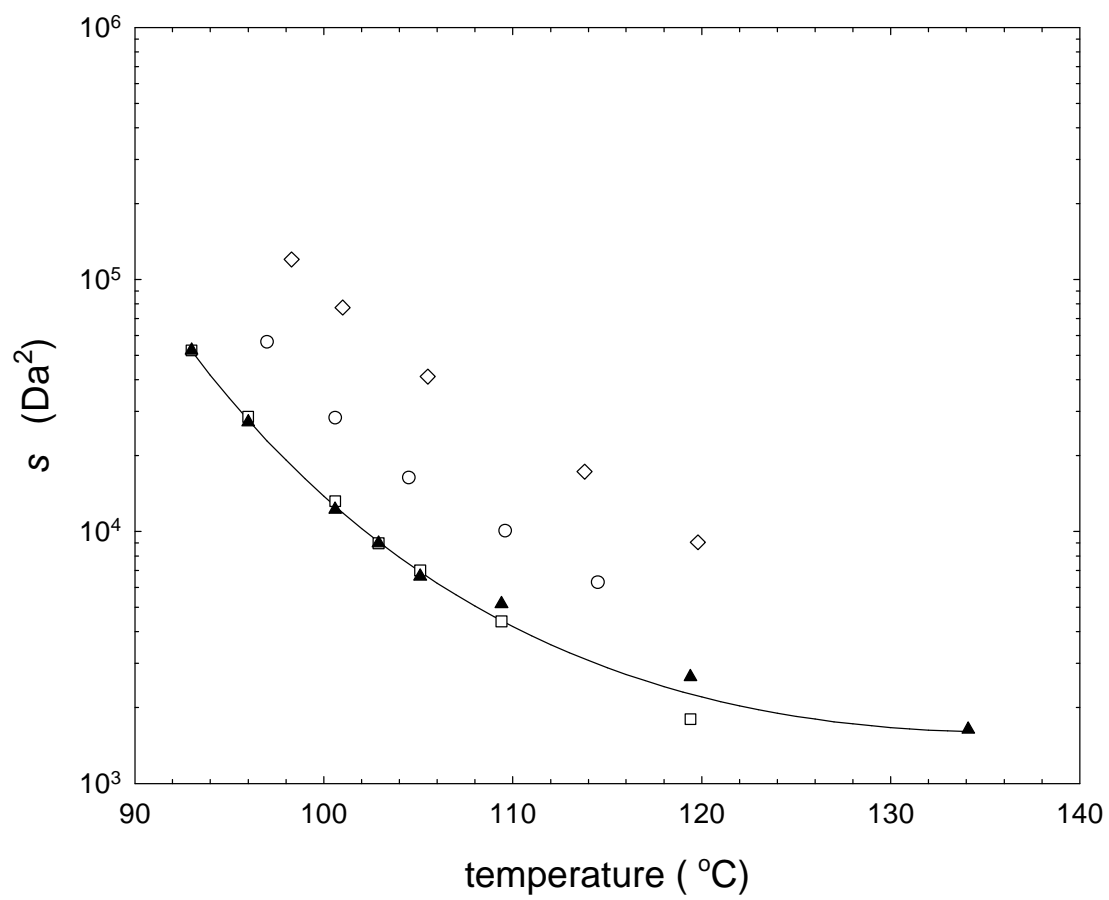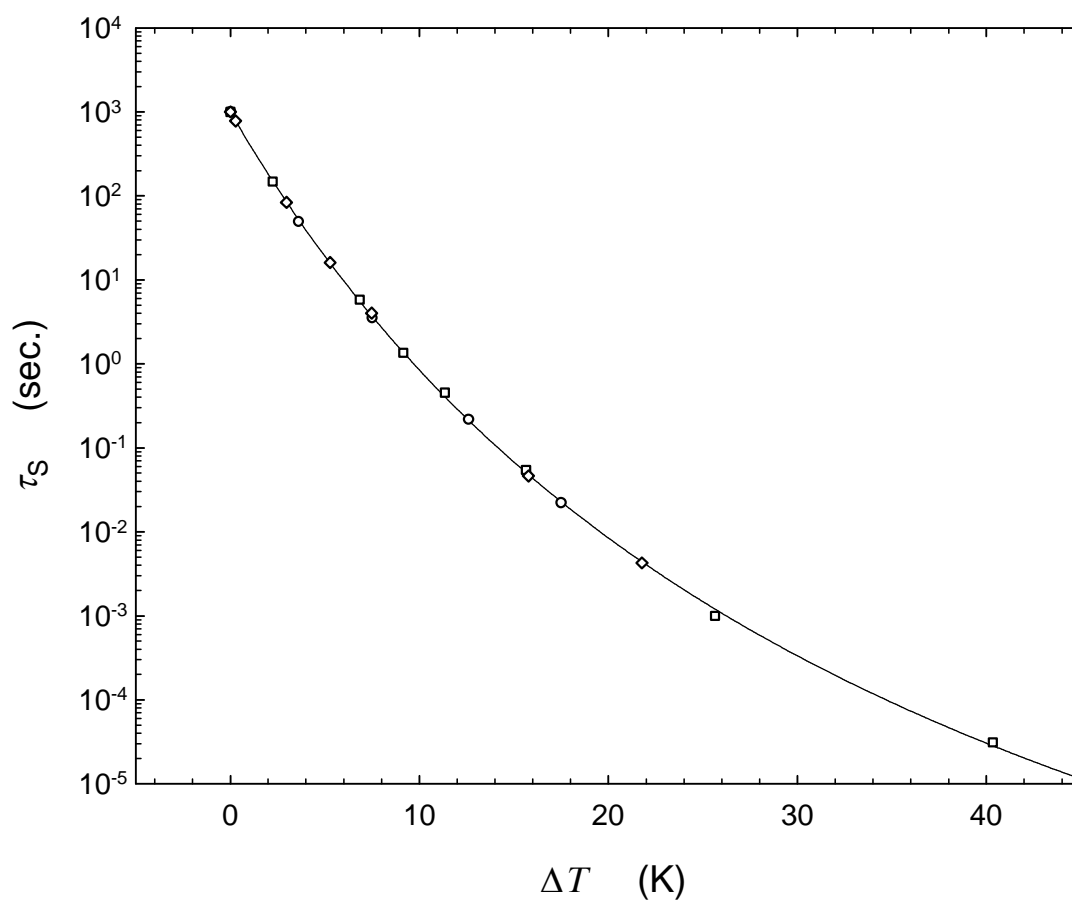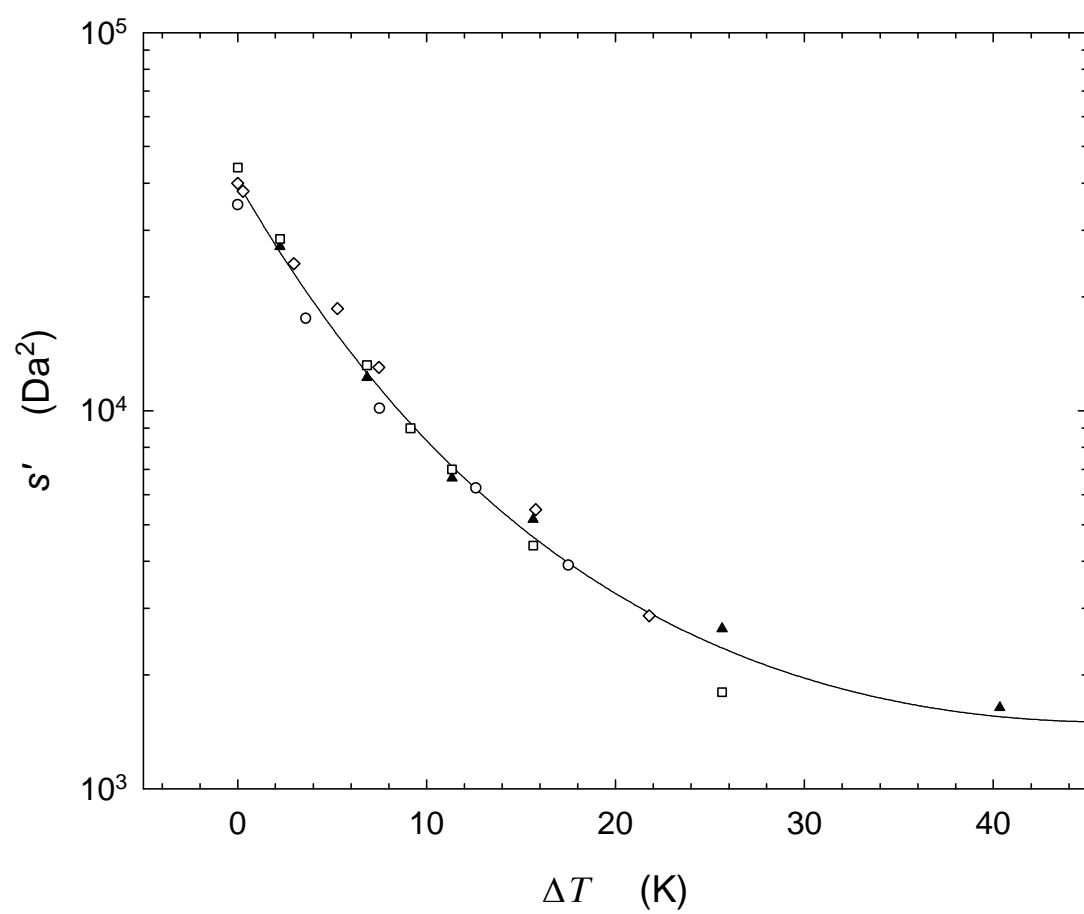
Figure 11

Figure 12

Thermorheological Complexity in Polystyrene Melts

and

Breakdown of the Stokes‒Einstein Relation in *o*-Terphenyl. 4

Y.-H. Lin[63]

Department of Applied Chemistry

National Chiao Tung University

Hsinchu, Taiwan

Abstract

In paper 1,[64] based on the structural-growth parameter *s* (or *s'*) which increases with decreasing temperature as extracted from analyzing the creep compliance $J(t)$ line shapes of two nearly monodisperse entangled polystyrene melts, it was shown that the basic mechanism for the thermorheological complexity (TRC) in polystyrene should be also responsible for the breakdown of the Stokes‒Einstein relation (BSE) in *o*-Terphenyl (in *tris*-naphthylbenzene as well).   It has been reported in paper 3[65] that TRC as related to glass transition in polystyrene melts behaves in a universal way within the polystyrene system, *entangled or not*. Benefiting from this new

---

[63] E-mail: yhlin@mail.nctu.edu.tw

64 Lin, Y.-H. *J. Phys. Chem. B* **2005**, *109*, 17654.

65 Lin, Y.-H. *J. Phys. Chem. B*, submitted. (paper 3)

understanding, we have made a closer analysis and comparison of the TRC in polystyrene and BSE in o-Terphenyl. It is shown from the analysis that the ratio of the structural-growth parameter s' at temperature T to its plateau value s_0' at high temperatures, $s'(T)/s_0'$, is equivalent to the enhancement parameter $\mu(T)$ in o-Terphenyl as determined from the data of the diffusion constant D_{g} and rotational relaxation time τ_{rot}. The enhancement parameter being of different magnitude for different materials, this conclusion is supported by the plotted curve of $\log\!\left(s'(T)/s_0'\right)$ versus the temperature difference $(\Delta T = T - T_{\mathrm{g}})$ from the glass transition temperature in polystyrene being similar in shape to those of $\log\!\left(\mu(T)\right)$ in o-Terphenyl and $tris$-naphthylbenzene. Our general description of the mechanism for the TRC in polystyrene and BSE in o-Terphenyl is compared with the two-state model proposed by Stillinger and Hodgdon for explaining the BSE in o-Terphenyl, showing a one-to-one correspondence and illustrating the similar ideas involved.

Thermorheological Complexity in Polystyrene Melts

and

Breakdown of the Stokes–Einstein Relation in *o*-Terphenyl. 4

Y.-H. Lin

Department of Applied Chemistry

National Chiao Tung University

Hsinchu, Taiwan

1. Introduction

As the glass transition temperature T_g is approached from above, two interesting effects occur in glass-forming fluids: the thermorheological complexity (TRC) in glass-forming polymer melts and the breakdown of the Stokes–Einstein relation (BSE) in fragile glass-forming liquids.   The former is represented by the different temperature dependence between the short-time and long-time regions in the creep compliance $J(t)$ of polystyrene melts as first observed by Plazek;[1,2,66,67,68] the latter is exemplified by the temperature dependence of translational diffusion being weaker than that of viscosity η or rotational relaxation time τ_{rot} in *o*-Terphenyl (OTP)[69,70,71,72,73] (in *tris*-naphthylbenzene[74,75] as well). These two effects are

66 Plazek, D. J. *J. Phys. Chem.* **1965**, *69*, 3480.

67 Plazek, D. J. *J. Polym. Sci., Part A*-2: *Polym. Phys.* **1968**, *6*, 621.

68 Plazek, D. J.; O'Rourke, V. M. J. *Polym. Sci. A*-2: *Polym. Phys.* **1971**, *9,* 209.

69 Fujara, F.; Geil, B.; Sillescu, H.; Fleischer, G.   *Z. Phys. B: Condens. Matter*

interesting because the basic mechanisms for them should be much related to the glass

transition phenomenon, which still does not have a fully clear theoretical

interpretation, even though much understanding has been gained from various studies

on it for the past few decades.[76,77,78,79,80]　The BSE in glass-forming liquids has been

actively studied in the last decade, and various models[81,82,83,84,85] have been proposed

to explain it.　On the other hand, the TRC in polystyrene had been puzzling to

1992, *88*, 195.

70 Cicerone, M. T.; Ediger, M. D. *J. Phys. Chem.* **1993**, *97*, 10489.

71 Kind, R.; Liechti, N.; Korner, N.; Hulliger, J. *Phys. Rev. B* **1992**, *45*, 7697.

72 Chang, I.; Fujara, F.; Geil, B.; Heuberger, G.; Mangel, T.; Sillescu, H. *J. Non-Cryst.*
Solids **1994**, *172–174*, 248.

73 Mapes, M. K.; Swallen, S. F.; Ediger, M. D. *J. Phys. Chem. B* **2006**, *110*, 507.

74 Chang, I.; Sillescu, H. *J. Phys. Chem. B* **1997**, *101*, 8794.; and references therein.

75 Swallen, S. F.; Bonvallet, P. A.; McMahon, R. J.; Ediger, M. D. *Phys. Rev. Lett.*
2003, *90*, 015901.

76 Angell, C. A. Science **1995**, *267*, 1924; and references therein.

77 Ediger M. D.; Angell, C. A.; Nagel, S. R. *J. Phys. Chem.* **1996**, *100*, 13200.

78 Sillescu, H. *J. Non-Crystal. Solids* **1999**, *243*, 81; and references therein.

79 Weeks, E. R.; Crocker, J. C.; Levitt, A. C.;　Schofield, A.; Weitz, D. A. *Science*
2000, *287*, 627.

80 Donati C.; Glotzer, S. C.; Poole, P. H.; Kob, W.; Plimpton, S. *J. Phys. Rev.E* **1999**, *60*, 3107.

81 Stillinger, F. H.; Hodgdon, J. A. *Phys. Rev. E* **1994**, *50*, 2064.

82 Tarjus, G.; Kivelson, D. *J. Chem. Phys.* **1995**, *103,* 3071.

83 Cicerone, M. T.; Wagner, P. A.; Ediger, M. D. *J. Phys. Chem. B* **1997**, *101*, 8727.

84 Xia, X.; Wolynes, P. G. *J. Phys. Chem.* **2001**, *105*, 6570.

85 Jung, Y. J.; Garrahan, J. P.; Chandler, D. *Phys. Rev. E* **2004**, *69*, 061205.

polymer rheologists until quantitative analyses were made on the $J(t)$ line shapes of two entangled melts as reported in paper 1 (ref 1). Based on the length-scale and time-scale (or equivalently the structural-growth parameter s) extracted from the $J(t)$ analyses, which increase with temperature approaching T_g from above, the basic mechanism for the TRC was analyzed. It has been shown that the basic mechanism should be also responsible for the BSE as occurring in OTP. In paper 3 (ref 2), it has been found that TRC as related to T_g behaves in a universal way within the polystyrene system, *entangled or not*, advancing our understanding of the structural-growth parameter s (or s') extracted from the analyses of the $J(t)$ results. Benefiting from this new understanding, we present a closer analysis and comparison of the two effects in this paper. Viscoelastic and dynamic results of glass-forming polymers[86,87,88,89,90] in general indicate that the glassy-relaxation process (or the α- or structural-relaxation process) has a stronger temperature dependence than that of the dynamics involving the whole molecule—namely, the terminal relaxation—suggesting that the TRC is a general phenomenon. At the same time, the BSE occurs in different fragile glass-forming liquids.[6−12] Here, we shall use polystyrene and OTP as the (representative) subjects under study, with the understanding that the analyses as

86 Plazek, D. J. *J. Rheol.* **1996**, *40,* 987.

87 Plazek, D. J. *Polymer J.* **1980**, *12*, 43.

88 Okamoto, H.; Inoue, T.; Osaki, K. *J. Polym. Sci: Part B: Polym. Phys.* **1995**, *33*, 417.

89 Inoue, T.; Hwang, E. J.; Osaki, K. *J. Rheol.* **1992**, *36*, 1737.

90 Adachi, K.; Hirano, H. *Macromolecules* **1998**, *31*, 3958.

presented here may be generalized to other glass-forming polymers or liquids.

2.   Basic Mechanism for TRC and BSE

In paper 1,[1] using the successful description of the rubber(like)-to-fluid region of

the creep compliance $J(t)$ in terms of the extended reptation theory (ERT)[91,92,93,94,95,96]

as the reference frame, the glassy-relaxation processes $\mu_G(t)$ occurring in the

short-time/ small-compliance region of $J(t)$ of two nearly monodisperse entangled

polystyrene melts (sample A with M_w=46900 and sample B with M_w=122000)[3,4] have

been analyzed in a perspective way.   In terms of a stretched exponential form for

$\mu_G(t)$ incorporated into ERT, the $J(t)$ line shapes over the whole range have been

quantitatively analyzed, indicating that the TRC occurring in $J(t)$ of polystyrene is due

to the temperature dependence of the energetic interactions-derived glassy-relaxation

process being stronger than that of the entropy-derived dynamic processes as

described in ERT.   The stronger temperature dependence is expressed by the increase

with decreasing temperature in the normalized glassy-relaxation time or

structural-growth parameter s, defined by

91 Lin, Y.-H. *Macromolecules* **1984**, *17*, 2846.

92 Lin, Y.-H. *Macromolecules* **1986**, *19*, 159.

93 Lin, Y.-H. *Macromolecules* **1986**, *19*, 168.

94 Lin, Y.-H. *Macromolecules* **1987**, *20*, 885.

95 Lin, Y.-H. *Macromolecules* **1989**, *22*, 1437.

96 Lin, Y.-H. *Polymer Viscoelasticity: Basics, Molecular Theories, and*

Experiments; World Scientific: Singapore, 2003.

$$s = \frac{\langle \tau \rangle_{\mathrm{G}}}{K} \qquad (1)$$

where $\langle \tau \rangle_{\mathrm{G}}$ is the average relaxation time of $\mu_{\mathrm{G}}(t)$ and K is the frictional factor,

$$K = \frac{\zeta \langle b^2 \rangle}{kT\pi^2 m^2} = \frac{\langle b^2 \rangle}{D\pi^2 m^2} \qquad (2)$$

associated with the Rouse segment with mass m, mean square length $\langle b^2 \rangle$ and

diffusion constant D.   In paper 3,[2] the creep compliance $J(t)$ and steady-state

compliance J_{e}^0 results of an entanglement-free nearly monodisperse polystyrene melt

(sample C with $M_{\mathrm{w}}=16400^5$; as explained in detail in section 3 of paper 3, due to the

molecular-weight distribution of sample C being not extremely narrow, it has to be

treated as an entanglement-free case even though its M_{w} value is a little higher than

$M_{\mathrm{e}}=13500$) have been equally well analyzed in terms of an equivalent scheme using

the Rouse theory[30,33,97,98,99] instead of ERT as the reference frame.   Both ERT and

the Rouse theory use the Rouse segment as the most basic structural unit; theoretically

the frictional factor K carries the temperature dependence of all the entropy-derived

dynamics processes: $\mu_{\mathrm{A}}(t)$, $\mu_{\mathrm{X}}(t)$, $\mu_{\mathrm{B}}(t)$, and $\mu_{\mathrm{C}}(t)$ in ERT or $\mu_{\mathrm{R}}(t)$ of the Rouse theory

97 Lin, Y.-H.; Juang, J.-H. *Macromolecules* **1999**, *32*, 181.

98 Rouse, P. E. Jr. *J. Chem. Phys.* **1953**, *21*, 1271.

99 Bird, R. B.; Curtiss, C. F.; Armstrong, R. C.; Hassager, O. *Dynamics of Polymeric Liquids, Vol. 2, Kinetic Theory,* 2nd ed.; Wiley: New York, 1987.

(see the previous papers[1,2,28-32] or ref 33 for the physical meanings and functional forms of the processes), which in general follows the Fulcher and Tammann‒Hesse (FTH) equation or the Williams‒Landel‒Ferry (WLF) equation.[100] The frictional factor has been studied in detail by extensive testing of the two theories with experiments.[28-33,101] The obtained key behavior and relationships as to the frictional factor are summarized in the following; we refer to the previous studies for the details:

(1) At and above 127.5°C,[29,33,38] it has been shown that the frictional factor K in the $\mu_X(t)$, $\mu_B(t)$, and $\mu_C(t)$ processes (as appearing in the expressions for τ_X, τ_B, and τ_C) for polystyrene melts in the entanglement region is independent of molecular weight, as expected from the theory.

(2) However, the frictional factor in the Rouse‒Mooney process $\mu_A(t)$ denoted by K' (as appearing in the expression for τ_A^1) is greater than the frictional factor K in the $\mu_X(t)$, $\mu_B(t)$, and $\mu_C(t)$ processes by the molecular weight-dependent factor $R_K(M)$ (see eq 5 of ref 32 or eq 11.6 of ref 33),[1,2,29,31-33] which has a plateau value 3.3 in the high-molecular-weight region; starts to decline with decreasing molecular weight at around $10M_e$ or $10M_e'$ ($M_e' = M_e/W_2$ with W_2 being the weight faction of the entangled component in a blend solution); and reaches 1 as the molecular weight reaches M_e or M_e'.

(3) The K value in the $\mu_X(t)$, $\mu_B(t)$, and $\mu_C(t)$ processes of ERT is in quantitative

100 Ferry, J. D. *Viscoelastic Properties of Polymers*, 3rd ed.; Wiley: New York, 1980.

101 See Table 1 and Appendix B of ref 1 and note at ref 38 of ref 2.

agreement with the frictional factor K in the Rouse theory (as appearing in the Rouse relaxation time τ_R^1; see Figure 20 of ref 31 or Figure 11.1 of ref 33), meaning that both theories have the same footing at the Rouse-segmental level.[2,31,33]

As indicated by the observation $R_K(M) \rightarrow 1$ as $M \rightarrow M_e$ or $M_e^{'}$, K' being greater than K by the factor $R_K(M)$ is due to the topological constraint of entanglement.   At temperatures close to T_g, in the relatively short yet macroscopic time scales of $\langle \tau \rangle_G$ and τ_S (non-ergodic times; see Table 2 of paper 1) the strong energetic interactions among segments keep many configurations from being explored, while in the long time scales of τ_A^1, τ_X, τ_B, and τ_C or τ_R^1 (ergodic times) there is enough time to explore the configurational space effectively, leading to entropy-derived modulus (as represented by the entropy force constant; see the note at ref 39)[102] and dynamics (as described by the Langevin equation; see the note at ref 40).[103]   Thus, except for the factor $R_K(M)$ due to the topological constraint effect of entanglement, there is not a fundamental difference between K' and K.   The expression for K (eq 2) is equally

---

102 This is indicated by the fact that no shift along the compliance coordinate is required in the quantitative analyses of $J(t)$ line shapes of polystyrene melts in the expected entropic region using ERT (in paper 1)[1] or the Rouse theory (in paper 3)[2] as the reference frame, even when the temperature is very close to T_g.

103 The successful quantitative analyses of the $J(t)$ line shapes of polystyrene melts in the expected entropic region indicate that the functional forms for the relaxation processes in the stress-relaxation modulus and the structural factors of the relaxation times as given in ERT or in the Rouse theory remain valid, even when the temperature is very close to T_g.[1,2]

applied to *K'*; namely

$$K' = \frac{\zeta' \langle b^2 \rangle}{kT\pi^2 m^2} = \frac{\langle b^2 \rangle}{D'\pi^2 m^2} \tag{3}$$

where the diffusion constant *D'* is smaller than *D* by the factor $R_K(M)$.

As detailed in section 4 of paper 3,[2] for more directly reflecting the close relation between the $\mu_G(t)$ and $\mu_A(t)$ processes—the two processes occurring next to each other in time, the normalized glassy-relaxation time *s* has been modified by introducing *s'* as defined by

$$s' = \frac{s}{(K'/K)} = \frac{\langle \tau \rangle_G}{K'} \tag{4}$$

Then the structural-relaxation time defined by $\tau_S = 18 \langle \tau \rangle_G$ (see ref 41 (paper 3) for a detailed study of the structural-relaxation time)[104] can be expressed by

$$\tau_S = 18sK = 18s'K' \tag{5}$$

$R_K(M) \to 1$ as $M \to M_e$ indicates that, when the tube (of the reptational model) is disappearing and the Rouse theory becoming applicable, the dynamics in the system has only one *K* and becomes isotropic as it should. As detailed in section 4 of paper 3,[2] in an entanglement-free system (sample C), *s* can be regarded as *s'* and *K* as *K'*.

---

104 Lin, Y.-H. *J. Phys. Chem. B* **2005**, *109*, 17670.

As far as sample C is concerned in the discussions below; s and s', and K and K' will be used interchangeably without further explanation. As s or s' decreases with increasing temperature, the entropic region shifts more away from the glassy region as can be observed in Figures 6 and 7 of ref 1 and in comparing Figures 8 and 9 of ref 2.

In the literature,[11-13,105,] τ_S reaching $100 \sim 1000$ sec has often been used as the criterion for defining T_g. Following this practice, the glass transition point T_g has been defined as the temperature where $\tau_S = 1000$ sec for all the three samples whose $J(t)$ results have been analyzed, two entangled and one entanglement-free. The thus defined T_g provides a common reference point equivalent for all samples, with respected to which the structural and dynamic quantities τ_S, s' and K' obtained from analyzing the $J(t)$ results may be compared in a perspective way; the effect of the T_g difference among samples on τ_S, s' and K' can be accounted for by expressing them as a function of the temperature difference from T_g, $\Delta T = T - T_g$. It has been found that τ_S, s' and K' values of the three samples plotted as a function of individual ΔT fall on a common curve, indicating that TRC as closely related with the glass transition behaves in a universal way within the polystyrene system, *entangled or not*.

When the temperature is significantly closer to T_g than 127.5$^\mathrm{o}$C, the formation of structure as related to the increase in s' starts to affect K through K'; in other words, K behaves in such a way that K' values as a function of ΔT fall on a universal curve$-K'$ differs from K by the factor $R_K(M)$. As a result, below $\sim 120^\mathrm{o}$C, K begins to deviate from the behavior purely controlled by the topological constraint of

105 Angell, C. A. *J. Non-Cryst. Solids* **1991**, *131-133*, 13.

entanglement–namely, being independent of molecular weight and thus the difference in T_g–which holds at higher temperatures. However, below ~ 120°C, ERT remains valid in describing the topological effect on the line shape of the viscoelastic responses as explained in section 8 of paper 3 even though K becomes gradually dependent on molecular weight as the temperature approaches T_g (see Figure 11 of paper 3)[2]. Because the effect of the formation of structure becomes dominant in the close proximity of T_g, we should use K' and its conjugate structural parameter s' to discuss the T_g-related effects instead of K and s as used in paper 1. However, the basic mechanism for the TRC developed in terms of K and s in paper 1 remains equally valid as the only difference is a proportional constant. In an entangled case, as the Rouse–Mooney process occurs right after the glassy-relaxation process $\mu_G(t)$, using K' and s' instead of K and s also indicates the need to shift our focus to the shorter-time region for studying the T_g-related effects.

Being Brownian motion, the diffusion constant of a Rouse segment can generally be expressed as

$$D' = \frac{kT}{\zeta'} \approx \frac{l^2}{\Delta t} \qquad (6)$$

where l is the step length that the Rouse segment has moved in a time interval Δt. The only criterion for choosing Δt and l is that the steps are independent of one another; then after sufficiently large number of steps of movement have taken place, the central limit theorem ensures that the dynamic process becomes Gaussian as required

by the Langevin equation being applicable.[28,33,106,107]   At high temperatures, there is

a wide range down to very small values to choose l and Δt to satisfy eq 6; the dynamic

process is often referred to as the continuous (small-step) or "free" diffusion.[11,108]   At

a temperature close to T_g, the structure is formed with a certain lifetime τ_S which has

increased greatly with s'; then, the smallest independent time step that can be chosen

is of the order of the lifetime of the structure $\Delta\tau \approx \tau_S = 18\langle\tau\rangle_G$. We can choose $\Delta\tau$ as

the time step because it is still much shorter than τ_A^1, τ_X, τ_B, and τ_C or τ_R^1 (see Table 2

of paper 1 and Figure 8 of paper 3).[1,2]   Corresponding to $\Delta\tau$ being longer at lower

temperatures, a larger length-scale denoted by d is expected for the step length as

explained in the following: As K' (or K) has been determined from the quantitative

line-shape analysis of $J(t)$, so D' (or D) is defined.   Due to eq 3, the following

constraint is imposed on the system

$$\text{const} = D'K' \approx \left(\frac{d^2}{\Delta\tau}\right)K' \approx \left(\frac{d^2}{\tau_S}\right)K' = \left(\frac{d^2}{18s'}\right) \qquad (7)$$

where eq 5 has been used.   To maintain $D'K'$ being constant, d has to increase by

about 5 times as s' increases from about 1500 at temperatures higher than $\sim T_g + 40^o$ to

about 40000 at T_g (see Figure 5 of paper 3).

106 Mooney, M. *J. Polym. Sci.* **1959**, *34*, 599.

107 Doi, M. *J. Polym. Sci., Polym. Phys. Ed*. **1980**, *18,* 1005.

108 Thirumalai, D.; Mountain, R. D. *Phys. Rev. E* **1993**, *47*, 479.

The relaxation times in the long-time region (τ_{A}^{1}, τ_{X}, τ_{B}, and τ_{C} or τ_{R}^{1}) are proportional to $K \propto \zeta/kT \approx \Delta\tau /d^2$ or $K' \propto \zeta'/kT \approx \Delta\tau /d^2$ while the structural relaxation time is $\tau_{S} \approx \Delta\tau \propto \langle\tau\rangle_{G}$. With decreasing temperature, $\Delta\tau$ increases more than $\Delta\tau/d^2$ as the structure is formed following the increase in s'. This difference in temperature dependence is the basic mechanism for the TRC as concluded from the analyses of the polystyrene $J(t)$ curves reported in papers 1 and 3.

It was pointed out in paper 1 that this basic mechanism should be also the reason for the breakdown of the Stokes–Einstein equation in relating the translational diffusion constant D_{g} with the shear viscosity η or rotational relaxation time τ_{rot} as observed in OTP, when T_{g} is approached from above. Without the entropy-derived modes of motion—as described by ERT or by the Rouse theory—in OTP,

$$\eta \propto \int_0^{\infty} \mu_{G}(t)dt = \langle\tau\rangle_{G} \propto \tau_{S} \approx \tau_{rot} \approx \Delta\tau \qquad (8)$$

What is explained above for the diffusion of the Rouse segment in polystyrene melts can similarly be applied to the molecular diffusion D_{g} in OTP;

$$D_{g} \approx \frac{d^2}{\Delta\tau} \qquad (9)$$

Thus, from eqs 8 and 9, one sees that $D_{g}\tau_{rot}$ increases with increasing d as T_{g} is approached from above, meaning BSE.

To characterize the BSE, a translational diffusion enhancement parameter μ has

been defined by

$$\mu = \frac{D_g}{D_{SE}} \tag{10}$$

where D_{SE} is the translational-diffusion constant expected when the Stokes–Einstein relation holds.   As the Stokes–Einstein relation holds at temperatures far above T_g in OTP, its μ value at a temperature T close to T_g may be calculated from

$$\mu(T) = \frac{D_g(T)\tau_{rot}(T)}{D_g(T_{high})\tau_{rot}(T_{high})} \tag{11}$$

where T_{high} stands for a high temperature in the region where the Stokes–Einstein relation holds.

As s' for the polystyrene system reaches a plateau value of about 1500 as the temperature is more than 40° above T_g, under the constraint imposed by eq 7, d should reach a lower limiting value at high temperatures, which is denoted by d_0.   Denoting the plateau value of s' at high temperatures by s_0' (≈ 1500 for polystyrene), then the s' value at a temperature T close to T_g may be expressed by

$$s'(T) = s_0' \left(\frac{d(T)}{d_0} \right)^2 \tag{12}$$

Applying the same idea to the translational diffusion enhancement parameter in OTP and substituting eqs 8 and 9 into eq 11, the μ value at a temperature T close to T_g may

be expressed by

$$\mu(T) = \left(\frac{d(T)}{d_0}\right)^2 \tag{13}$$

On the basis of comparing eqs 12 and 13, we conclude that $\mu(T)$ for OTP is equivalent to $s'(T)/s_0'$ for polystyrene melts, reflecting the same mechanism.

3. Comparison of the Results of $\mu(T)$ and $s'(T)/s_0'$

The data of $\mu(T)$ for OTP and *tris*-naphthylbenzene (TNB) as defined by eq 11 have recently been compiled by Mapes et al[10] from diffusion results obtained by NMR[6] and isothermal desorption[109] for the former and by NMR[11] and forward recoil spectrometry[12] for the latter and the results of rotational relaxation time.[6,11,110] In Figure 1, we compare the $\mu(T)$ results of OTP and TNB with the $s'(T)/s_0'$ values of the three polystyrene samples: A, B and C as a function of $\Delta T = T - T_g$. The magnitude of the enhancement factor $\mu(T)$ is different for different materials. The similarity in shape of the three sets of data plotted as a function of ΔT in Figure 1 supports the conclusion of the analysis given above that $\mu(T)$ for OTP and TNB plays the same role as $s'(T)/s_0'$ for polystyrene.

109 Mapes, M. K.; Swallen, S. F.; Kearns, K. L.; Ediger, M. D. *J. Chem. Phys.* **2005**, *123*, 1.

110 Zemke, K.; Schmidt-Rohr, K.; Magill, J. H.; Sillescu, H.; Spiess, H. W. *Mol. Phys.* **1993**, *80*, 1317.

The magnitude of $s'(T)/s_0'$ in polystyrene is smaller than those of $\mu(T)$ in OTP and TNB as well as $\mu(T)$ of smaller probe molecules: tetracene and 9,10-bis(phenylethynyl)anthracene, in polystyrene but is about the same as that of a larger probe: rubrene, in polystyrene.[111,112,113] The magnitude of $s'(T)/s_0'$ in polystyrene being in general smaller than those of $\mu(T)$ in the cases mentioned above may have to do with the chain connectivity existing in a polymer, which has the effect of keeping the translational motion of a segment from being as uninhibited as that of a molecule in a glass-forming liquid—the translational motion takes place mainly when the "window of opportunity" for the cooperative jumping motion opens up (see the discussion below).

4. Discussion

In paper 1, we have pointed out that to satisfy the conditions imposed by eq 7 for choosing $\Delta\tau$ and d, a likely dynamic process for the Rouse segment to take is by cooperative large-step jumping involving more than one Rouse segment. Such a general description is consistent with the picture that the molecular (or segmental) motion becomes spatially heterogeneous and dynamically correlated as revealed by molecular dynamics simulations for glass-forming Lennard–Jones mixtures at low temperatures[17,114] and observed directly by confocal microscopy in the colloidal

111 Cicerone, M. T.; Blackburn, F. R.; Ediger, M. D. *Macromolecules* **1995**, *28*, 8224.

112 Cicerone, M. T.; Ediger, M. D. *J. Chem. Phys.* **1996**, *104*, 7210.

113 Wang, C.-Y.; Ediger, M. D. *Macromolecules* **1997**, *30*, 4770.

114 Thirumalai, D.; Mountain, R. D. *Phys. Rev. E* **1993**, *47*, 479.

fluids near T_g.[16] Dynamic heterogeneity in glass-forming liquids and polymers in the

vicinity of T_g has also been indicated by various studies using different

techniques.[115,116,117,118,119] For explaining the enhancement of translational diffusion,

several models of spatially heterogeneous dynamics have been proposed. In

particular, one can find a one-to-one correspondence between the two-state model

proposed by Stillinger and Hodgdon (SH)[18] for explaining BSE in OTP and the

analysis originally proposed in paper 1 and further elaborated above for explaining

TRC in polystyrene and BSE in OTP. Such a comparison is made in the following,

which may illustrate the similar ideas involved.

The two-state picture proposed by SH consists of flickering fluidized domains in

an essentially solid matrix; in the fluidized domains stress can be released quickly and

the molecule can move faster. The fluidized domains in the SH picture was described

in terms of four temperature-dependent average characteristics:

(1)   domain volume v_0;

(2)   domain appearance rate per unit volume, r_0;

(3)   domain lifetime t_0;

(4)   domain internal viscosity η_0.

115 Cicerone, M. T.; Ediger, M. D. *J. Chem. Phys.* **1995**, *103*, 5684.

116 Schiener,B.; Bohmer, R.; Loidl, A.; Chamberlin, R. V. *Science* **1996**, *274*, 752.

117 Richert, R. *J. Phys. Chem. B* **1997**, *101,* 6323.

118 Russell, E. V.; Israeloff, N. E. *Nature* **2000**, *408*, 695.

119 Tracht, U.; Wilhelm, M.; Heuer, A.; Feng, H.; Schmidt-Rohr, K.; Spiess, H. W.

Phys. Rev. Lett. **1998**, *81*, 2727.

η_0 must reflect the fluidized nature of the domains, and thus its magnitude must be substantially less than the macroscopically measured viscosity η. Following SH, as the volume fraction ϕ_0 of the system that is interior to the fluidized domains is given by

$$\phi_0 = r_0 v_0 t_0 ; \qquad (14)$$

the structural relaxation time τ_S is expressed as

$$\tau_S \left(\approx \tau_{rot} \right) = \frac{1}{r_0 v_0} = \frac{t_0}{\phi_0} \qquad (15)$$

and the viscosity η as

$$\eta \approx G_\infty \tau_S = \frac{G_\infty}{r_0 v_0} \qquad (16)$$

A key assumption in the SH model is that the system's overall translational diffusion constant D_g is a simple volume average over fluidized domains and surrounding static matrix; thus

$$D_g = \phi_0 D_0 + (1 - \phi_0) \times 0 = \phi_0 \left(\frac{kT}{6\pi \eta_0 R} \right) \qquad (17)$$

where the Stokes–Einstein equation is assumed to hold in the fluidized domains; and

R is the effective radius of the diffusing molecule. Then using eqs 14 and 16, the enhancement parameter μ as defined by eq 10 is expressed as

$$\mu = \frac{\phi_0\left(\dfrac{kT}{6\pi\eta_0 R}\right)}{\left(\dfrac{kT}{6\pi\eta R}\right)} = r_0 v_0 t_0 \frac{\eta}{\eta_0} \approx G_\infty \frac{t_0}{\eta_0} \qquad (18)$$

As observed, μ increases with decreasing temperature; so must t_0/η_0 do. In other words, using eqs 15 and 17, we may have from eq 9

$$d^2 \approx D_g \Delta\tau \approx D_g \tau_S = \left(\frac{kT}{6\pi\eta_0 R}\right)t_0 \propto \mu \qquad (19)$$

which increases with decreasing temperature and is in agreement with eq 13. One sees that the step length d that the segment or molecule jumps after a waiting period $\Delta\tau \approx \tau_S$ as indicated by the analysis given in section 2 is equivalent to the distance the molecule moves by diffusion in a fluidized domain over the domain's lifetime t_0 in the SH two-state model.

While the SH fluidized domain model offers an explanation that is consistent with our general description, clearly the uniqueness of the SH model or any other model which may turn out to be consistent with our general description needs to be checked by various studies.

5. Summary

In paper 1,[1] it was shown that the basic mechanism for the TRC in polystyrene should be also responsible for the BSE in OTP. It has been found as reported in paper 3[2] that τ_S, *s'* and *K'* values of the three studied polystyrene samples plotted as a function of individual $\Delta T = T - T_g$ fall on a common curve, indicating that TRC as closely related with the glass transition behaves in a universal way within the polystyrene system, entangled or not. Benefiting from this new understanding, we have made a closer analysis and comparison of the TRC in polystyrene and BSE in OTP. It is shown from the analysis that the $s'(T)\big/s_0^{'}$ values extracted from the $J(t)$ line shapes of the three polystyrene samples play the same role as the enhancement parameter $\mu(T)$ as calculated from the diffusion constant D_g and rotational relaxation time τ_{rot} in OTP and TNB.   Such an expectation is supported by the results obtained for polystyrene, OTP and TNB as shown in Figure 1.   This result is particularly significant considering that the BSE in OTP or TNB is based on a set of measurements that is very different from the creep measurement, in which the TRC in polystyrene is observed.   As they are observed in different ways, the BSE and TRC had been treated as two totally different and unrelated phenomena until the study reported in paper 1.

We have also compared our general description of the mechanism for the TRC in polystyrene and BSE in OTP with the two-state model proposed by Stillinger and Hodgdon for explaining the BSE in OTP, illustrating the similar ideas involved.

Figure Caption:

Figure 1

Comparison of $s'(T)/s_0'$ values (with $s_0'=1500$) of polystyrene samples: A (M_w=46900; ○); B(M_w=122000; ◇) and C (M_w=16400; □ from the $J(t)$ line-shape analysis; △ from matching the steady-state compliance J_e^0 values) with the enhancement factors $\mu(T)$ of OTP (●isothermal desorption; ▲NMR) and TNB (■ forward recoil spectrometry; ▼NMR) as a function of $\Delta T = T - T_g$. The solid line is calculated from the modified FTH equation (eq 19 of ref 2) which best fits the $s'(T)/s_0'$ results of the three polystyrene samples collectively.

Figure 1
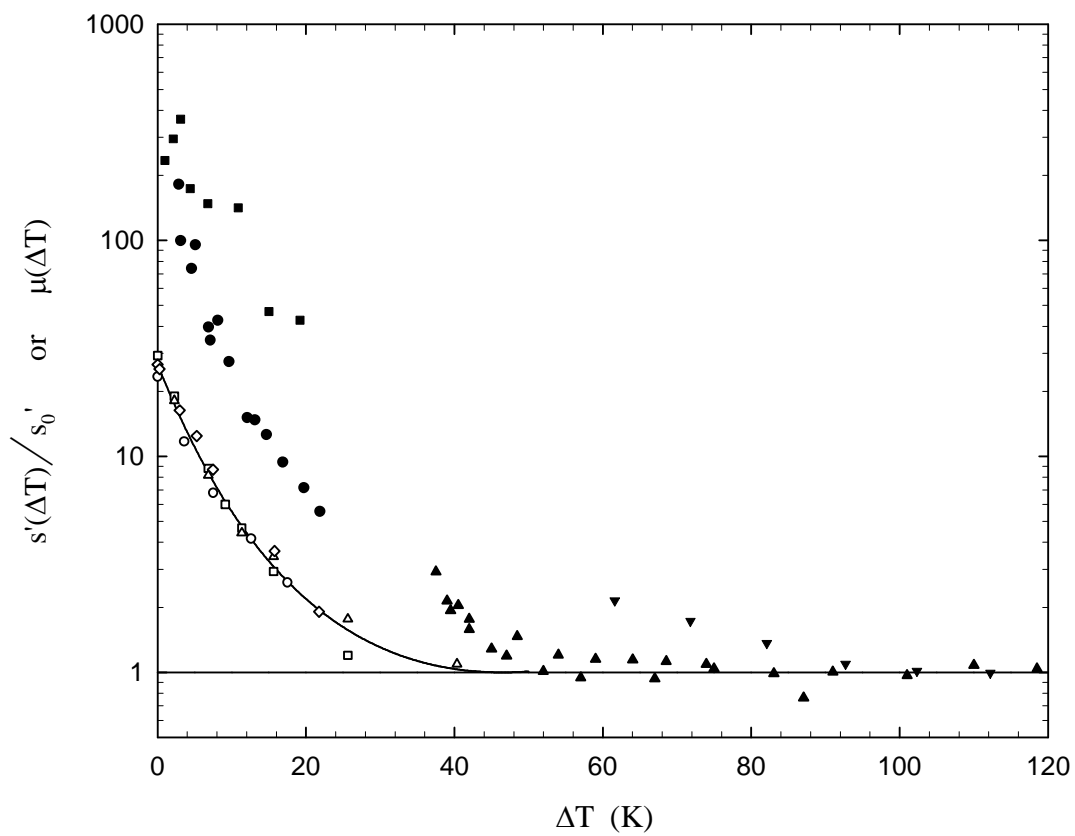
95

Range of Universality

Regarding the T_g-Related Thermorheological Complexity

in Polystyrene Melts. 5

Y.-H. Lin[120]

Department of Applied Chemistry

National Chiao Tung University

Hsinchu, Taiwan

Abstract

The creep compliance $J(t)$ curves over the whole time range of three nearly monodisperse polystyrene samples have been previously quantitatively analyzed in terms of the proposed scheme using the extended reptation theory as the reference frame for the entangled system or the Rouse theory as the reference frame for the entanglement-free system, yielding important T_g-related dynamic and structural quantities: the structural-relaxation time τ_S, the structural-growth parameter s' and the frictional factor K'. These quantities individually fall on the same curves, if expressed as a function of the temperature difference $\Delta T = T - T_g$ from the individual glass transition points of the samples, which are defined as the temperatures where the structural relaxation time τ_S=1000 sec. These results covering the molecular-weight

[120] E-mail:yhlin@mail.nctu.edu.tw

range from 16400 to 122000 strongly indicate that universality associated with the T_g-related dynamics occurs in the polystyrene system, *entangled or not*. In this report, the viscoelastic spectra $G^*(\omega)$ reported by Inoue et al[11] at molecular weights just below the entanglement molecular weight $M_\mathrm{e}=13500$ and well below M_e are quantitatively analyzed in terms of the same scheme. Quantities in both the glassy region (A_G^f, β and τ_S or $\langle\tau\rangle_\mathrm{G}$) and entropic region (*s'* and *K'*) extracted from the analyses are consistent with those obtained previously from the analyses of the $J(t)$ results. It is shown that the ΔT dependences of *s'*, *K'* and τ_S merge into their respective universal curves at around $M_\mathrm{w}=12000$. At the same time, the universal curve of τ_S is shown in agreement with the temperature dependences of the shift factors obtained by Plazek from the recoverable compliance $J_\mathrm{r}(t)$ results, supporting the expected extension of the T_g-related universality to higher molecular weights than covered by the previous analyses.

Range of Universality

Regarding the T_g-Related Thermorheological Complexity

in Polystyrene Melts. 5

Y.-H. Lin

Department of Applied Chemistry

National Chiao Tung University

Hsinchu, Taiwan

1. Introduction

It has recently been shown[121,122,123] that the creep compliance $J(t)$ curves over the whole time range of three nearly monodisperse polystyrene samples (as denoted by s-A, -B and -C in Table 1) measured by Plazek[124,125,126] can be quantitatively and profitably analyzed in terms of the scheme using the extended reptation theory (ERT)[127,128] as the reference frame for the entangled system (s-A and s-B) and the

---

[121] Lin, Y.-H. *J. Phys. Chem. B* **2005**, *109*, 17654.

[122] Lin, Y.-H. *J. Phys. Chem. B* **2005**, *109*, 17670.

[123] Lin, Y.-H. *J. Phys. Chem. B* submitted. (paper 3)

[124] Plazek, D. J. *J. Phys. Chem.* **1965**, *69*, 3480.

[125] Plazek, D. J. *J. Polym. Sci., Part A*-2: *Polym. Phys.* **1968**, *6*, 621.

[126] Plazek, D. J.; O'Rourke, V. M. *J. Polym. Sci. A*-2: *Polym. Phys.* **1971**, *9,* 209.

[127] Lin, Y.-H. *Macromolecules* **1984**, *17*, 2846; **1986**, *19*, 159; **1987**, *20*, 885.

[128] Lin, Y.-H. *Polymer Viscoelasticity: Basics, Molecular Theories, and Experiments*;

Rouse theory[8,129,130] as the reference frame for the entanglement-free system (s-C),

yielding important T_g-related dynamic and structural quantities.   From the analyses,

it has been shown that the structural- or α-relaxation time τ_S can be separated into two

decoupled factors: the structural-growth parameter *s'* and the frictional factor *K'*

$(\tau_S = 18 s' K')$ by a fundamentally clean-cut process: Firstly, *s'*, characterizing the

thermorheological complexity, is entirely determined by the line shape of $J(t)$; then,

K' is determined from the time-scale shift factor.   It is found that all the three

quantities τ_S, *s'* and *K'* individually fall on the same curve if they are expressed as a

function of the temperature difference $\Delta T = T - T_g$ from the individual glass transition

points of the samples, which are defined as the temperatures where τ_S=1000 sec.

These results strongly indicate that the universality associated with the T_g-related

dynamics occurs in the polystyrene system, *entangled or not*.   The details of the

studies are referred to the previous papers.[1−3] As these studies represent a new way of

analyzing the creep compliance $J(t)$ results, it is of importance and interest to compare

the results of these studies with other results of measurements and analyses. While

serving this purpose, this report also shows where deviations from the T_g-related

universality would begin to occur from analyzing the viscoelastic spectra $G^*(\omega)$ of

low molecular weight polystyrene samples reported by Inoue et al.[131]

World Scientific: Singapore, 2003.

[129] Rouse, P. E. Jr. *J. Chem. Phys.* **1953**, *21*, 1271.

[130] Bird, R. B.; Curtiss, C. F.; Armstrong, R. C.; Hassager, O. *Dynamics of Polymeric*

Liquids, Vol. 2, *Kinetic Theory,* 2nd ed.; Wiley: New York, 1987.

[131] Inoue, T.; Onogi, T.; Yao, M.-L.; Osaki, K. *J. Polym. Sci.: Part B: Polym. Phys.*

2. Viscoelastic Spectra as Analyzed

As all the samples L10, A5000, A2500 and A1000, whose viscoelastic spectra are analyzed in this study have M_w values, as listed in Table 1, below the entanglement molecular weight $M_e=13500$,[8,132,133] the scheme of analysis is the one using the Rouse theory as the reference frame, as detailed in paper 3.[3] The technical details of calculating the $G^*(\omega)$ spectra have been described in the Appendix of paper 2.[2] The comparisons of the measured spectra $G^*(\omega)$ with the calculated including the contribution of the Rouse (entropic) component for samples L10, A5000, and A2500 at several temperatures are shown in Figures 1–3, respectively. As the contribution of the entropic component is negligible in A1000 because of its extremely low molecular weight, only the glassy-relaxation function

$$G_G(t) = A_G^f \exp\left(-\left(t/\tau_G\right)^\beta\right) \tag{1}$$

is used to fit its viscoelastic spectra as shown in Figure 4. In these figures, the spectrum at a certain temperature is chosen (105°C for L10; 100°C for A5000; 80°C for A2500; and 25°C for A1000 as chosen by Inoue et al) as the reference to which the line shape in the glassy region of the spectrum measured at different temperatures are

1999, *37*, 389.

[132] Lin, Y.-H. *Macromolecules* **1987**, *20*, 3080.

[133] Fetters, L. J.; Lohse, D. J.; Richter, D.; Witten, T. A.; Zirkel, A. *Macromolecules* **1994**, *27*, 4639.

superposed on it, forming a composite spectrum and yielding the time-scale shift factors a_G. With the average glassy-relaxation time denoted by $\langle \tau \rangle_G$, the structural relaxation time is defined as

$$\tau_S = 18\langle \tau \rangle_G \qquad (2)$$

For each sample the average glassy-relaxation time $\langle \tau \rangle_G$ at the reference temperature can be determined from matching the calculated spectrum with the composite spectrum over the glassy region. With the thus obtained $\langle \tau \rangle_G$ value, the τ_S values at different temperatures can be calculated from the shift factors a_G for each sample. At the same time the parameters A_G^f and β are extracted from fitting to the line shapes of the composite spectra over the glassy region. As listed in Table 1, the values of A_G^f and β obtained for L10, A5000 and A2500 are very consistent with the values for s-A, -B and -C obtained previously, supporting the trustworthiness of the two sets of data. In A1000, there are a large number of components having chain lengths as short as or smaller than the length scale associated with the glassy-relaxation process; as a result, its glassy-relaxation time distribution is directly broadened by its molecular-weight distribution which is not particularly narrow, leading to a β value smaller than for the other samples.

The structural-growth parameter s' and the frictional factor K' for L10, A5000 and A2500 can only be obtained from a spectrum that simultaneously covers both the glassy and entropic regions; as a result, the s' and K' values are obtained from their

101

spectra only at a few temperatures. As *s'* decreases with increasing temperature, the entropic region of the spectrum shifts more away from the glassy region as shown in Figures 1–3 for L10, A5000 and A2500, respectively.

2. τ_S, *s'* and *K'* Results in Comparison with the Universal Curves

The obtained τ_S values for the four samples, L10, A5000, A2500 and A1000, are shown in Figure 5 along with the results obtained for s-A, -B and -C, which have been collectively closely fitted by the FTH equation:

$$\log(\tau_S) = a + \frac{b}{(\Delta T + c)} \qquad (3)$$

with $a = -11.5045$, $b = 539.3497$ and $c = 37.1827$.[3] For showing the τ_S results of L10, A5000, A2500 and A1000 as a function of ΔT in Figure 5, their glass transition temperatures T_g defined as the point where $\tau_S=1000$ sec need to be determined individually first. As the longest τ_S values for the samples, except for A1000, are around 100~200 sec as extracted from the data of Inoue et al, the T_g values cannot be determined by interpolation. Under the circumstance, one may do two things: one is by doing extrapolation based on the FTH equation that best fits the available data; the other is by superposing the longest τ_S data point on the curve calculated from eq 3 by shifting along the ΔT coordinate. The T_g values determined in these two ways differ by less than 0.3°; either way does not lead to a difference in interpretation. The $T_g(\tau_S=1000$ sec) values as listed in Table 1 and used in calculating ΔT for plotting the

τ_S points in Figure 5 are the results of the extrapolation way.   As shown in Table 1, these T_g values are consistent with the values determined by DSC[134] as much as those of s-A, s-B and s-C are.   In the case of A1000, the temperature dependence of τ_S results are fitted to the FTH equation, from which the T_g point where τ_S=1000 sec is determined by interpolation.

The τ_S results of L10, A5000 and A2500 shown in Figure 5 indicate that the small deviations from the universal curve increase with decreasing molecular weight towards the direction of the curve for A1000; the largest change occurs in the molecular-weight range between A2500 and A1000.   In particular, the data points of L10 closely cling to the curve calculated from eq 3, indicating that the universality of the ΔT dependence of τ_S obtained previously should extend to a molecular weight between those of s-C and L10.   Similar closeness to the universal curves of s' and K' ($s=s'$ and $K=K'$ when the molecular weight is below the entanglement molecular weight, as explained in section 4 of paper 3; here we keep using the notations s' and K' as used in paper 3) as a function of ΔT have been observed for the s' and K' values of L10 as extracted from the line-shape analyses shown in Figures 1–3.

Shown in Figures 6 and 7, respectively, are the s' and K' values obtained for L10, A5000 and A2500 in comparison with the results of s-A, -B and -C, which have been closely fitted by a modified FTH equation (for s') or FTH equation (for K') collectively,[3] as shown by the calculated curves in the figures.   These curves of s' and K' together with that of τ_S as a function of ΔT representing the coverage of the

---

[134] Lin, Y.-H. *Macromolecules* **1990**, *25*, 5292.

molecular-weight range of from 16400 to 122000 indicate that the T_g-related

dynamics behave in a universal way in the polystyrene system, entangled or not, as

discussed in detail in paper 3.   In the very low molecular-weight region as covered in

this study, with decreasing molecular weight, deviations from the calculated universal

curves increase in general.   The K' values are virtually on the universal curve, with

only slightly noticeable deviation towards the lower side in the case of A2500.   The

success of using ΔT to account for the change in T_g with molecular weight is indeed

extraordinary in the case of K' considering the fact that the T_g values of L10, A5000

and A2500 have dropped from the maximum value by 10, 18 and 40 degrees,

respectively.   Thus, as $\tau_S = 18K's'$, the deviation of s' to the higher side is mainly

correlated with τ_S deviating towards the same side.   As shown in Figure 6, being a

little beyond the fluctuation-of-errors range from the calculated curve, the s' data

points of L10 appear on the verge of deviating from the universal curve.   When

multiplied by a constant, the calculated universal curve can be shifted upwards to

superpose well on the s' data points of L10, A5000 and A2500 individually as shown

by the dotted lines in Figure 6.   By extrapolating the thus obtained multiplication

factors to the no-shift point, it is estimated that the deviation from the universal curve

begins around M_w=12000, which is between the M_w value of L10 and the

entanglement molecular weight M_e=13500.   Thus, although as shown previously, the

universal curve is applicable in both the entangled and entanglement-free regions, the

range of the applicable entanglement-free region is quite narrow.   Note that although

the M_w value of s-C being a little higher than M_e=13500, its creep compliance $J(t)$

results can be best analyzed using the Rouse theory as the reference frame because its

molecular-weight distribution is not extremely narrow, as explained in detail in paper 3. The M_w value of s-C being higher than M_e also helps keep the system inside the region where the universal ΔT dependence of s' is applicable.

4. Structural Relaxation Time as Embedded in the Recoverable Compliance

The short-time/small-compliance region of the creep compliance $J(t)$ contains the information of the glassy-relaxation process. Because of the convolution integral involved in converting the relaxation modulus $G(t)$ into creep compliance $J(t)$, as shown in section 4.1 of paper 1, the separate relaxation processes are "smeared" and the $J(t)^{-1}$ line shape is different from that of $G(t)$. As a result, the extraction of the glassy relaxation process–as characterized by the A_G^f, β, and $\langle \tau \rangle_G$ values–from $J(t)$ is not as direct as from $G(t)$. Nevertheless, the time-scale shift factor with a temperature change in the small-compliance region reflects that of the glassy-relaxation process. In Figure 8, the time-scale shift factors of s-A, s-C, P19 and P60 (see Table 1) obtained by Plazek from the recoverable compliance $J_r(t)$ results are compared with the curve calculated from eq 3; in making the superposition the shift factors of these samples have been individually multiplied by a proper factor. The comparison shown in Figure 8 is more extensive than shown for s-A only in Figure 5 of ref 2. The close superposition supports that the creep compliance $J(t)$ results of s-A and s-C obtained by Plazek have been faithfully analyzed.[135] Although

---

[135] Note: For very good reasons, several shift factors listed by Plazek have to be excluded: For s-C, the steady-state compliance J_e^0 becomes much reduced at 96 and

105

the range of ΔT from 0 to 20, over which the universal curve calculated from eq 3 is shown in agreement with the shift factor results, is not as wide as the full range of the calculated curve, the maximum uncertainty of ΔT allowed is 1K; if a shift of 1K along the ΔT coordinate is made, even with the vertical-shift adjustment being permitted, systematic deviations of the shift factors from the universal curve become very visible. In other words, the shown agreement is actually quite unique.   Thus, the agreement of the calculated curve with the shift-factor results of P19 and P60 supports the universality expected to cover molecular weights higher than that of s-B.

5. Discussion and Summary

As presented in papers $1-3$,[1-3] the scheme of analysis using the extended reptation theory (ERT) as the reference frame for the entangled system (s-A and s-B) or the Rouse theory as the reference frame for the entanglement-free system (s-C) allows us to convert the creep compliance $J(t)$ faithfully into the form of relaxation modulus $G(t)$ or viscoelastic spectrum $G^*(\omega)$ (see the Appendix of ref 2).   Here, we have analyzed the viscoelastic spectra of very low molecular-weight polystyrene samples (L10, A5000, A2500) in terms of the same scheme.   From analyzing the two sets of data, consistent results are obtained, including:

93°C, greatly limiting the range of the $J_r(t)$ curve (see Figure 2 of ref 6); as a result,

the shift factors at these two temperatures are prone to large errors.   For s-A, the $J_r(t)$

curves at 125° and 133.8^{o}C only cover a very small time period in the "knee" region

(see Figure 3 of ref 4), which is most susceptible to the temporal-unevenness effect as

discussed in section 4 of ref 1.

(a) Equally well characterized glassy-relaxation process as represented by the closeness of the values of the glassy-relaxation strength A_G^f and stretching parameter β extracted from $J(t)$ and from $G^*(\omega)$ as listed in Table 1.

(b) The closeness of the values of the structural-relaxation time τ_S, structural-growth parameter s' and frictional factor K' in the case of the L10 sample to the universal curves obtained from analyzing the $J(t)$ results previously[1-3] over the molecular-weight region from 122000 to 16400, whose low end is higher than that of L10 by about 6000.   The small deviations in the case of L10 from the universal curves are in the directions as expected from the larger deviations observed in the other samples of even smaller molecular weights; in other words, the small deviations in L10 should be caused by other effects that would set in when the molecular weight is significantly lower than the entanglement molecular weight M_e=13500.   One important factor may be the disappearing of the hindrance to segmental movement as the chain connectivity is sufficiently diminished.   Such a view is supported by the constraint (see eq 7 of ref 16)[136]

$$\frac{d^2}{s'} = \text{const} \qquad (4)$$

whereby, as s' becomes larger with decreasing molecular weight, a larger jumping step length d may be allowed.

Indicating that the experimental results of Plazek[4-6] and Inoue et al[11] have been

---

[136] Lin, Y.-H. *J. Phys. Chem. B* submitted. (paper 4)

linked in quantitative way, the agreements as summarized above further support the validity and accuracy in practice of the analysis scheme.   It is also shown in this study that as the molecular weight of polystyrene is around M_w=12000, the ΔT dependences of τ_S, s' and K' merge into the universal curves obtained previously. Since it is hard to imagine that other factors could set in to interfere the universality as the molecular weight increases beyond M_w=122000, the observed universality is expected to extend to higher molecular weights.   This expectation is supported by the agreement of the ΔT dependence of the shift factors obtained by Plazek from the recoverable compliance $J_r(t)$ results with the universal curve of τ_S.

Acknowledgement

Table 1: Characteristics M_w, M_w/M_n and T_g (based on DSC and defined at τ_S=1000 sec) and the Parameters A_G^f, β and Z Extracted from the Analyses of Creep Compliance Curves $J(t)$ or Viscoelastic Spectra $G^*(\omega)$ of Samples Whose Structural-Relaxation Times τ_S, Structural-Growth parameters s' and Frictional Factors K' (from ref 3 and from this report) Displayed in Figures 5−7 or Shift Factors (SF; from refs 4 and 6) Displayed in Figure 8.

Sample	M_w	M_w/M_n	T_g(°C) DSC[137]	T_g(°C) τ_S=1000sec	$A^f_G \times 10^{-10}$ dynes/cm²	β	Z	Displayed in Figures 5–7	Displayed in Figure 8
s-A	46900	1.05[138]	97	97	1.295	0.41	20	τ_S, s', K' from $J(t)$	SF from $J_r(t)$
s-B	122000	1.05[b]	100	99.6[139]	0.973[140]	0.41	20	τ_S, s', K' from $J(t)$	
s-C	16400	1.05[b]	93.4	93.8	0.993	0.42	20	τ_S, s', K' from $J(t)$	SF from $J_r(t)$
L10	10500	1.02	90	(90.03)[141]	0.993	0.42	50	τ_S, s', K' from $G^*(\omega)$	
A5000	5970	1.02	82	(81.64)[e]	1.09	0.42	50	τ_S, s', K' from $G^*(\omega)$	
A2500	2630	1.05	(59.6)[142]	(59.43)[e]	1.09	0.42	20	τ_S, s', K' from $G^*(\omega)$	
A1000	1050	1.13	(5)[f]	6.22	1.14	0.36		τ_S, s', K' from $G^*(\omega)$	
P19	189000	1.02	100						SF from $J_r(t)$
P60	600000	1.06	100						SF from $J_r(t)$

[137] Values based on the DSC results shown in Figure 3 of ref 14.
[138] Calculated from the polydispersity parameter Z; see refs 1 and 3 for details.
[139] "Restored" to the uncontaminated state; see ref 3 for details.
[140] This value is low due to contamination by residual plasticizers in the sample (see refs 1 and 5).
[141] Calculated by extrapolation from the FTH equation best fitted to the τ_S values.
[142] Estimated from the T_g values determined by DSC as reported in ref 11 which appear to be greater than the DSC values given by Figure 3 of ref 14 by 3.8° in average.

Figure Captions:

Figure 1

Comparison of the viscoelastic spectra $G^*(\omega)$ of L10 measured at different temperatures ($\triangledown$ at 92°C; $\triangle$ at 95°C; $\diamond$ at 99°C; ● at 105°C; ▲ at 110°C; ■ at 120°C; and ◆ at 130°C)[11] with the calculated (—— in the glassy region; in the entropic region: —— at 105°C; − − at 110°C; − – at 120°C; and – – – at 130°C); the reference temperature is 105°C.

Figure 2

Comparison of the viscoelastic spectra $G^*(\omega)$ of A5000 measured at different temperatures ($\triangledown$ at 85°C; $\triangle$ at 88°C; $\diamond$ at 92°C; ● at 100°C; ■ 110°C; ◆ at 120°C)[11] with the calculated (—— in the glassy region; in the entropic region: —— at 100°C; −− at 110°C; and − − at 120°C); the reference temperature is 100°C.

Figure 3

Comparison of the viscoelastic spectra $G^*(\omega)$ of A2500 measured at different temperatures ($\triangledown$ at 62°C; $\triangle$ at 65°C; $\diamond$ at 70°C; ● at 80°C; ■ at 90°C)[11] with the calculated (—— in the glassy region; in the entropic region: —— at 80°C; and − − at 90°C); the reference temperature is 80°C.

Figure 4

Comparison of the viscoelastic spectra $G^*(\omega)$ of A1000 measured at different temperatures ($\triangledown$ at 5°C; $\triangle$ at 10°C; $\diamond$ at 15°C; $\square$ at 20°C; ● at 25°C and ■ at

30°C)[11] with the calculated (——); the reference temperature is 25°C.

Figure 5

The structural-relaxation time, τ_S, of L10 (●), A5000 (■), A2500 (◆; with the best fitting FTH curve ····) and A1000 (▲; with the best fitting FTH curve −−) as a function of the temperature difference ΔT from individual T_g in comparison with the universal curve (——) calculated from the FTH equation (eq 3) best fitted to the τ_S values of s-A (○), s-B (◇) and s-C (□) collectively.

Figure 6

The structural-growth parameter, s', of L10 (●), A5000 (■), A2500 (◆) as a function of the temperature difference ΔT from each individual T_g in comparison with the universal curve (——) calculated the modified FTH equation (eq 19 in ref 3) best fitted to the s' values of s-A (○), s-B (◇) and s-C (□ obtained from the $J_p(t)$ line-shape analysis; ▲ from the analysis of J_{ep}^0) collectively. The dotted lines each represent the universal curve multiplied by a constant factor to superpose on the data points of L10 (×1.23), A5000 (×1.9) and A2500 (×2.2) individually.

Figure 7

The frictional factor, K', of L10 (●), A5000 (■), A2500 (◆) as a function of the temperature difference ΔT from each individual T_g in comparison with the universal curve (——) calculated from the FTH equation (eq 18 as explained in section 6 of ref 3)

best fitted to the K' values of s-A ($\bigcirc$), s-B ($\diamondsuit$) and s-C ($\square$) collectively.

Figure 8

Comparison of the universal curve (——) calculated from eq 3 with the temperature dependences of the shift factors (SF) obtained by Plazek from the recoverable compliance $J_r(t)$ results of s-A ($\bigcirc$), s-C ($\square$), P19 ($\triangle$) and P60 ($\triangledown$)[4,6] (see Table 1 and the text).
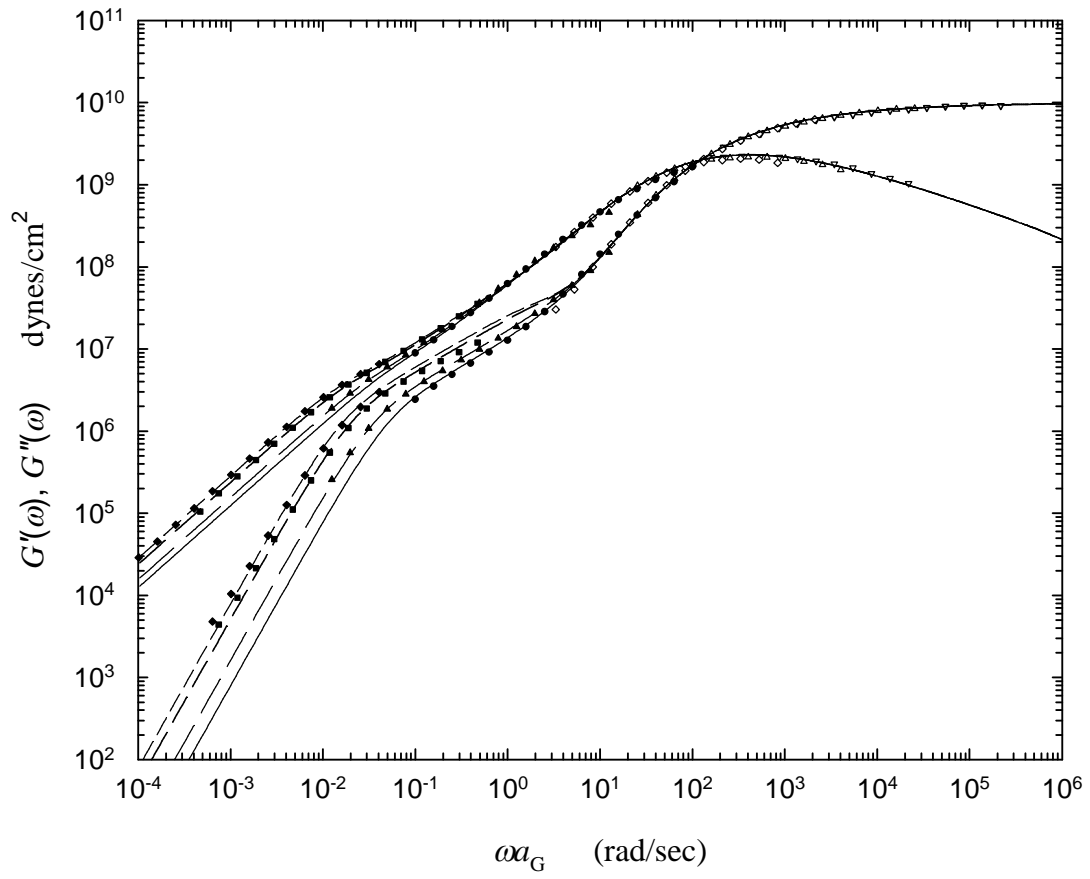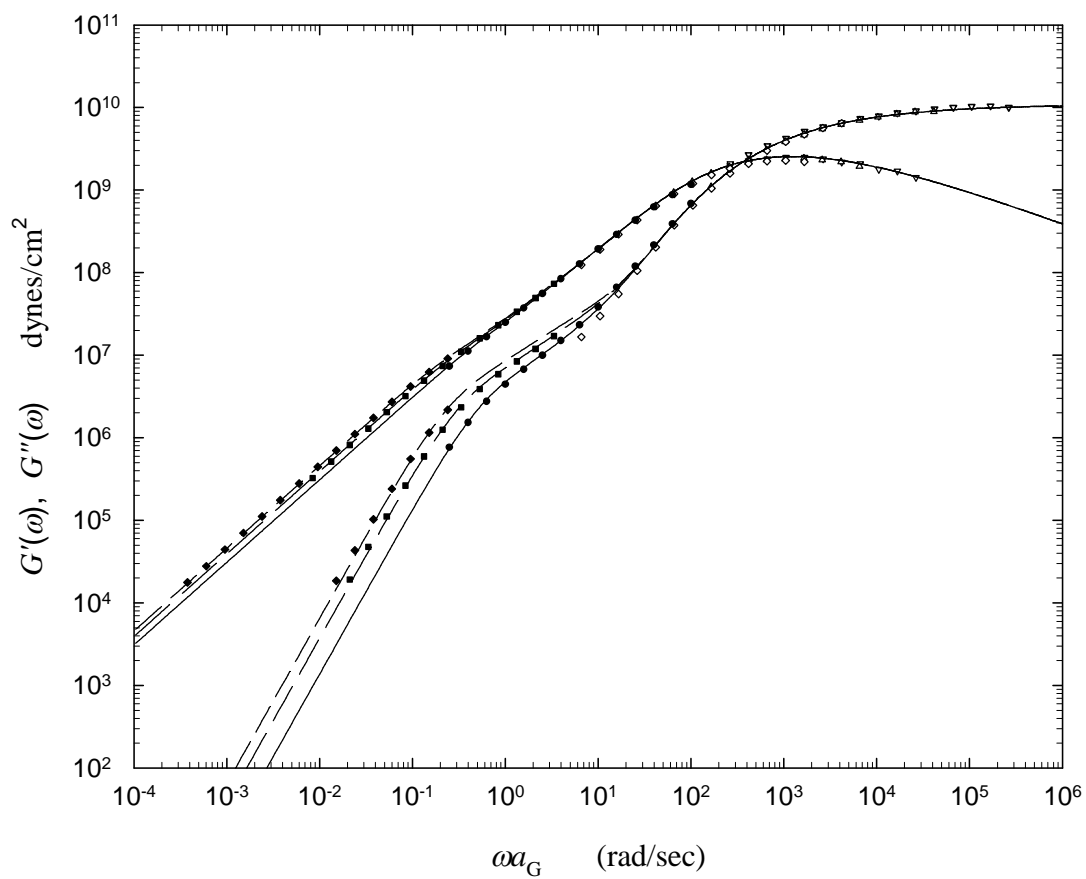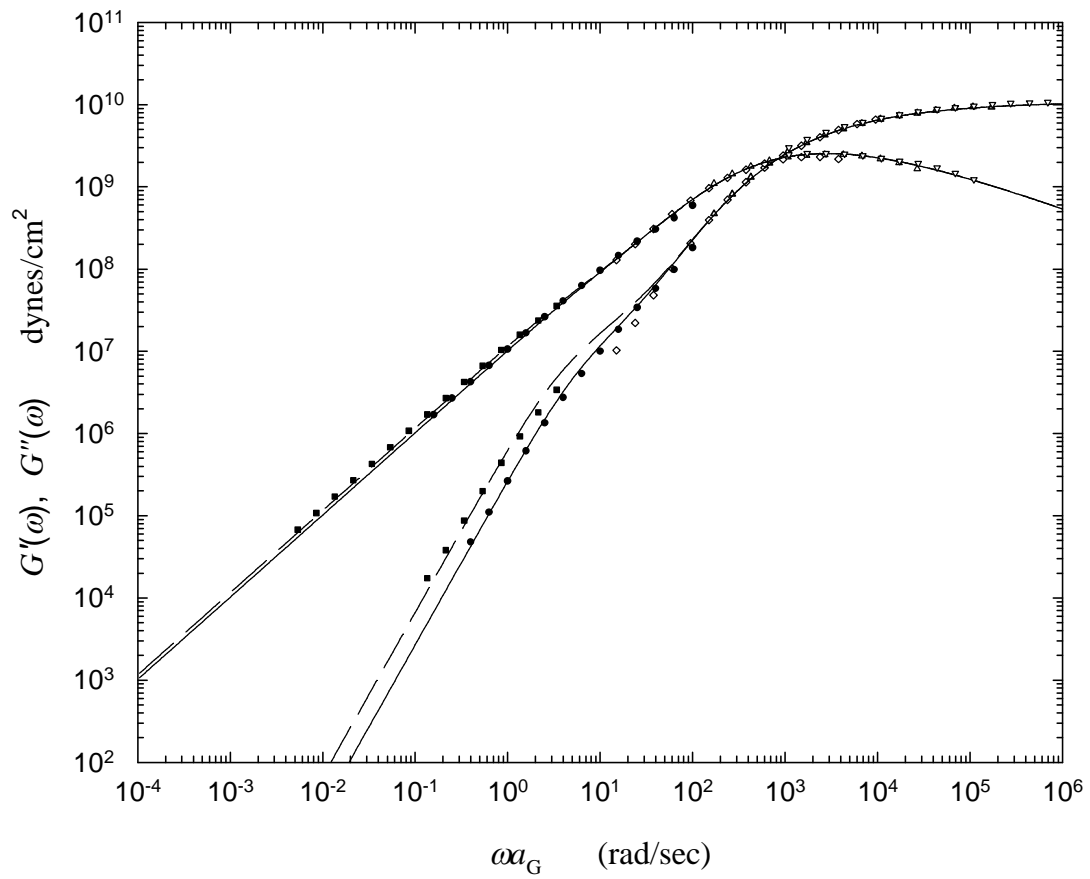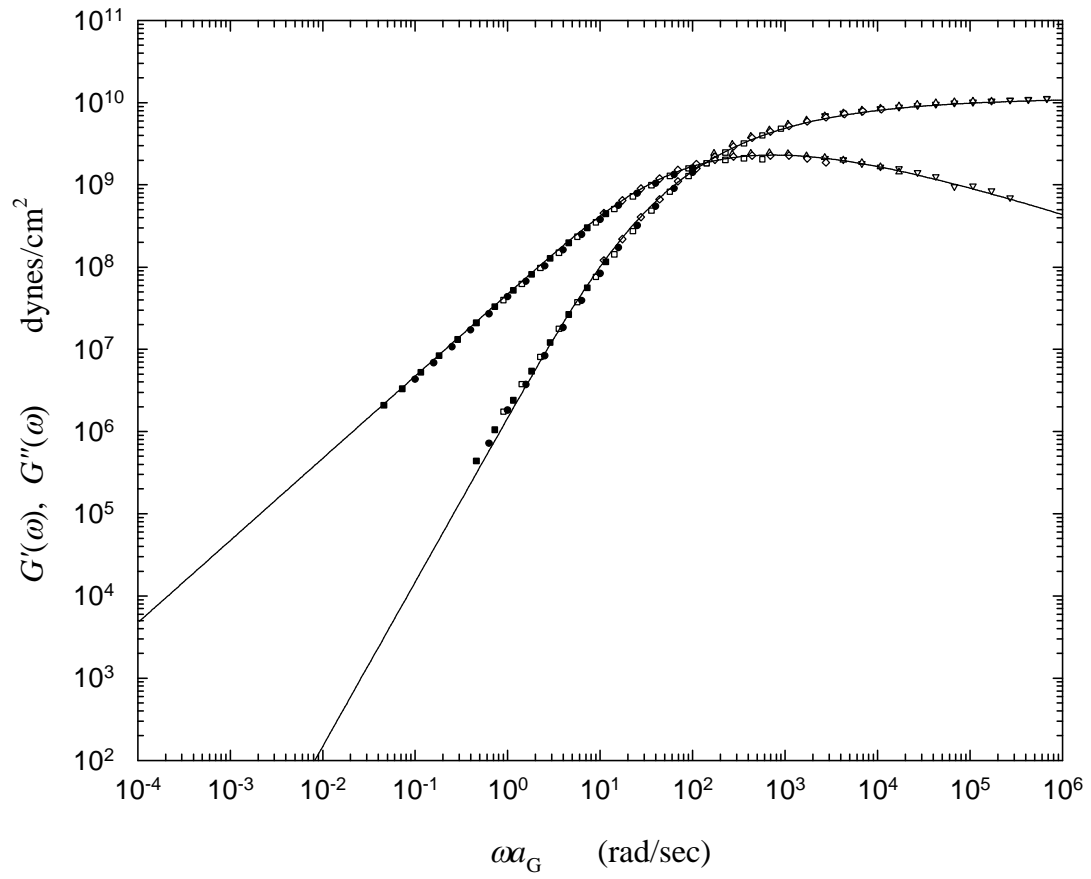
Figure 1

Figure 2
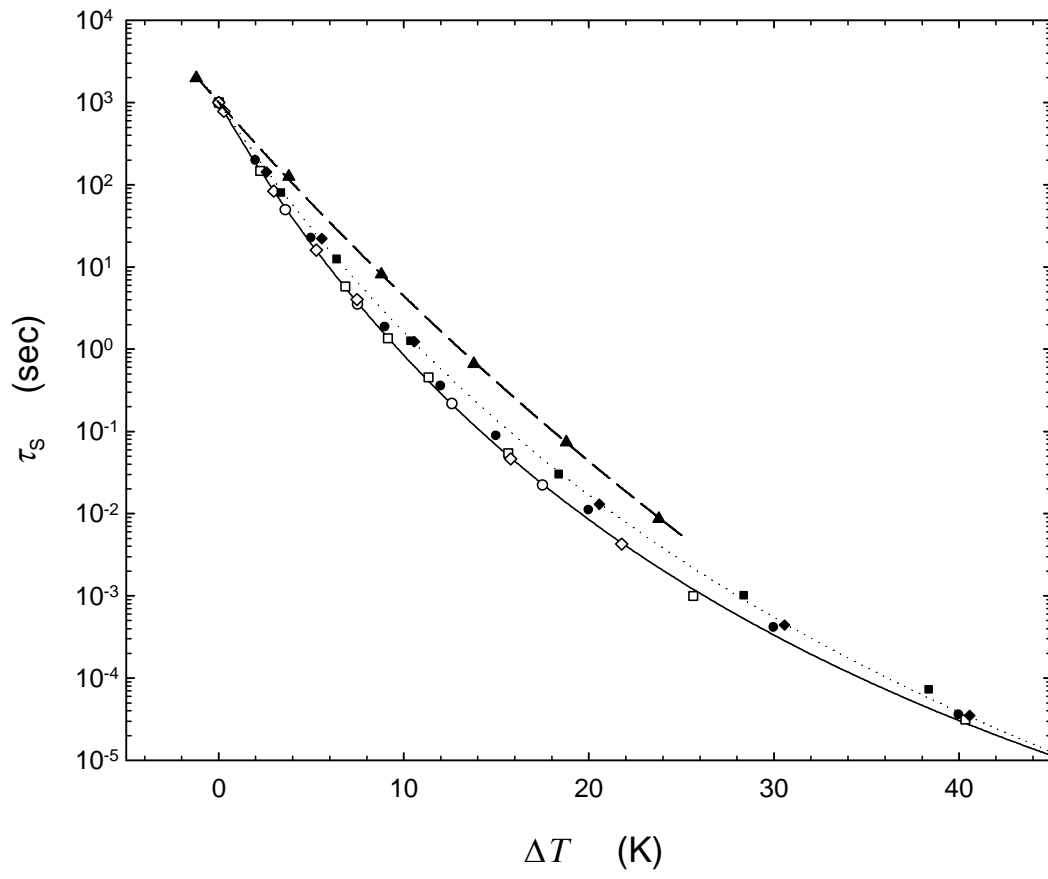
Figure 3

Figure 4

117

Figure 5

118

Figure 6

119
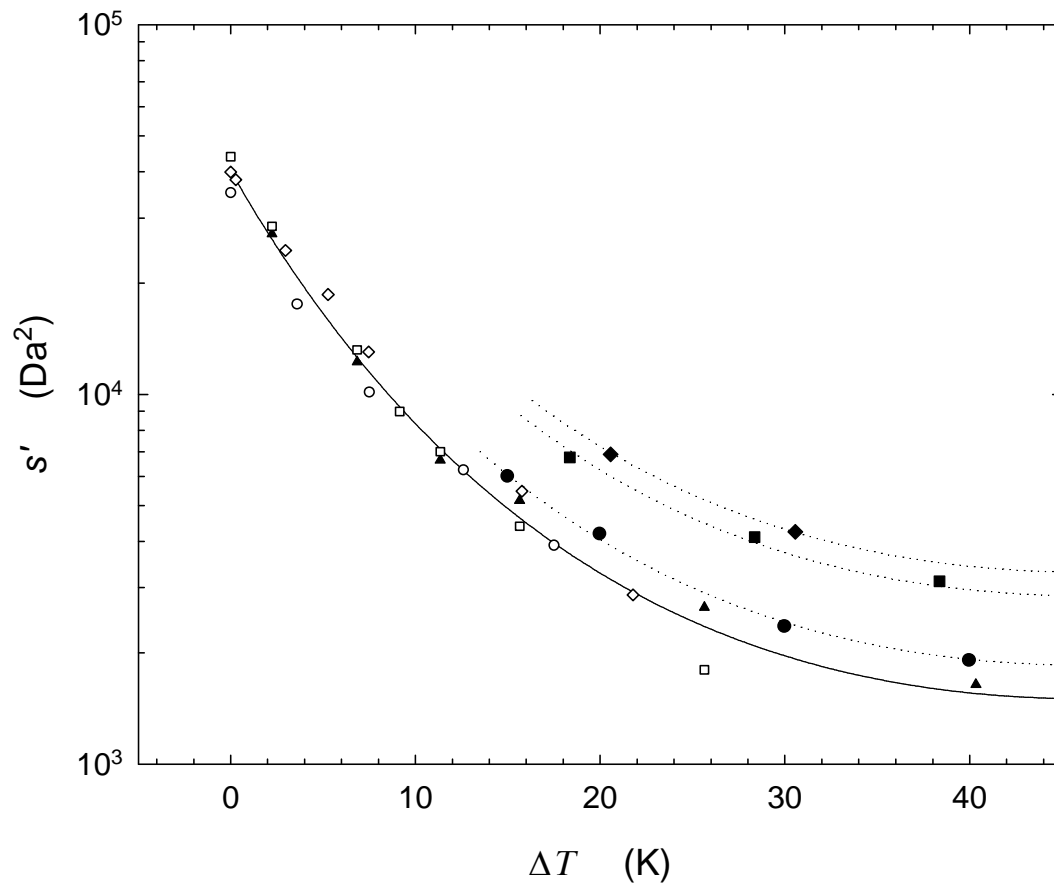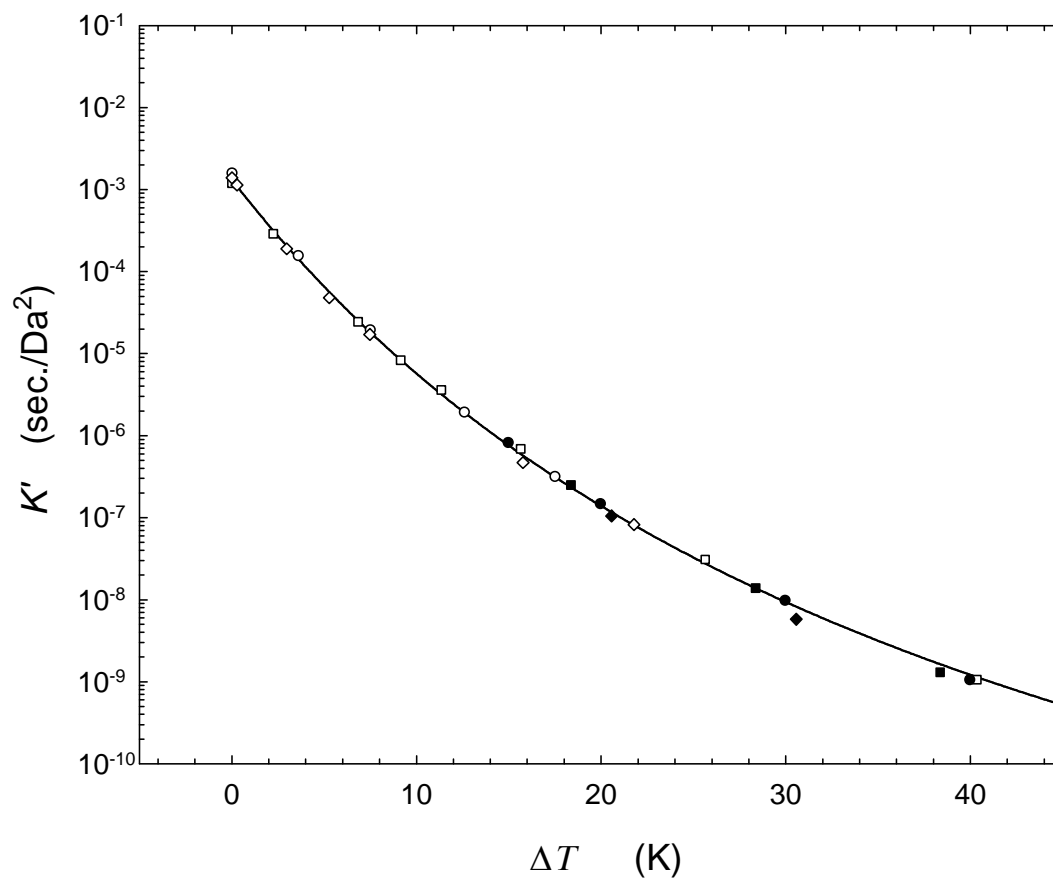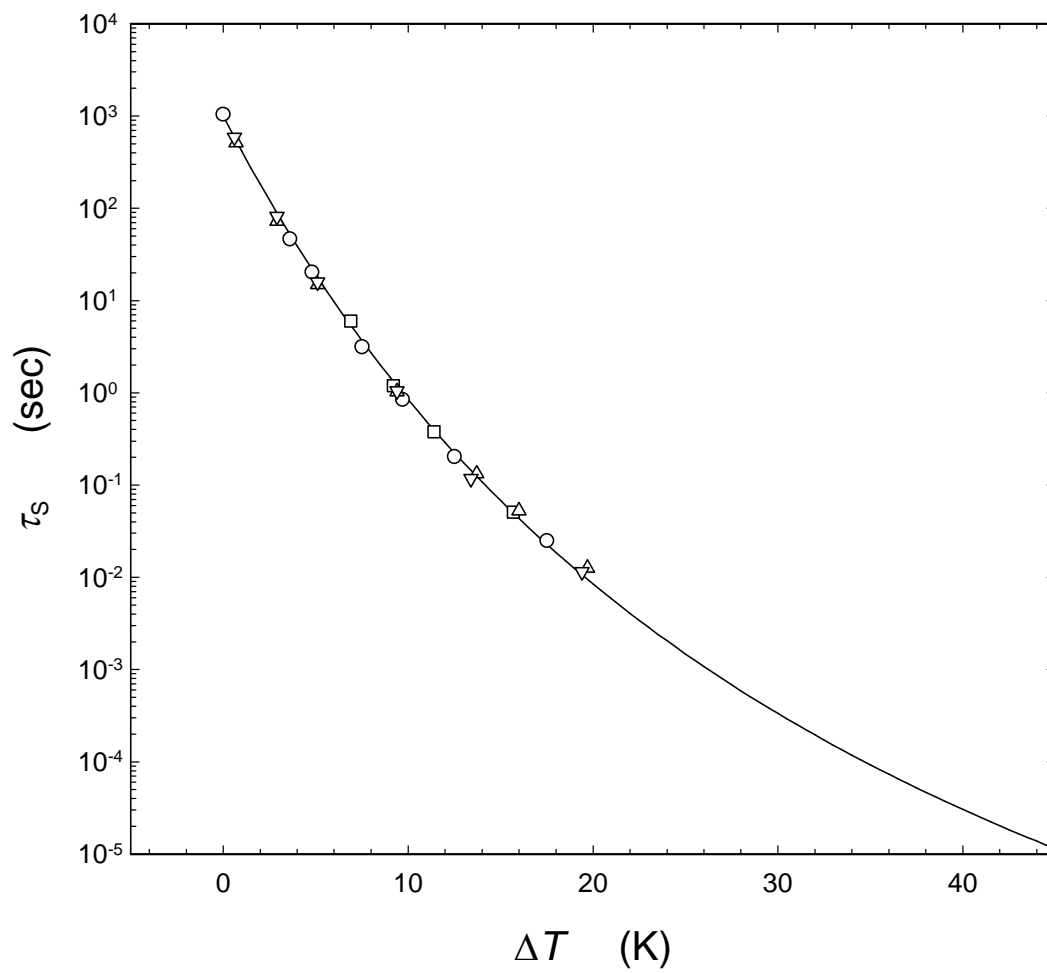
Figure 7

Figure 8

Monte Carlo Simulations

of Stress Relaxations of Entanglement-Free Fraenkel Chains. 1:

Linear Polymer Viscoelasticity

Y.-H. Lin and A. K. Das

Department of Applied Chemistry

National Chiao Tung University

Hsinchu, Taiwan

Abstract

Shear-stress relaxation modulus $G_S(t)$ curves of entanglement-free Fraenkel chains have been calculated using Monte Carlo simulations based on the Langevin equation, carrying out both in the equilibrium state and following the application of a step deformation. While the fluctuation‒dissipation theorem is perfectly demonstrated in the Rouse-chain model, only a quasi version of the fluctuation‒dissipation theorem is observed in the Fraenkel-chain model. In both types of simulations on the Fraenkel-chain model, two distinctive modes of dynamics emerge in the relaxation modulus: a fast energetic interactions-derived mode and a slow entropy-derived mode, giving a $G_S(t)$ line shape typically observed experimentally. It has been shown through analysis that the fast mode arises from the segment-tension fluctuations or reflects the relaxation of the segment-tension arising

from segments being stretched by the applied step strain; and the slow mode arises from the fluctuating segmental-orientation anisotropy or represents the randomization of the segmental-orientation anisotropy induced by the step deformation. Furthermore, it is demonstrated that the slow mode is well described by the Rouse theory in all aspects: the magnitude of modulus, the line shape of the relaxation curve and the number-of-beads dependence of the relaxation times. In other words, with one Fraenkel segment substituting for one Rouse segment, it has been shown that the entropic-force constant on each segment is not a required element to give rise to the Rouse modes of motion which have been typically observed in the long-time region of the linear viscoelastic response of an entanglement-free polymer. This conclusion provides an explanation resolving a long-standing fundamental paradox in the success of Rouse-segment-based molecular theories for polymer viscoelasticity—namely, the paradox between the Rouse segment size being of the same order of magnitude as that of the Kuhn segment and the meaning of the Rouse segment as defined in the Rouse chain model. A comparison of the simulation result with experiment suggests that the Fraenkel-chain model, while being still relatively simple, has captured the basic element of the energetic interactions—the rigidity on the segment—in a polymer system.

Monte Carlo Simulations

of Stress Relaxations of Entanglement-Free Fraenkel Chains. 1:

Linear Polymer Viscoelasticity

Y.-H. Lin and A. K. Das

Department of Applied Chemistry

National Chiao Tung University

Hsinchu, Taiwan

1. Introduction

It has been extensively shown that the linear viscoelastic response of an entanglement-free polymer melt is well described by the Rouse theory.[143,144,145,146,147] However, the agreement between theory and experiment is limited to the region below the modulus level corresponding to the molecular weight of a single Rouse segment that can be assigned to the polymer system—for instance, below $\sim \rho RT/m = 3.8 \times 10^7$

[143] Rouse, P. E. Jr. *J. Chem. Phys.* **1953**, *21*, 1271.

[144] Bird, R. B.; Curtiss, C. F.; Armstrong, R. C.; Hassager, O. *Dynamics of Polymeric Liquids, Vol.* 2, *Kinetic Theory,* 2nd ed.; Wiley: New York, 1987.

[145] Lin, Y.-H. *Polymer Viscoelasticity: Basics, Molecular Theories, and Experiments*; World Scientific: Singapore, 2003.

[146] Lin, Y.-H. *Macromolecules* **1986**, *19*, 168.

[147] Lin, Y.-H.; Juang, J.-H. *Macromolecules* **1999**, *32*, 181.

dynes/cm^2 corresponding to the Rouse-segmental molecular weight $m \approx 850$ in the case of polystyrene;[148,149,150,151152,153,154,155,156,157,158] in other words, the agreement occurs only in the time or frequency region slower than the motion associated with a single Rouse segment or equivalently the relaxation rate of the highest Rouse mode. Because of the entropic-force constant on the Rouse segment, this region may be referred to as the entropic region and the relaxation processes in it as entropy-derived dynamics. In the entropic region the entire viscoelastic response follows the same temperature dependence indicating that thermorheological simplicity is followed, as expected from the Rouse theory—the frictional factor associated with the Rouse segment carries the temperature dependence of the viscoelastic response.   In the time or frequency region faster than the motion of a single Rouse segment, the modulus of

[148] Inoue T.; Okamoto, H.; Osaki, K. *Macromolecules* **1991**, *24*, 5670.

[149] Inoue, T.; Hayashihara,H.; Okamoto, H.; Osaki, K. *J. Polym. Sci. Polym. Phys. Ed.*
1992, *30*, 409.

[150] Inoue, T.; Osaki, K. *Macromolecules* **1996**, *29*, 1595.

[151] Inoue, T.; Uematsu, T.; Osaki, K. *Macromolecules* **2002**, *35*, 820.

[152] Lin,Y.-H. *J. Polym. Res.* **1994**, *1*, 51.

[153] Lin, Y.-H.; Lai, C. S. *Macromolecules* **1996**, *29,* 5200.

[154] Lai, C. S.; Juang, J.-H.; Lin, Y.-H. *J. Chem. Phys.* **1999**, *110*, 9310.

[155] Lin, Y.-H. J. Chin. Chem. *Soc.***2002**, *49*, 629.

[156] Lin,Y.-H.; Luo, Z.-H. *J. Chem. Phys.* **2000**, *112*, 7219.

[157] Lin, Y.-H. *J. Phys. Chem. B* **2005**, *109*, 17654.

[158] Lin, Y.-H. *J. Phys. Chem. B* **2005**, *109*, 17670.

the dynamic response is much higher–ranging from $\sim 4 \times 10^7$ to $\sim 10^{10}$ dynes/cm^2 for polystyrene. The high modulus is due to the strong energetic interactions among segments, both intra-chain and inter-chain; the dynamics in this region may be properly referred to as energetic interactions-derived dynamics, which has also been referred to in the literature as the glassy relaxation or the structural relaxation or the α relaxation. It has been widely observed that as the temperature approaches the glass transition temperature, T_g, from above, the energetic interactions-derived dynamics has a temperature dependence stronger than that of the entropy-derived. [159,160,161,162,163,164,165,166] Thus, when the whole range of the viscoelastic response is included in the consideration, the thermorheological simplicity does not hold. Recently, the basic mechanism for the thermorheological complexity in polystyrene has been analyzed, showing that the effect as related to T_g behaves in a universal way within the polystyrene system, entangled or not,[15,167] and that the same basic mechanism is also responsible for the break-down of the

[159] Plazek, D. J. *J. Phys. Chem.* **1965**, *69*, 3480.

[160] Plazek, D. J. *J. Polym. Sci., Part A-2: Polym. Phys.* **1968**, *6*, 621.

[161] Plazek, D. J.; O'Rourke, V. M. J. *Polym. Sci. A-2: Polym. Phys.* **1971**, *9*, 209.

[162] Plazek, D. J. *J. Rheol.* **1996**, *40*, 987.

[163] Plazek, D. J. *Polymer J.* **1980**, *12*, 43.

[164] Okamoto, H.; Inoue, T.; Osaki, K. *J. Polym. Sci: Part B: Polym. Phys.* **1995**, *33*, 417.

[165] Inoue, T.; Hwang, E. J.; Osaki, K. *J. Rheol.* **1992**, *36*, 1737.

[166] Adachi, K.; Hirano, H. *Macromolecules* **1998**, *31*, 3958.

[167] Lin, Y.-H. *J. Phys. Chem. B*, submitted.

Stokes–Einstein equation in relating the translational diffusion constant and viscosity or molecular rotational relaxation time in fragile glass-forming liquids,[168] such as OTP[169,170,171,172,173] and TNB.[174,175] While it has been extensively demonstrated that the molecular theories: the Rouse theory[1–5] for the entanglement-free region of molecular weight and the extended reptation theory (ERT)[3,176,177,178] for the entangled region, describe the viscoelastic responses in the entropic region successfully in a quantitative way, the glassy-relaxation process can only be analyzed phenomenologically, often in terms of a stretched exponential form. In other words, we have quite limited understanding about the glassy-relaxation process at the molecular level. In this study, using the Monte Carlo simulation based on the Langevin equation,[3,14] we compute the relaxation modulus curves of the model

[168] Lin, Y.-H. *J. Phys. Chem. B*, submitted.

[169] Fujara, F.; Geil, B.; Sillescu, H.; Fleischer, G. *Z. Phys. B: Condens. Matter* **1992**, *88*, 195.

[170] Cicerone, M. T.; Ediger, M. D. *J. Phys. Chem.* **1993**, *97*, 10489.

[171] Kind, R.; Liechti, N.; Korner, N.; Hulliger, J. *Phys. Rev. B* **1992**, *45*, 7697.

[172] Chang, I.; Fujara, F.; Geil, B.; Heuberger, G.; Mangel, T.; Sillescu, H. *J. Non-Cryst. Solids* **1994**, *172–174*, 248.

[173] Mapes, M. K.; Swallen, S. F.; Ediger, M. D. *J. Phys. Chem. B* **2006**, *110*, 507.

[174] Chang, I.; Sillescu, H. *J. Phys. Chem. B* **1997**, *101*, 8794.; and references therein.

[175] Swallen, S. F.; Bonvallet, P. A.; McMahon, R. J.; Ediger, M. D. *Phys. Rev. Lett.* **2003,** *90*, 015901.

[176] Lin, Y.-H. *Macromolecules* **1984**, *17*, 2846.

[177] Lin, Y.-H. *Macromolecules* **1986**, *19*, 159.

[178] Lin, Y.-H. Lin *Macromolecules* **1987**, *20*, 885.

systems which contain elements of energetic interactions—the Fraenkel chains,[179] shedding light on the coexistence of and the interrelation between the energetic interactions-derived and entropy-derived dynamic processes.

2. Monte Carlo Simulation Based on the Langevin Equation

In the Monte Carlo simulation, the continuous change in time, dt, in the Langevin equation is replaced by a small time-step, Δt.   For a chain with the positions of the beads at time step i denoted by $\{\mathbf{R}_n(i)\}$, the simulation form of the Langevin equation is expressed by

$$\mathbf{R}_n(i+1) = \mathbf{R}_n(i) + \frac{d^2}{2}\left(\frac{\mathbf{F}_n(i)}{kT}\right) + \mathbf{d}_n(i) \qquad (1)$$

where $\mathbf{F}_n(i)$ is the force on the nth bead at the ith time step arising from the interaction potential; the random step vector $\mathbf{d}_n(i)$ is characterized by the following first and second moments:

$$\langle \mathbf{d}_n(i) \rangle = 0 \qquad (2)$$

and

$$\langle \mathbf{d}_n(i)\, \mathbf{d}_m(j) \rangle = d^2 \mathbf{I} \delta_{nm} \delta_{ij} \qquad (3)$$

---

[179] Fraenkel, G. K. *J. Chem. Phys.*, **1952**, *20*, 642.

where **I** is a unit tensor.

Then the relaxation modulus can be calculated from the Monte Carlo simulation after a step shear deformation

$$\mathbf{E} = \begin{pmatrix} 1 & \lambda & 0 \\ 0 & 1 & 0 \\ 0 & 0 & 1 \end{pmatrix} \tag{4}$$

is applied to the polymer chain in an equilibrium state at $t=0$. Following the application of the step deformation **E**, the evolution of $\{\mathbf{R}_n(i)\}$ is calculated according to eq 1; and the stress relaxation of a chain with N beads is given by

$$S_{xy}(\lambda, i) = \sum_{n=1}^{N} F_{nx}(i) Y_n(i) \tag{5}$$

For the simulation, a large number of identical relaxation processes following a step deformation are repeated and accumulated for averaging. Before a new cycle is repeated, the system must run for a sufficiently large number of time steps to reach an equilibrium state. To prevent some residual memory from accumulating, the step deformation may be applied in a cyclic manner, as done in this study; if the **E** given by eq 4 is referred to as a deformation in the x direction and denoted by x, the deformation cycle: $x \rightarrow -x \rightarrow y \rightarrow -y \rightarrow z \rightarrow -z$ is repeated and following each step deformation, the physically equivalent stress component is collected for averaging. Although the cyclic scheme is used for averaging throughout the

simulation study as reported in this paper and the companion paper,[180] to conveniently discuss the anisotropy introduced by the deformation, the obtained results will be discussed with respect to eq 4 as the chosen direction of deformation—namely, in terms of the *xy* component. Denoting the thus averaged stress relaxation as $S(\lambda,i)$, the relaxation modulus normalized to that corresponding to a single segment is given as

$$G_S(i) = -\frac{S(\lambda,i)}{\lambda(N-1)} \tag{6}$$

In this study, we are mainly interested in the linear relaxation modulus. In accordance with the fluctuation-dissipation theorem, the relaxation modulus equivalent to that given by eq 6 in the linear region of λ can be calculated from[181,182,183]

---

[180] Lin, Y.-H.; Das, A. K. *J. Chem. Phys.* (submitted; paper 2)

[181] Doi, M.; Edwards, S. F. *The Theory of Polymer Dynamics*; Oxford Univ. Press: Oxford, 1986.

[182] McQuarie, D. A. *Statistical Mechanics*; Harper & Row: New York, 1976.

[183] From applying the fluctuation-dissipation theorem, eq 7 is the expression for the relaxation modulus based on the molecular expression for the stress tensor as given in ref 39 (Namely, eq 5 here; the sign system used here for the stress tensor is opposite to that used in ref 39), which is also in agreement with the expression for the zero-shear viscosity as given in ref 40 (page 519). Note: In the Monte Carlo simulation based on the Langevin equation, the velocity distribution is assumed to be at equilibrium, namely, described by the Maxwellian distribution;[2,3] thus, the momentum flux terms only contribute to the isotropic part of the normal stresses and

$$G_S(i) = \frac{1}{6(N-1)kT} \sum_{\alpha \neq \beta} \left\langle J_{\alpha\beta}(0) J_{\alpha\beta}(i) \right\rangle = \frac{1}{6(N-1)kT} \sum_{\alpha \neq \beta} \overline{J_{\alpha\beta}(0) J_{\alpha\beta}(i)}$$

(7)

$$= \frac{1}{6I(N-1)kT} \sum_{i_0=1}^{I} \sum_{\alpha \neq \beta} J_{\alpha\beta}(i_0) J_{\alpha\beta}(i_0+i); \quad \text{with } \alpha, \beta \text{ denoting } x, y, z$$

where I represents a very large number of iteration (typically $\sim 10^3 - 10^4$, depending on the time window, namely the limit of i) and

$$J_{xy}(i) = \sum_{n=1}^{N} F_{nx}(i) Y_n(i)$$

(8)

Although in the simulation we use all the six combinations of $J_{\alpha\beta}(t)$ (with $\alpha \neq \beta$) for averaging in calculating the time-correlation function, in our discussion below, we shall use the xy component as the representative of the shear stress. The simulation result as obtained through eq 6 is referred to as the step strain-simulation $G_S(t)$, as opposed to the equilibrium-simulation $G_S(t)$ obtained through eq 7.

For a Rouse chain, the force on an internal bead is given by[2,3]

$$\mathbf{F}_n(i) = -\frac{3kT}{\langle b^2 \rangle} \left(2\mathbf{R}_n(i) - \mathbf{R}_{n+1}(i) - \mathbf{R}_{n-1}(i) \right)$$

(9)

An equivalent equation can be written for the end beads: $n=1$ or N. Throughout our

need not be included in the stress expressions in this paper.

calculations we have set $\langle b^2 \rangle = 1$.

The relaxation modulus of a Rouse chain with N beads or molecular weight M is given by[2,3]

$$kT\mu_R(t,M) = kT\sum_{p=1}^{N-1}\exp\left(-\frac{t}{\tau_p}\right) \qquad (10)$$

where the relaxation time of the pth normal mode, τ_p, is given by

$$\tau_p = \frac{\zeta\langle b^2 \rangle}{24kT\sin^2(p\pi/2N)} = \frac{K\pi^2 M^2}{24N^2\sin^2(p\pi/2N)} \qquad (11)$$

with $K = \zeta\langle b^2 \rangle\big/kT\pi^2 m^2$ being the frictional factor associated with the Rouse segment.[3] The frictional factor carries the temperature dependence of the relaxation times of a polymer in the entropic region of its relaxation modulus, which is usually described by the Fulcher and Tammann–Hesse (FTH) equation or the Williams–Landel–Ferry (WLF) equation.[184,185,186] In the simulation the time-step depends on the step-length d chosen; the relaxation time τ_p can be expressed in terms of the time-step as[14]

[184] Fulcher, G. S. *J. Am. Chem. Soc.*, **1925**, 8, 339, 789; Tammann, G. and Hesse, G.,
Z. *Anorg. Allg. Chem.* **1926**, *156*, 245.

[185] Williams, M. L.; Landel, R. F.; Ferry, J. D. *J. Am. Chem. Soc.* **1955**, *77*, 3701.

[186] Ferry, J. D. *Viscoelastic Properties of Polymers*, 3rd ed.; Wiley: New York, 1980.

$$\frac{\tau_p}{\Delta t} = \frac{\langle b^2 \rangle}{12d^2 \sin^2(p\pi/2N)} \tag{12}$$

For a chain whose nearest neighboring beads interact through the Fraenkel potential:

$$U_F = \frac{H_F}{2} \sum_{n=1}^{N-1} \left(\frac{|\mathbf{r}_n - \mathbf{r}_{n+1}|}{b_0} - 1 \right)^2 \tag{13}$$

the force on an internal bead is given by

$$\begin{aligned}
\mathbf{F}_n(i) = & -\frac{H_F}{b_0^2} \left(2\mathbf{R}_n(i) - \mathbf{R}_{n+1}(i) - \mathbf{R}_{n-1}(i) \right) \\
& + \frac{H_F}{b_0} \left[\frac{\mathbf{R}_n(i) - \mathbf{R}_{n-1}(i)}{|\mathbf{R}_n(i) - \mathbf{R}_{n-1}(i)|} + \frac{\mathbf{R}_n(i) - \mathbf{R}_{n+1}(i)}{|\mathbf{R}_n(i) - \mathbf{R}_{n+1}(i)|} \right]
\end{aligned} \tag{14}$$

An equivalent equation can be written for the end beads: $n=1$ or N. Throughout our calculation, we have set $b_0=1$ and $H_F = 400kT$.

3. Equilibrium-Simulation $G_S(t)$

3.1 Rouse chains. The relaxation time in terms of time steps as expressed by eq 12 allows one to compare the simulation $G_S(t)$ curve based on a Rouse chain with that calculated from the analytical equation.   In Figure 1, such a comparison is made for two-bead, five-bead and ten-bead chains; in the comparison, both the simulated and theoretical results are normalized to that as corresponding to one single segment with

kT set as 1—namely, $G_S(t) = \mu_R(t)/(N-1)$ (see eq 10). This way of normalization will be adopted throughout this paper (Note: kT is shown in equations of this report to indicate the relationship to entropy or average kinetic energy; however, throughout the simulation as well as in the shown results, kT is set to be 1 or equivalently kT is the unit of energy), except for the comparison between simulation and experiment, where the experimental $G(t)$ will be used. The close agreement in both the modulus and time-step coordinates as shown in Figure 1 supports the validity of the simulation.

3.2 Chains consisting of Fraenkel Segments. When the entropic force in the Rouse segment is replaced by that derived from the Fraenkel potential, the stiffness of the segment is greatly enhanced. Because the Fraenkel force is a non-linear function of the bead positions, an analytical solution cannot be obtained from the corresponding Langevin equation. In this case, the Monte Carlo simulation becomes very important and useful, illustrating how enhancing the stiffness of the segment will affect the viscoelastic response.

The simulations based on chains consisting of Fraenkel segments (referred to as Fraenkel chains below) give rise to two distinct modes in $G_S(t)$ as shown in Figure 2 for a five-bead chain—the "bead," as in the Rouse chain model, is actually a volume-less point; with this understanding, we still refer to it as a bead. In Figure 2, the simulation results obtained with the step length d chosen at 0.01 and 0.03 are compared, with each time step for the latter being treated as nine times—the expected ratio—longer than the one for the former. The close agreement between the two indicates that the step length $d=0.03$ is sufficiently short, causing virtually no distortion to the obtained $G_S(t)$ curve; at the same time, no additional information

particularly significant can be gained from using the much more time-consuming

choice, d=0.01.　Thus, all of our simulations reported in this study and in the

companion paper[38] are based on d=0.03. In Figure 3, the $G_S(t)$ curves for two-bead,

five-bead, ten-bead and twenty-bead Fraenkel chains are compared; their line shapes

are similar to what have been observed experimentally.　We shall show below that

the fast mode is an energetic interactions-derived dynamic process while the slow

mode is an entropy-derived one.

In Figure 3, the results of simulation in the equilibrium state are compared with

the Rouse theoretical curves each for a chain with the corresponding number of beads.

To obtain the shown close superposition of the Rouse theoretical curves on the

simulation results in the long-time region, we need to apply small shifting factors to

the Rouse curves along the modulus coordinate. The multiplication factors

representing the shifts are 0.69, 0.85, 0.88, and 0.95 for the dumbbell, five-bead chain,

ten-bead chain and twenty-bead chain, respectively.　The close agreement of the

slow modes with the Rouse $G_S(t)$ curves as shown in Figure 3 with only a small

shifting factor in the modulus coordinate strongly indicates that the slow mode is well

described by the Rouse theory; most significantly, N dependence of the relaxation

time as given by eq 12 is well followed.　Such agreements mean that the slow mode

is of entropic nature as the Rouse modes of motion. Considering the fact that potential

function on the Fraenekel segment represents a strong energetic interaction between

two beads─much stiffer than the Rouse segment, the emergence of the entropic slow

mode is indeed intriguing. The energetic nature of the fast mode and the entropic

nature of the slow mode are analyzed below in detail. For the sake of simplicity, we

will consider the Fraenkel dumbbell case; then, the extension of the analysis to a

Fraenkel chain with more than two beads will be discussed.

If there is no attractive interaction potential between two beads, the thermal

fluctuations in an equilibrium state will eventually separate them far apart.

Therefore, at equilibrium the average distance between the two beads (or the average

distance over a long period of time) is not that corresponding to the tensionless point

of the potential—namely, when the bond length is equal to b_0 in the case of the

Fraenkel segment—but larger. There are different ways to define the average as will be

discussed below; however, this is true in all cases.   Hence, the two beads are each

more often than not under a tension to bring them closer.   This is so with a Rouse

segment as well as with a Fraenkel segment. These tensile forces on the bonds play

important roles contributing to the stress tensor of the chain. Because the Fraenkel

potential rises up sharply with a deviation from the tensionless point, the average

bond length in the equilibrium state should be larger than b_0 by only a small amount

δ_0 in any way of averaging.   Physically, the small δ_0 is responsible for the existence

of the entropy-derived slow mode; in an approximate way, the small δ_0 allows the

tensile force on the segment to be expressed as a linear function of the bond vector as

occurring in the Rouse theory.

For the Fraenkel dumbbell, the Langevin equation in terms of the bond vector,

$\mathbf{b}(t) = \mathbf{R}_2(t) - \mathbf{R}_1(t)$, is given by

$$\frac{d\mathbf{b}(t)}{dt} = -\left(\frac{2}{\zeta}\right)\frac{H_F}{b_0^2}\left[1 - \frac{b_0}{|\mathbf{b}(t)|}\right]\mathbf{b}(t) + \mathbf{g}(t) \qquad (15)$$

where the fluctuation term is given by $\mathbf{g}(t) = \mathbf{g}_2(t) - \mathbf{g}_1(t)$ with $\mathbf{g}_1(t)$ and $\mathbf{g}_2(t)$ being the fluctuations on beads 1 and 2, respectively.

Eq 15 can be similarly expressed in the discrete form for simulation purpose as described in Section 2.   Defining

$$1 - \frac{b_0}{|\mathbf{b}(t)|} = \frac{\delta(t)}{b_0} \qquad (16)$$

eq 15 is rewritten as

$$\frac{d\mathbf{b}(t)}{dt} = -\left(\frac{2}{\zeta}\right)\frac{H_F}{b_0^3}\delta(t)\mathbf{b}(t) + \mathbf{g}(t) \qquad (17)$$

Corresponding to eq 17, the xy shear stress component is given by

$$J_{xy}(t) = -\frac{H_F}{b_0^3}\delta(t)b_x(t)b_y(t) \qquad (18)$$

Hence

$$G_S(t) = \frac{1}{kT}\left\langle J_{xy}(0)J_{xy}(t)\right\rangle = \frac{H_F^2}{kTb_0^6}\left\langle \delta(0)b_x(0)b_y(0)\delta(t)b_x(t)b_y(t)\right\rangle \qquad (19)$$

As expected, the simulation results obtained for the Fraenkel dumbbell based on the combination of eqs 7 and 8 and on eq 19 are identical.   In the simulation, the fluctuation in $\delta(t)$ as defined by eq 16 can be monitored separately allowing the time

correlation function $\langle \delta(0)\delta(t) \rangle$ to be calculated. Physically, $\delta(t)$ approximately represents the deviation of $|\mathbf{b}(t)|$ from b_0. Any small change in $|\mathbf{b}(t)|$ leads to a large relative change in $\delta(t)$ (for instance a change in $|\mathbf{b}(t)|$ from 1.005 to 1.01 doubles the value of $\delta(t)$); as a result, compared to the motion associated with the bond vector $\mathbf{b}(t)$ itself, $\delta(t)$ represents fast fluctuations with large relative fluctuation amplitude, giving rise to a fast relaxation process in $G_S(t)$ as shown below. As $\delta(t)$ originates from the particular form of Fraenkel potential, representing the fluctuations in the tension on the Fraenkel segment, the fast relaxation mode may be very well referred to as an energetic interactions-derived dynamic process. Because of the large difference between the fluctuation rate of $\delta(t)$ and that associated with $b_x(t)b_y(t)$, eq 19 may be approximated by

$$G_S(t) \approx \frac{H_F^2}{kTb_0^6} \langle \delta(0)\delta(t) \rangle \left\langle \big(b_x(0)b_y(0)\big)\big(b_x(t)b_y(t)\big) \right\rangle$$

$$\tag{20}$$

$$= \frac{H_F^2}{kTb_0^6} \left[\langle \Delta\delta(0)\Delta\delta(t) \rangle + \delta_0^2 \right] \left\langle \big(b_x(0)b_y(0)\big)\big(b_x(t)b_y(t)\big) \right\rangle$$

where formally

$$\delta(t) = \Delta\delta(t) + \delta_0 \tag{21}$$

with

$$\langle \Delta\delta(t) \rangle = 0 ; \quad \text{and} \quad \langle \delta(t) \rangle = \delta_0 \tag{22}$$

138

As explained above, δ_0 is always greater than zero. Eq 20 suggests two distinct relaxation processes in $G_S(t)$, as observed. At long times when $\langle\Delta\delta(0)\Delta\delta(t)\rangle$ has diminished, $G_S(t)$ transits into a slow relaxing region, which would be described by

$$\frac{1}{kT}\langle J_{xy}(0)J_{xy}(t)\rangle = \frac{H_F^2}{kTb_0^6}\left[\delta_0^2\right]\left\langle\left(b_x(0)b_y(0)\right)\left(b_x(t)b_y(t)\right)\right\rangle \qquad (23)$$

In the short-time region where the process $\langle\Delta\delta(0)\Delta\delta(t)\rangle$ is dominant, the approximation as used in eq 20 is expected to be good. By contrast, over a long period of time, as the non-vanishing residual fluctuations in $\delta(t)$ are small and more comparable in (relative) magnitude to the slow fluctuations in $b_x(t)b_y(t)$, the separation into the product of δ_0^2 and $\left\langle\left(b_x(0)b_y(0)\right)\left(b_x(t)b_y(t)\right)\right\rangle$ as done in eq 23 may not be well justified. Nevertheless, the approximate form, eq 20, helps us understand the distinctive coexistence of the fast and slow modes of motion as observed from the simulation. To somewhat make up for the deficiency of the approximation as represented by eq 20 in the long-time region, we use three different ways to calculate δ_0, from which an approximate $G_S(t)$ curve in each case can be obtained for comparison with the exact result, reflecting the key physical elements affecting $G_S(t)$. One, denoted by δ_N, is calculated from the natural base line of $\langle\delta(0)\delta(t)\rangle$. The second, denoted by δ_V, is the value 0.0075 expected from

considering the virial theorem.[187] As described in Appendix A the virial theorem is well confirmed in our simulation. The third, denoted by δ_F, gives a close fitting to the $G_S(t)$ curve obtained from simulation using the exact form, eq 19. In each case, the definition of $\Delta\delta(t)$ is changed accordingly with δ_0 of eq 21 replaced by δ_N, δ_V or δ_F.

Regardless of the choice for δ_0 for the time being, we shall first look at the approximate $G_S(t)$ functional form as given by eq 23 for the long-time region. Eq 23 represents the time-correlation function of the stress tensor component $J_{xy}(t)$ in the long-time region described by the Langevin equation:

$$\frac{d\mathbf{b}(t)}{dt} = -\left(\frac{2}{\zeta}\right)\frac{H_F\delta_0}{b_0^3}\mathbf{b}(t) + \mathbf{g}(t) \tag{24}$$

which is linear and of the same form as that of the Rouse dumbbell:

$$\frac{d\mathbf{b}(t)}{dt} = -\frac{6kT}{\zeta\langle\mathbf{b}^2\rangle_R}\mathbf{b}(t) + \mathbf{g}(t) \tag{25}$$

Thus, the slow mode is expected to behave very similarly to the single mode of motion in the Rouse dumbbell. If the δ_V value as obtained from the virial theorem ($\delta_V = 3kTb_0/H_F$, as from eq A1) is used for δ_0, eqs 24 and 25 are identical with $b_0 = \langle\mathbf{b}^2\rangle_R^{1/2} = 1$ as set in this study and will lead to the same time-correlation

---

[187] Goldstein, H. *Classical Mechanics*, 2nd ed.; Addison–Wesley: Reading, Massachusetts, 1980.

function of the bond vector as given by the Rouse dumbbell model:[3]

$$\langle \mathbf{b}(0) \cdot \mathbf{b}(t) \rangle = \langle \mathbf{b}^2 \rangle_R \exp\left(-\frac{t}{\tau}\right)$$ (26)

with
$$\tau = \frac{\zeta \langle \mathbf{b}^2 \rangle_R}{6kT} = \frac{\zeta b_0^2}{2H_F(\delta_V/b_0)}$$ (27)

(Note: Obtained from the simulation, the mean square bond length $\langle \mathbf{b}^2 \rangle$ of the Fraenekel dumbbell is greater than that of the Rouse dumbbell $\langle \mathbf{b}^2 \rangle_R$ by 1.3%; as this difference is very small, particularly, much smaller than the difference between δ_N, δ_V and δ_F, it is neglected here.) As shown in Figure 4, the shape of the $\langle \mathbf{b}(0) \cdot \mathbf{b}(t) \rangle$ curve from the simulation is well described by the single exponential form as that of the Rouse dumbbell model but with a relaxation time longer by about 45%. In other words, using the relaxation time of $\langle \mathbf{b}(0) \cdot \mathbf{b}(t) \rangle$ as the criterion for determining δ_0, the value, denoted by δ_τ, is obtained to be 0.0052.

In Figure 5, we show the $G_S(t)$ simulation curves obtained in four different ways: one uses the exact form, eq 19; the other three use the approximate form, eq 20, with δ_0 substituted by δ_N, δ_V or δ_F. The corresponding $\langle \delta(0)\delta(t) \rangle$ curves calculated on the basis of using δ_N, δ_V or δ_F are shown in Figure 6. One can notice that the fast dynamics occurring in the thus calculated $G_S(t)$ and $\langle \delta(0)\delta(t) \rangle$ have the same time-scale and that there is virtually no difference between the simulation results based on using δ_N, δ_V or δ_F. Clearly this is due to the fluctuation magnitude

141

in $\delta(t)$ or $\Delta\delta(t)$ being much larger than δ_N, δ_V and δ_F. For $G_S(t)$, the approximate results are also virtually indistinguishable from the exact in the most part (the early portion) of the fast-mode region. Clearly, these agreements occurring in the short-time region are due to the dominant effect of $\langle\Delta\delta(0)\Delta\delta(t)\rangle$ and indicates that the fast mode in $G_S(t)$ arises from the segment-tension fluctuation $\delta(t)$ —therefore, an energetic interaction-derived dynamic process. In the long-time region, large divergences between the curves based on using δ_N, δ_V or δ_F occur. Because of the separation of δ_0^2 from $\langle(b_x(0)b_y(0))(b_x(t)b_y(t))\rangle$ is not a well-justified approximation as explained above, using the natural base line of $\langle\delta(0)\delta(t)\rangle$, which is obtained to be $\delta_N = 0.0022$, much smaller than the value of δ_V or δ_F, leads to the poorest result. Allowing δ_0 adjustable, simulation using the approximate form can give a $G_S(t)$ curve which is virtually indistinguishable from that obtained from using the exact form. The very close fit shown in Figure 5 is obtained with $\delta_F = 0.01$, which is larger than $\delta_V = 0.0075$ by 33%. Hence, in this case the value from the virial theorem underestimates by about 33%, as opposed to giving an overestimate of the δ_0 value when the relaxation time of the time correlation function $\langle\mathbf{b}(0)\cdot\mathbf{b}(t)\rangle$ is used as the criterion. On the other hand, the comparison of the $G_S(t)$ relaxation time of the Rouse dumbbell with that of the slow mode in the $G_S(t)$ simulated from the exact form indicates that the virial theorem gives an accurate prediction of δ_0. This is also indicated in Figure 3 by the agreements between the Rouse theory and the simulation results in the slow-mode region for 5-bead, 10-bead and 20-bead chains.

Involving only a very small approximation (see eq A1) which is unrelated to the

separation into two time-correlation functions as done in eq 20, δ_V from the virial theorem can be regarded as independent and trustworthy. As opposed to the independence of δ_V, each of the equations (eqs 20, 23 and 24) as involved in estimating the different δ_0 values: δ_N, δ_τ and δ_F contains an element of approximation, which naturally distorts the real situation in different ways, the obtained values of δ_0 are not expected to be the same. Excluding the δ_N value, which is apparently based on a bad approximation, the obtained δ_0 values in various forms are within 40% from their average, which is very close to the value from the virial theorem. The closeness of these estimated δ_0 values to the expectation based on the virial theorem supports that the approximations involved in the above analyses are well justified and that the physical picture they present—the fast mode in $G_S(t)$ is an energetic interactions-derived dynamic process and the slow mode is an entropy-derived one as the Rouse modes of motion—is a valid description. The described basic natures associated with the fast and slow modes, respectively, will be further shown in a different way in the discussion of the step strain-simulation $G_S(t)$ below.

For a Fraenkel chain with more than two beads, the extension of the above analysis requires an examination. As opposed to eq 19 for a dumbbell, for an N-bead chain, the relaxation modulus is given by

$$G_S(t) = \frac{1}{(N-1)kT}\left\langle J_{xy}(0)J_{xy}(t)\right\rangle$$

$$= \frac{H_F^2}{(N-1)kTb_0^6}\left\langle\left(\sum_{i=1}^{N-1}\delta_i(0)b_{ix}(0)b_{iy}(0)\right)\left(\sum_{j=1}^{N-1}\delta_j(t)b_{jx}(t)b_{jy}(t)\right)\right\rangle$$

(28)

As being dynamically correlated, the contributions of the cross terms in eq 28 to $G_S(t)$ are not zero; the dynamic correlation is also expected in the Rouse-chain model.[188] As a result, applying the above conclusions for a single segment to an N-bead chain requires an analysis. As it turns out, the self terms of eq 28 as given by

$$G_S^{\text{self}}(t) = \frac{H_F^2}{(N-1)kTb_0^6} \sum_{i=1}^{N-1} \left\langle \delta_i(0)b_{ix}(0)b_{iy}(0)\delta_i(t)b_{ix}(t)b_{iy}(t) \right\rangle \qquad (29)$$

are virtually the solely-contributing terms to $G_S(t)$ in the short-time region; in other words, the cross terms only contribute to the long-time region. This is illustrated by the comparison of the curves of $G_S(t)$ and $G_S^{\text{self}}(t)$ for a five-bead chain in Figure 7. As also shown in the same figure, virtually the same relative weight between the self and cross terms in the long-time region occurs to the Rouse-chain model, further supporting the Rouse-chain nature of the slow mode. Since there is virtually no difference between $G_S(t)$ and $G_S^{\text{self}}(t)$ in the short-time region for the Fraenkel chain, we may use eq 29 to illustrate the effect of fluctuations in $\delta_i(t)$, which is dominant in the short-time region. Since the summation in eq 29 just represents a multiple of the single term in eq 19, the analysis based on the Fraenkel dumbbell as presented above can be readily applied to a N-bead chain. Thus, the conclusions of the analysis based

[188] Note: For the mean square end-to-end vector of a Fraenkel chain, which is a static property, there is no correlation between different segment, just as in the case of the freely jointed chain. But just as in a Rouse chain, the dynamic coupling between different segments cannot be neglected.

on the Fraenkel dumbbell as to the energetic interactions-associated nature of the fast

mode in $G_S(t)$ are basically equally applicable to the Fraenkel chains in general with

multiple beads.   In the slow-mode region, the contributions of the cross terms clearly

cannot be neglected.   This together with the lack of a good justification for

separating $\langle \delta(0)\delta(t)\rangle$ from $\langle \left(b_x(0)b_y(0)\right)\left(b_x(t)b_y(t)\right)\rangle$ in the long-time region makes an

analysis for the slow mode similar to that done to the Fraenkel dumbbell unwieldy.

Nevertheless, the entropic nature of the slow mode is clearly supported by the fact

that $G_S(t)$ is well described by the Rouse theory in all aspects: the line shape, the

magnitude of modulus and the N dependence of relaxation times. Furthermore,

through the fluctuation-dissipation theorem, it is found from the step strain-simulation

of $G_S(t)$ as discussed below that the slow mode should arise from fluctuations in the

segmental-orientation anisotropy−an entropic origin.

4. Step Strain-Simulation $G_S(t)$

Based on the fluctuation-dissipation theorem, the step strain-simulation $G_S(t)$ in

the linear region of the applied strain is expected to be equivalent to the

equilibrium-simulation $G_S(t)$.   In Figure 1, the step strain-simulation $G_S(t)$ curves

obtained at λ=0.5 for 2-bead, 5-bead and 10-bead Rouse chains are also shown. As

expected from the theory, no non-linear effect can be observed between the $G_S(t)$

curves obtained from the simulations at λ=0.5 and 1 for the Rouse chain model; in

other words, the shown step strain-simulation $G_S(t)$ curves are linear results. These

step strain-simulation results are in close agreement with the equilibrium-simulation

$G_S(t)$ results and the Rouse theoretical curves, illustrating the working of the fluctuation-dissipation theorem and confirming the validity of the simulations as presented in this study.

The equilibrium-simulation $G_S(t)$ and the step strain-simulation $G_S(t)$ curves obtained at λ=0.2 and 0.5 for the 2-bead, 5-bead, 10-bead and 20-bead Fraenkel chains are compared in Figure 8. There are clear differences between the equilibrium-simulation $G_S(t)$ and the step strain-simulation $G_S(t)$ at λ=0.2 in the 2-bead chain case, indicating that the fluctuation-dissipation theorem is not fulfilled totally. This may be due to λ=0.2 being not in the linear region yet as there is some small difference between the $G_S(t)$ results at λ=0.2 and 0.5 in the fast-mode region. In fact, the numerically calculated $G_S(0)$ as a function of the strain λ as shown in Figure 6 of the companion paper indicates that the linear region should be below λ=0.005. However, further investigation by decreasing the λ value indicates that this is not the main cause. With the λ value decreasing, the number of repeating cycles required to obtain a well-averaged $G_S(t)$ curve increases greatly. Prevented by the overwhelmingly long time involved, we limit our study to the Fraenkel dumbbell system—where the difference from the equilibrium-simulation $G_S(t)$ is also the most obvious—in comparing the $G_S(t)$ results at λ=0.004 and 0.2. Although there are some difference between the results at λ=0.004 and 0.2, the $G_S(t)$ result of the Fraenkel dumbbell at λ=0.004 does not appear to be closer to the equilibrium-simulation result as shown in Figure 9. As also shown in Figure 8, the difference between the equilibrium-simulation and step strain-simulation $G_S(t)$ curves begins to appear in an obvious way in the time region around the end of the fast mode and the early part of

the slow mode, where an effect related to the coupling between $\delta(t)$ and $b_x(t)b_y(t)$—a subject discussed in section 3—is most likely to occur. Thus, the difference suggests that the coupling between $\delta(t)$ and $b_x(t)b_y(t)$ may occur differently in the two types of simulations. Furthermore, the comparison the results shown in Figure 8 and 9 indicates that the agreement between the equilibrium-simulation and step strain-simulation $G_S(t)$ curves in the dumbbell case is not as good as the agreement in the 5-bead chain case, which in turn is not as successful as in the 10-bead chain and 20-bead chain cases. As the difference in coupling may be reduced by the decrease in the coupling itself, this trend may be explained by what we have observed in Figure 3 suggesting that the coupling between $\delta(t)$ and $b_x(t)b_y(t)$ is reduced making the slow mode better described by the Rouse theory as the number of modes of motion in the slow mode region increases. In other words, as being more removed from the fast mode, the lower modes (belonging to the slow mode) in an N-bead chain, may improve the overall decoupling of the fast and slow modes as N increases. In spite of the visible difference particularly when N is small, we still see an overall agreement between the equilibrium-simulation and step strain-simulation $G_S(t)$ curves, each revealing clearly two separate modes. We refer to such an overall agreement as a quasi version of the fluctuation-dissipation theorem.

In Figure 10, we show the mean square segment length $\langle \mathbf{b}^2(t) \rangle$; and its components: $\langle b_x^2(t) \rangle$, $\langle b_y^2(t) \rangle$ and $\langle b_y^2(t) \rangle$ of a five-bead Fraenkel chain as a function of time following the application of the step shear strain $\lambda=0.5$. Although $\lambda=0.5$ is not really in the linear region, we show these results at $\lambda=0.5$ because their

changes with time are discernible and at the same time, the corresponding $G_S(t)$ curve

does not differ from the one obtained from the equilibrium simulation very much.

Comparing these results can serve our purpose, as discussed below, better than

showing the results at $\lambda=0.2$.   As shown in Figure 10, the segment length is stretched

by the step strain and relaxes back to the equilibrium value, as opposed to the segment

length fluctuating around its mean value in the equilibrium simulation.   From

comparing the time-scales of the dramatic changes in $G_S(t)$ (Figure 8)

and $\langle \mathbf{b}^2(t) \rangle$ (Figures 10), it is clear that the fast mode occurring in the step-strain

simulation clearly reflects the large tension on the segments, arising from segments

being stretched by the step deformation, and that its relaxation reflects the decrease in

the average segment length back to the equilibrium value.   This segment-tension

relaxation is equivalent to the time-correlation function of the segment-tension

fluctuation $\langle \delta(0)\delta(t) \rangle$ as shown in Figure 6.

In the entropic region of the step strain-simulation $G_S(t)$, the mean square segment

length has reached the equilibrium value as shown in Figure 10, same as that

occurring all the times in the equilibrium simulation; however, as the differences

between the time dependences of the components $\langle b_x^2(t) \rangle$, $\langle b_y^2(t) \rangle$ and $\langle b_y^2(t) \rangle$

indicate, there is some net orientation anisotropy in the step-strain case as opposed to

maintaining isotropy in average in the equilibrium case.   As orientation does not

cause a change in the potential energy on the segment, the anisotropy of the segmental

orientation is of entropic nature. According to the fluctuation-dissipation theorem,

corresponding to the randomization of segmental orientation anisotropy as occurring

in the simulation following a step shear deformation, fluctuating segmental-orientation anisotropy should be present all the time in the equilibrium state; such fluctuations should be responsible for the entropic slow mode in the equilibrium-simulation $G_S(t)$. The close relationship between the slow mode in $G_S(t)$ and the segmental orientation anisotropy as further revealed in the nonlinear region of strain will be analyzed in great detail in the companion paper.

5. Comparison of Simulation with Experiment

Both the Rouse theory and the present Monte Carlo simulation using the Rouse chain model or the Fraenkel chain model are a mean-field representation, meaning that the bulk viscoelastic response of an entanglement-free polymer system (concentrated solution or melt) is the sum of the contributions from all the chains in a unit volume, each is represented by its statistically averaged dynamic behavior. In comparison with experimental results of polymer melts, the mean-field representation works very well in the long-time or entropic region of the viscoelastic response, as illustrated by the quantitative agreement of the measured viscoelastic spectra with the Rouse theory. Since in the entropic region, there is basically no difference between the Rouse theory and the simulation results based on the Fraenkel chains, we may compare the simulation results with experiment over the whole time range, shedding light on the viscoelastic response in the short-time or energetic-interactions region. Intuitively, the mean-field Fraenkel chain model should be an over-simplified representation for the viscoelastic behavior in the energetic-interactions region for a polymer in its melt state. However, the $G_S(t)$ results obtained from the Fraenkel

chain-based simulations have basically reflected the main features in the $G(t)$ curves

obtained experimentally in both the short-time and long-time regions, suggesting that

the simple model may have captured the key interactions in the real system.

The creep compliance $J(t)$ can be converted to the relaxation modulus $G(t)$

through the basic equation of linear viscoelasticity:

$$t = \int_0^t J(t')G(t-t')dt' \qquad (30)$$

The convolution integral of eq 30 can be solved numerically by the method of

Hopkins and Hamming,[189,190] as detailed in Appendix A of ref 15.   Recently, the

creep compliance $J(t)$ results of nearly monodisperse polystyrene samples obtained by

Plazek,[17-19] two entangled and one entanglement-free, have been quantitatively

analyzed through eq 30 in terms of a $G(t)$ functional form which incorporates a

stretched exponential form for the glassy-relaxation process into the extended

reptation theory for the entangled case[15,16] or into the Rouse theory for the

entanglement-free case.[25]   From such quantitative analyses, it has been shown that

the thermorheological complexity as related to the glass transition behaves in a

universal way within the polystyrene system, entangled or not. The details of the

---

[189] Hopkins, I. L.; Hamming, R. W. *J. Appl. Phys.* **1957**, *28,* 906; *J. Appl. Phys.*

1958, *29,* 742.

[190] Tschoegl, N. W. *The Phenomenological Theory of Linear Viscoelastic Behavior*;

Springer-Verlag: Berlin, 1989.

studies are referred to refs 15 and 25. Here, we will only use the result of the entanglement-free system—denoted by sample C in ref 25 and will also be so denoted here. The $G(t)$ functional form used for the entanglement-free case is expressed by

$$G(t) = A_{\mathrm{G}}^{\mathrm{f}} \mu_{\mathrm{G}}(t) + \rho RT \int \frac{f(M)}{M} \mu_{\mathrm{R}}(t,M) dM \qquad (31)$$

where $\mu_{\mathrm{R}}(t,M)$ is given by eq 10; ρ, R and T are the density, gas constant, and absolute temperature, respectively; $f(M)$ represents the molecular-weight distribution of the sample; and $A_{\mathrm{G}}^{\mathrm{f}}$ is the full relaxation strength of the glassy-relaxation process $\mu_{\mathrm{G}}(t)$, phenomenologically expressed by a stretched exponential. Note that eq 31 has a general functional form basically equivalent to the approximation as given by eq 20 for decoupling the modes of motion associated with $\delta(t)$ and with $b_x(t)b_y(t)$. As shown in section 3, with δ_0 being allowed as an adjustable fitting parameter, eq 20 can give rise to a result in close agreement with what is obtained from the exact expression (eq 19). As opposed to the slow mode arising from the fluctuations of $b_x(t)b_y(t)$ in the simulation using eq 20, the Rouse theory is used to describe the slow mode directly here.

In the quantitative $J(t)$ line-shape analyses, the effect of the molecular-weight distribution $f(M)$ of the studied samples, even though very narrow, need be included into the calculation. The molecular-weight distribution is assumed to be described

by the Schulz function,[191] whose distribution width is characterized by the single parameter Z ($M_w/M_n = (Z+1)/Z$). As a fitting parameter, the Z values obtained from the quantitative line-shape analyses are typically within the expected range, giving $M_w/M_n \leq 1.05$;[3-5,25] for instance, $M_w/M_n = 1.05$ is obtained for sample C.[25] As the Monte Carlo simulation carried out in the present study is for an ideally monodisperse system, for making a comparison between experiment and simulation, we use the parameters obtained for a nearly monodisperse sample—sample C—to calculate the $G(t)$ curve expected for an ideally monodisperse system.

Affecting the entropic region of the $G(t)$ of a nearly monodisperse sample are Z and the frictional factor K. Being phenomenologically described by the stretched exponential form,

$$\mu_G(t/\tau_G) = \exp\left(-(t/\tau_G)^\beta\right); \quad 0 < \beta \leq 1 \tag{32}$$

the glassy-relaxation region of $G(t)$ is affected by the three parameters: A_G^f, τ_G and β. The role of τ_G can be equivalently represented by the average glassy-relaxation time as given by

$$\langle \tau \rangle_G = \int_0^\infty \mu_G(t/\tau_G)dt = \frac{\tau_G}{\beta}\Gamma(1/\beta) \tag{33}$$

---

[191] Schulz, G. V. *Z. Physik. Chem., Abst. B* **1943**, *43*, 25; Tung, L. H. *Polymer Fractionation*; Cantow, M. J. R Ed.; Academic: New York, 1967.

where Γ is the gamma function. Much dynamic and structural information related to the glass transition is contained in the shapes of the $J(t)$ or $G(t)$ curves, which change with temperature—the thermorheological complexity. The scheme of analysis is to use the Rouse theory as the reference frame in time, with respect to which the relative position of the glassy relaxation process can be studied[25] (The same scheme is used for the entangled system, where ERT is used as the reference frame instead of the Rouse theory[15]). As the relaxation times of all the Rouse normal modes are proportional to the frictional factor K, the relative position of the glassy-relaxation process can be conveniently characterized by the ratio of the average glassy-relaxation time to the friction factor

$$s' = \frac{\langle \tau \rangle_{\mathrm{G}}}{K'} \tag{34}$$

where K' in the most general way includes $K' = K$ for an entanglement-free system whose entropic region of $G(t)$ is described by the Rouse theory as well as represents the frictional factor in the Rouse–Mooney normal modes of motion of an entangled system.[192] It has been shown that the uneven thermorheological complexity observed in the $J(t)$ results of polystyrene is fully described by a simple increase in s' with decreasing temperature. Furthermore, it has been shown that both s' and K' values for the three studied samples, two entangled and one entanglement-free, as a function of

---

[192] Note: see ref 25 for the details.

the temperature difference from individual T_g, $\Delta T = T - T_g$, individually fall on the same curve, indicating that the T_g-related effect behaves in a universal way within the polystyrene system. s' reaches a plateau value of about 1500 at $\Delta T \geq 40^{\circ}$ and is about 40000 at $\Delta T = 0$ or at T_g.[25] It has been shown[15,16,25] that the increase in s' with decreasing temperature is due to the formation of a structure, whose length scale increases with decreasing temperature and greatly exceeds that of a single Rouse segment at T_g. The formation of the structure also indicates that non-ergodicity[15,16,25,193] gradually becomes an important effect as the temperature approaches T_g. The use of the Langevin equation in the present study implies that the system has to be ergodic.[3,34] Thus, the high-temperature limit s'=1500 is the one that should be used in calculating the $G(t)$ curve for comparison with the simulation result.

For polystyrene, the molecular weight for a single Rouse segment, m, is about 850;[6-16] with $M_w = 16400$, sample C is equivalent to a chain with 20 beads in average (see the note at ref 52).[194] Shown in Figure 11 is the comparison of the equilibrium-simulation $G(t)$ curve for a 20-bead Fraenkel chain with H_F=400kT and the expected "experimental" curve for an ideally monodisperse polystyrene with molecular weight equal to the M_w value of sample C at high temperatures—that is,

---

[193] Sillescu, H. *J. Non-Crystal. Solids* **1999**, *243*, 81; and references therein.

[194] Note: The weight-average molecular weight of sample C, $M_w = 16400$, is a little

higher than the entanglement molecular weight, $M_e = 13500$, for polystyrene.

However, as explained in detail in ref 25, because the molecular weight distribution of

sample C is not extremely narrow, its viscoelastic behavior in the entropic region has

to be analyzed in terms of the Rouse theory rather than the extended reptation theory.

calculated with $s'=1500$ for $\Delta T \geq 40^{\circ}$. As shown, the "experimental" curve is calculated using an arbitrary K value: 10^{-4}; and the simulation curve has been multiplied by a proper factor in both the modulus and time coordinates to obtain a close superposition between the two curves. As the shift factor along the time coordinate depends on the K value used in the calculation and the step-length d employed in the simulation, its value is of no particular meaning. However, the shift factor along the modulus coordinate is much related to the entropic nature of the slow mode as discussed in section 3 regarding the results shown in Figure 3. The vertical multiplication factor used for obtaining the close superposition is 4.2×10^7, which is very near the value 3.7×10^7 expected if the entropic region of the simulation $G(t)$ is in perfect agreement with the Rouse theory. The ratio of 3.7/4.2 also agree closely with the value 0.95 used to superpose the Rouse theoretical curve on the simulation $G_S(t)$ curve of the 20-bead Fraenkel chain shown in Figure 3. The agreement in the general shape between the two $G(t)$ curves is indeed very encouraging, considering the simplicity of the chain model used in the simulation. The discrepancy in the short-time region between the two curves may have to do with the choice of the H_F value. Although improving the agreement in the very short-time region, an increase in H_F leads to a faster relaxation rate for the fast mode, causing some disagreement in the lower part of the fast mode. As we don't believe that a mean-field chain model can really adequately describe the viscoelastic behavior of a polymer melt in the energetic-interactions region, where some sorts of intermolecular interactions should contribute to the modulus as well, we don't think a fine tuning of the H_F value would serve a particularly meaningful purpose.

In Figure 11, the relaxation times of the 19 Rouse normal modes for a 20-bead chain are also indicated. As contrasted with the positions in time of these relaxation times, the relaxation of the tension on the Fraenkel segment as revealed by the simulation has basically finished before the highest Rouse mode begins to relax in a substantial way. As explained above, the simulation result is only applicable to a polymer system at temperatures sufficiently above T_g. As opposed to such a situation, the glassy-relaxation process as extracted from the measured creep compliance $J(t)$ at T_g extends to times much larger than the relaxation time of the highest Rouse mode, indicating vitrification at the Rouse-segmental level.[15,16,25]

6. **Discussion**

Two distinct relaxation modes of fundamentally different physical nature have been observed in both the equilibrium-simulation and step strain-simulation $G_S(t)$ curves for the Fraenkel chains. The general agreements between the two sets of results are basically in accordance with the fluctuation-dissipation theorem; the small differences between the two may be due to the fact that the dynamic quantity $J_{xy}(t)$ is actually a product of two parts with very different time dependence and strain dependence (opposite in sign, as clearly visible in the nonlinear region studied in the companion paper) and the difference in coupling between the two kinds of dynamics. Regarding the general agreement between the equilibrium-simulation and step strain-simulation $G_S(t)$ curves as representing a quasi version of the fluctuation-dissipation theorem, we may conclude: While the fast mode arises from

the segment-tension fluctuations or reflects the relaxation of the segment-tension arising from segments being stretched by the applied step strain—thus, an energetic interactions-derived dynamic process, the slow mode arises from the fluctuating segmental-orientation anisotropy or represents the randomization of the segmental-orientation anisotropy induced by the step deformation—thus, an entropy-derived dynamic process. Segmental orientation anisotropy being responsible for the entropic nature of the slow mode in the Fraenkel-chain case is an important conclusion derived from this study, indicating that in modeling the polymer viscoelastic behavior one does not need to put the entropic-force constant into the segment to obtain the modes of motion as occurring in the Rouse theory, which is well-known to describe very well the linear viscoelastic behavior in the long-time (entropic) region of the entanglement-free polymer system.

The proper size that can be assigned to a Rouse segment of a particular polymer has been studied in recent years by different techniques.[6-16] In the studies analyzing the whole range of the viscoelastic response, covering both the glassy-relaxation and entropic regions, it is in general assumed that $G(t)$ is expressed as a sum of the dynamic processes derived from energetic interactions and entropy. Using the quantitatively successful description of the entropic region of the linear viscoelastic response by ERT in the entangled case and by the Rouse theory in the entanglement-free case as the reference frame in time, the incorporation of a stretched exponential form (eq 32) into ERT or the Rouse theory (see eq 31) as detailed previously[15,25] and summarily described in the previous section has allowed us to analyze the glassy-relaxation process occurring in the short-time region in a

meaningful and profitable way, revealing the basic mechanism of the thermorheological complexity and showing that the effect as related to the glass transition behaves in a universal way within the polystyrene system, entangled or not.[15,16,25]   As opposed to the incorporation of the glassy-relaxation process into ERT or the Rouse theory being done phenomenologically, the segment-tension relaxation process emerges naturally on the top of the slow mode in the simulated $G_S(t)$ curve for the entanglement-free Fraenkel chain as presented in this study.   Very significantly, the curves calculated from the Rouse theory, which describe the slow mode very well, are each based on a chain with the *same* number of beads; the close agreement between simulation and theory indicates that the size of the Fraenkel segment is the same as that of the Rouse segment.   In other words, this result strongly suggests that the size that can be properly assigned to a "Rouse segment" for describing the *linear* entropic viscoelastic response actually has a considerable degree of rigidity.   The general agreement between the simulated and experimental $G(t)$ curves as shown in Figure 11 supports such a picture.   As will be shown in the companion paper, in spite of the rigidity in such a "Rouse segment," the slow mode as occurring in the nonlinear $G_S(t,\lambda)$ is as much of entropic nature as in the linear $G_S(t)$.

7. Summary

In this study, based on the entanglement-free Rouse-chain and Fraenkel-chain models, we have carried out Monte Carlo simulations of relaxation modulus in the equilibrium state and following a step shear deformation.   In the case of the Rouse chain, the validity of the simulation is confirmed by the agreement with the analytical

results; the fluctuation-dissipation theorem is also perfectly illustrated by the comparison of results from both kinds of simulations. In the case of the Fraenkel chain, while a quasi version of the fluctuation-dissipation theorem is illustrated; two distinct modes of relaxation in the relaxation modulus are revealed, describing the basic features as typically observed in an experimentally measured $G(t)$.   The physical natures of the two modes are analyzed in detail: The fast one corresponding to the segment-tension fluctuation or relaxation is classified as an energetic interactions-derived process; and the slow one well described by the Rouse theory is classified as entropy-derived.   A very important concept derived from this study is that segmental-orientation anisotropy is responsible for the entropic nature of the slow mode; in other words, in modeling one does not need to put the entropic-force constant into the segments in order to obtain the modes of motion as occurring in the Rouse theory.   From the comparison of the Rouse theory with the slow mode obtained from the simulation, it is shown that basically one Fraenkel segment substitutes for one Rouse segment.   This conclusion provides an explanation resolving a long-standing fundamental paradox in the success of modern molecular theories of polymer viscoelasticity developed based on the Rouse segment as the most basic structural unit, as the entropic-force constant on the Rouse segment is generally regarded as too soft from considering the persistence length or the Kuhn segment length of a polymer chain—the Fraenkel chain is basically equivalent to the freely jointed chain.   As listed in Table 1 of ref 8, the Rouse segment size m for various polymers is of the same order of magnitude as that of the Kuhn segment M_K. The authors of ref 8 have particularly pointed out such a paradox between $m \approx M_K$ and the definition of a Rouse segment based on the Gaussian probability distribution in

the Rouse chain model.[1-3] Furthermore, the comparison of the simulation with the experimental result strongly suggests that, even though still being a mean-field single-chain model, the Fraenkel chain has captured the key interactions in a polymer system, having the potential of serving as a more realistic substitute for the Rouse model.

Acknowledgement

Appendix A: The Application of the Virial Theorem to the Fraenkel Dumbbell.

The average kinetic energy for each degree of freedom being $kT/2$ is a built-in element of the Langevin equation.[40] For simplicity, we consider the Fraenkel dumbbell case; however, the analysis as presented here can be extended to a Fraenkel chain with any number of beads. For a dumbbell, according to the virial theorem[45] $\overline{T} = -\frac{1}{2}\sum_{i=1}^{2}\overline{\mathbf{F}_i \cdot \mathbf{R}_i} = \frac{H_F}{2b_0^3}\overline{\delta(t)\mathbf{b}(t)\cdot\mathbf{b}(t)}$; here $\overline{T}$ is the average internal kinetic energy and is $\frac{3kT}{2}$. This relation is confirmed by our simulation. Since as indicted by the simulation $\mathbf{b}(t)\cdot\mathbf{b}(t)$ does not fluctuate more than 10% from its mean value, which is only larger than b_0^2 by less than 1.3%, the virial theorem for the Fraenkel dumbbell can be well represented by

$$\frac{H_F}{b_0}\overline{\delta(t)} = 3kT \qquad (A1)$$

160

For $H_{\mathrm{F}} = 400kT$, $\overline{\delta(t)} = 0.0075$.

Figure Captions

Figure 1

Comparison of the equilibrium-simulation $G_S(t)$ curves of two-bead, five-bead and ten-bead Rouse chains ($\triangle$ for $N=2$; $\square$ for $N=5$; $\bigcirc$ for $N=10$) with the step strain-simulation $G_S(t)$ results ($\blacktriangle$ for $N=2$; $\blacksquare$ for $N=5$; $\bullet$ for $N=10$) and the Rouse theoretical curves ($---$ for $N=2$; $---$ for $N=5$; $\underline{\quad\quad}$ for $N=100$).

Figure 2

Comparison of the equilibrium-simulation $G_S(t)$ curves of the five-bead Fraenkel chain using the step length $d=0.01$ ($\underline{\quad\quad}$) and $d=0.03$ ($\bigcirc$).

Figure 3

Comparison of the equilibrium-simulation $G_S(t)$ curves of two-bead, five-bead, ten-bead and twenty-bead Fraenkel chains ($\triangle$ for $N=2$; $\diamond$ for $N=5$; $\square$ for $N=10$ and $\bigcirc$ for $N=20$) with the Rouse theoretical curves ($---$ for $N=2$; $---$ for $N=5$; $--$ for $N=10$ and $\underline{\quad\quad}$ for $N=20$). See the text.

Figure 4

Comparison of the time correlation function $\langle \mathbf{b}(0) \cdot \mathbf{b}(t) \rangle$ obtained from the simulation on the Fraenkel dumbbell ($\bullet$) and multiplied by 1.45 along the time coordinate with the theoretical curve of the Rouse dumbbell ($\underline{\quad\quad}$).

Figure 5

The equilibrium-simulation $G_S(t)$ curves of the Fraenkel dumbbell: exact (using eq 19; —) and approximations (using eq 20 with $\delta_0 = \delta_N = 0.0022$, △; $\delta_0 = \delta_V = 0.0075$, □; and $\delta_0 = \delta_F = 0.01$, ○).

Figure 6

Time-correlation functions $\langle \delta(0)\delta(t) \rangle$ obtained from simulation on the Fraenkel dumbbell with $\delta(t)$ defined by eq 21: △ with $\delta_0 = \delta_N = 0.0022$; □ with $\delta_0 = \delta_V = 0.0075$; and ○ with $\delta_0 = \delta_F = 0.01$.

Figure 7

Comparison of the equilibrium-simulation $G_S(t)$ (● based on eq 28) and $G_S^{self}(t)$ (○ based on eq 29) for the five-bead Fraenkel chain; also shown are the equilibrium-simulation $G_S(t)$ (—) and $G_S^{self}(t)$ (- - -) for the five-bead Rouse chain.

Figure 8

Comparison of the step strain-simulation $G_S(t)$ curves for the two-bead, five-bead, ten-bead and twenty-bead Fraenkel chain at $\lambda = 0.2$ (△ for $N=2$; ◇ for $N=5$; □ for $N=10$; ○ for $N=20$) and 0.5 (▲ for $N=2$; ◆ for $N=5$; ■ for $N=10$; ● for $N=20$) with the equilibrium-simulation curve (- - - for $N=2$; – – – for $N=5$; – – for $N=10$; —— for $N=20$).

Figure 9

Comparison of the step strain-simulation $G_S(t)$ curves for the Fraenkel dumbbell at $\lambda=0.004$ ($\bigcirc$) and 0.2 ($\triangle$) with the equilibrium-simulation curve (——).

Figure 10

The time-step dependences of $\langle \mathbf{b}^2(t) \rangle$ and the components $\langle b_x^2(t) \rangle$, $\langle b_y^2(t) \rangle$ and $\langle b_y^2(t) \rangle$ for the five-bead Fraenkel chain following a step strain $\lambda=0.5$.

Figure 11

Comparison of the equilibrium-simulation $G(t)$ curve ($\mathbf{o}$) for the 20-bead Fraenkel chain with $H_F=400kT$ and the expected "experimental" curve (——) for an "ideally monodisperse polystyrene sample" with the molecular weight equivalent to $N=20$; also shown are the points ($+$) representing the relaxation times of the 19 Rouse normal modes. See the text.
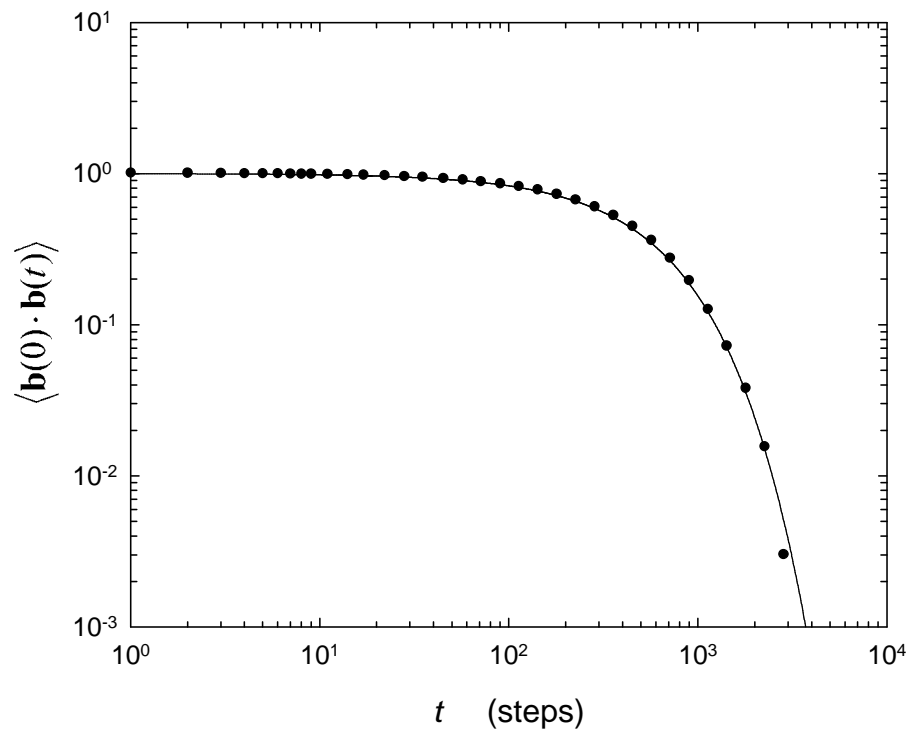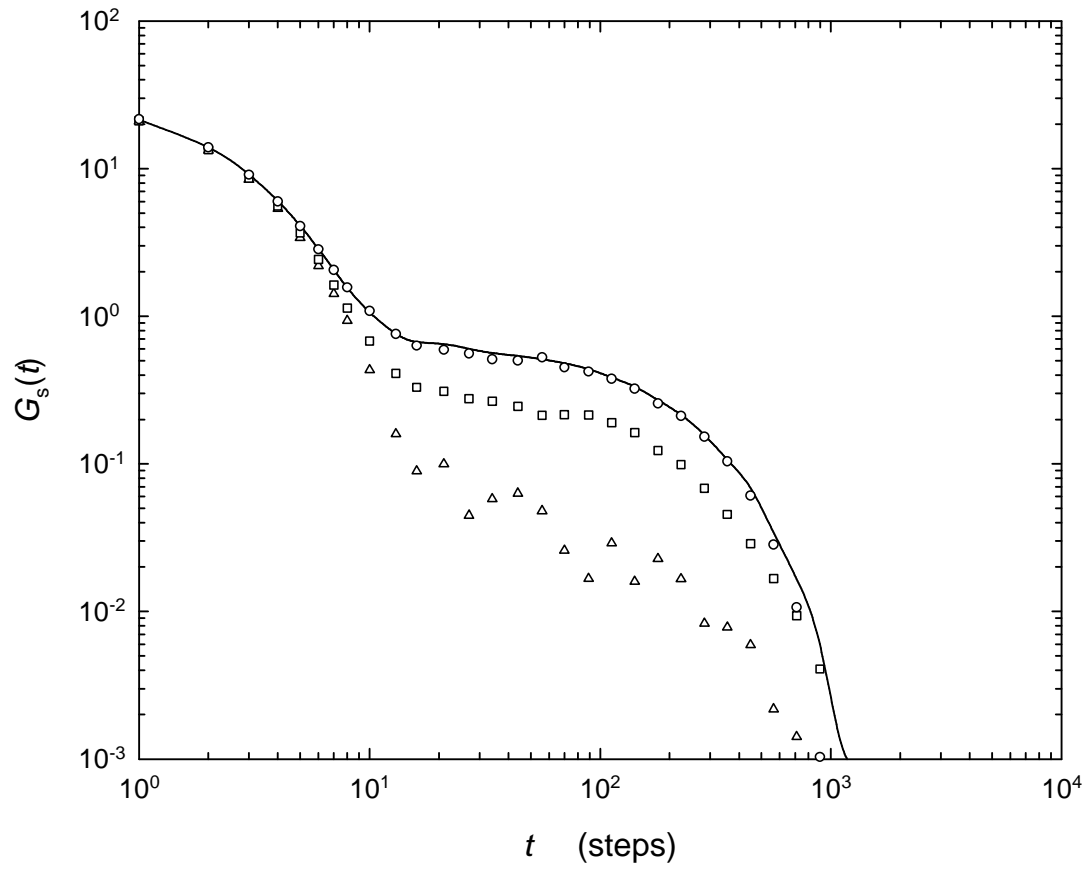
Figure 1

Figure 2

166

Figure 3

Figure 4

Figure 5

Figure 6

The figure shows a log-log plot with t (steps) on the horizontal axis ranging from 10^0 to 10^4, and $\langle \delta(0)\delta(t) \rangle$ on the vertical axis ranging from 10^{-6} to 10^{-2}.
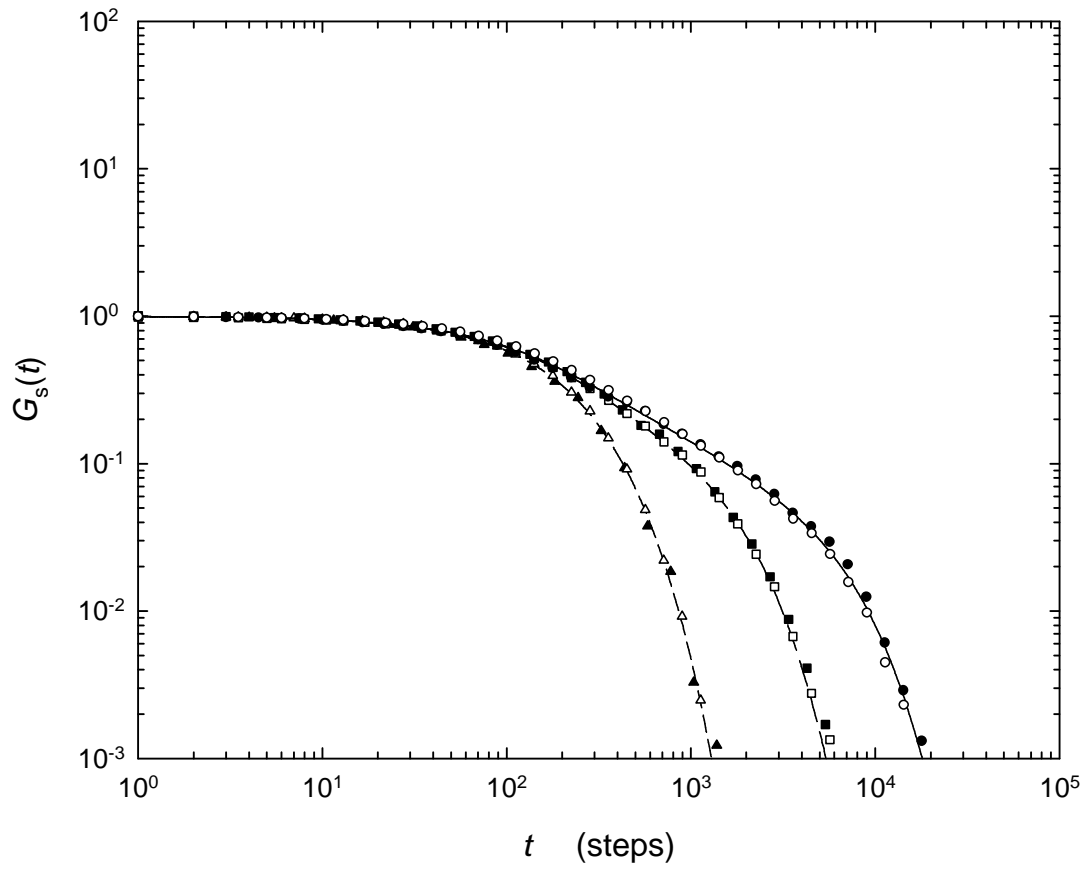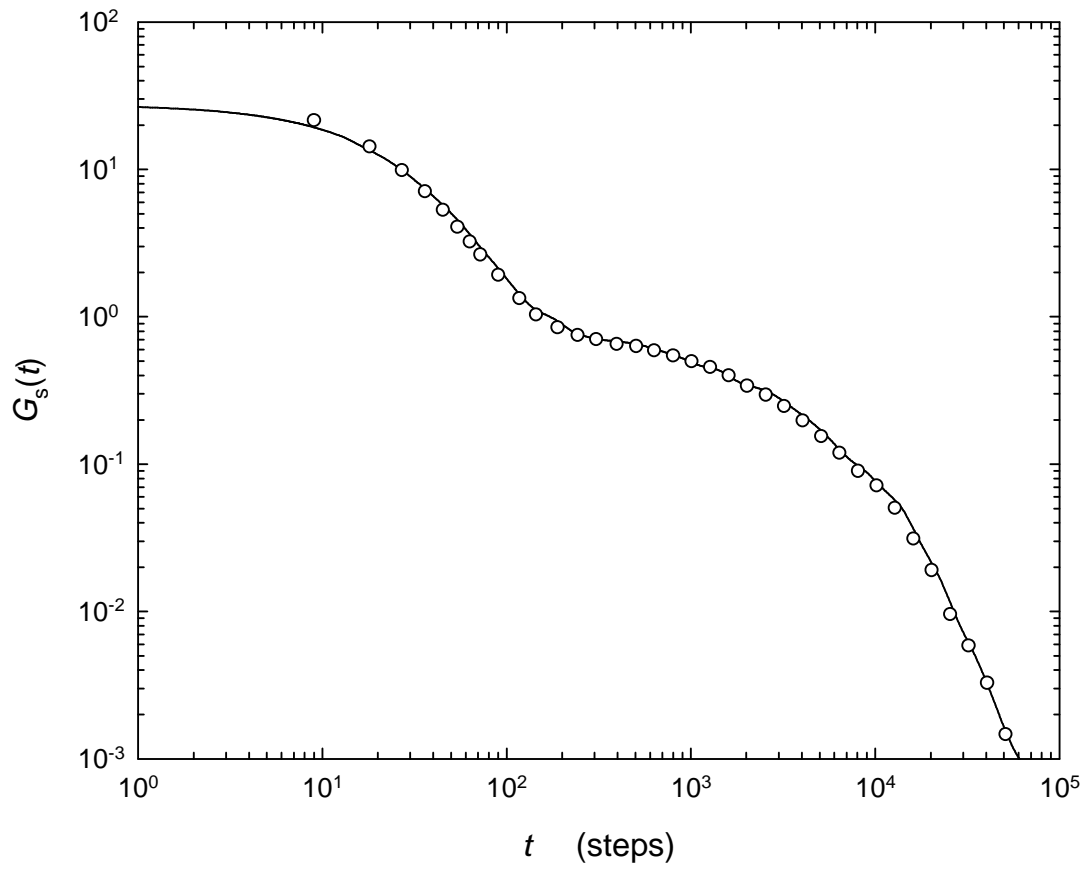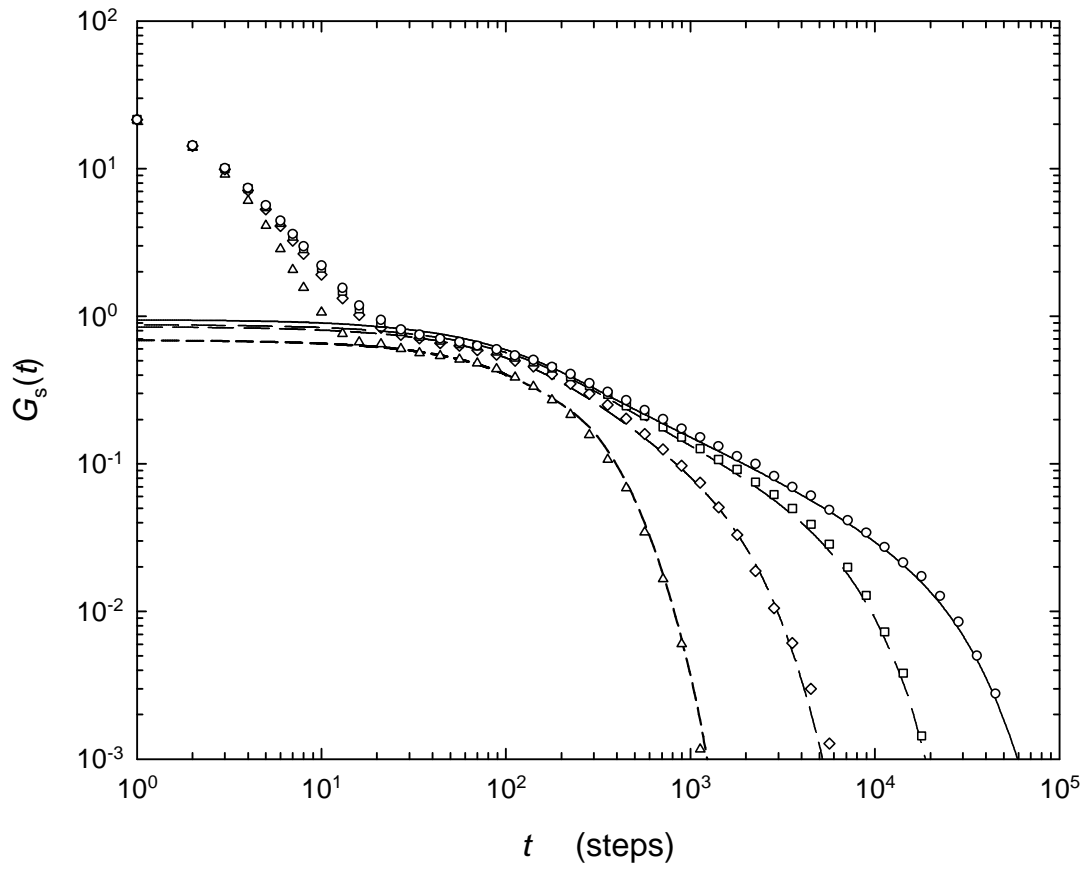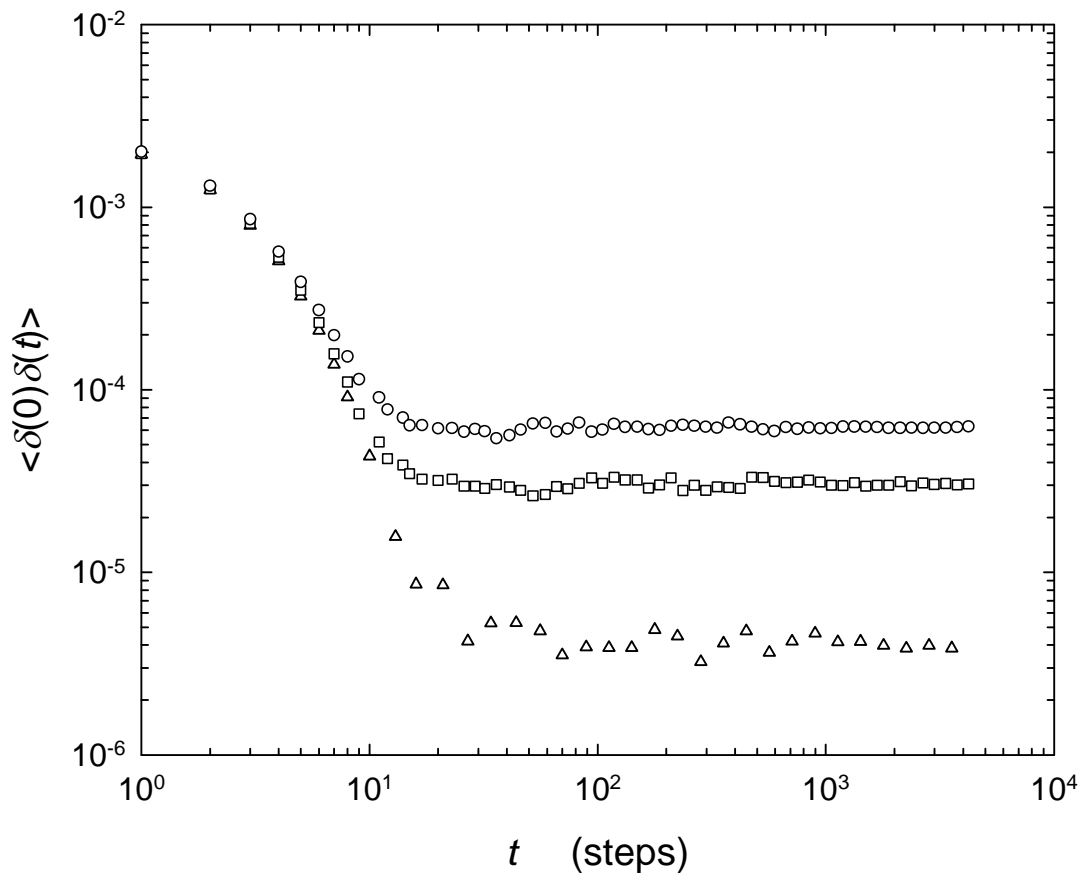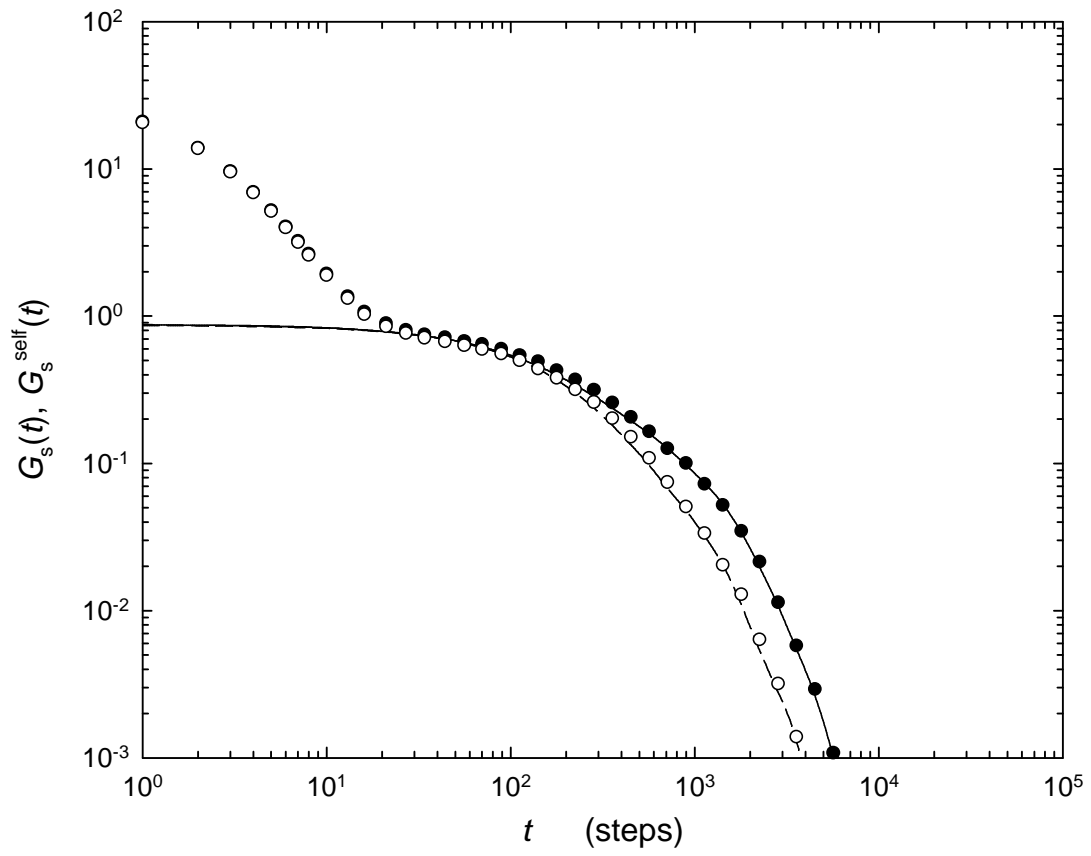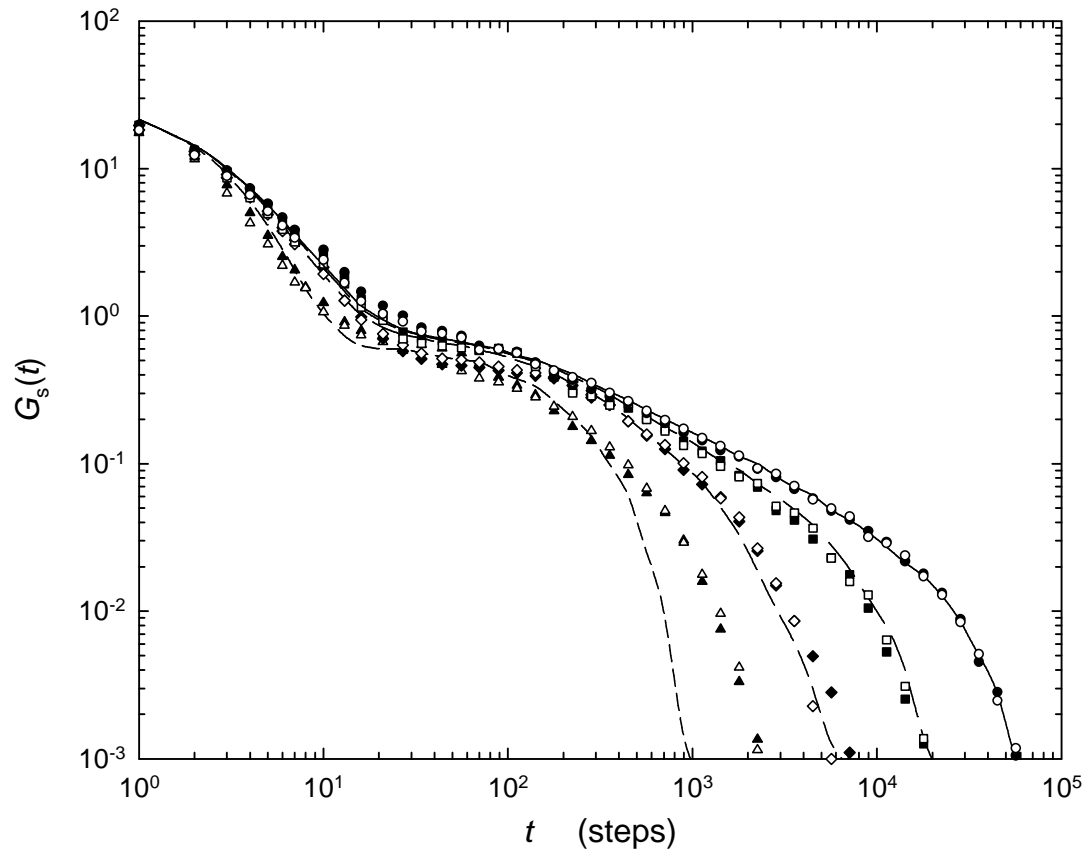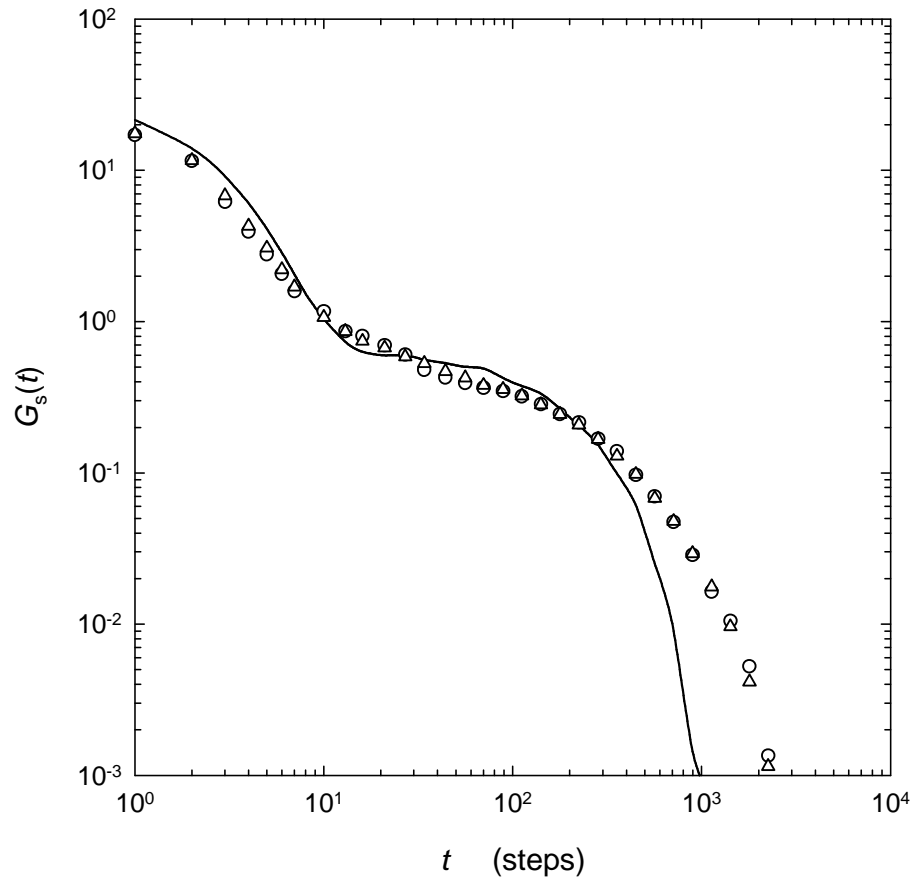
Figure 7

Figure 8

Figure 9

Figure 10
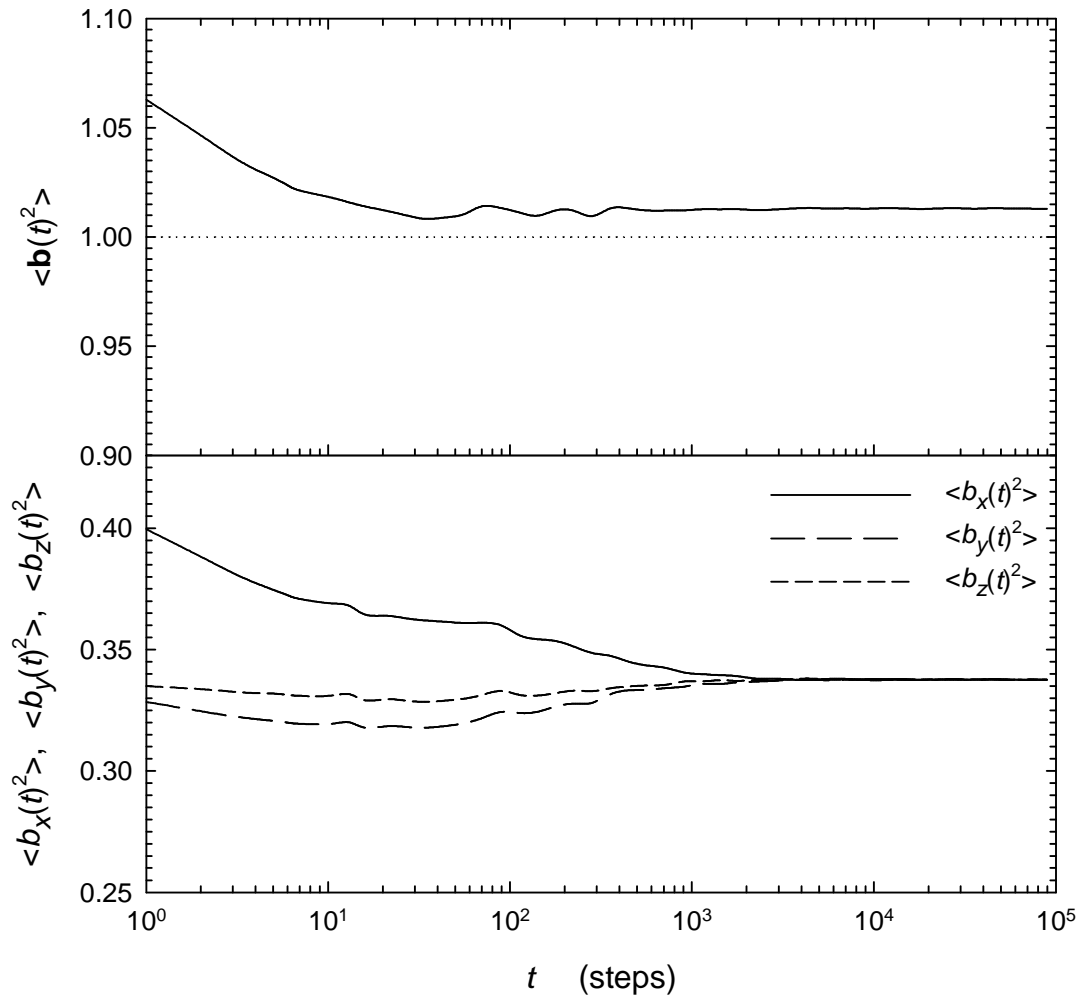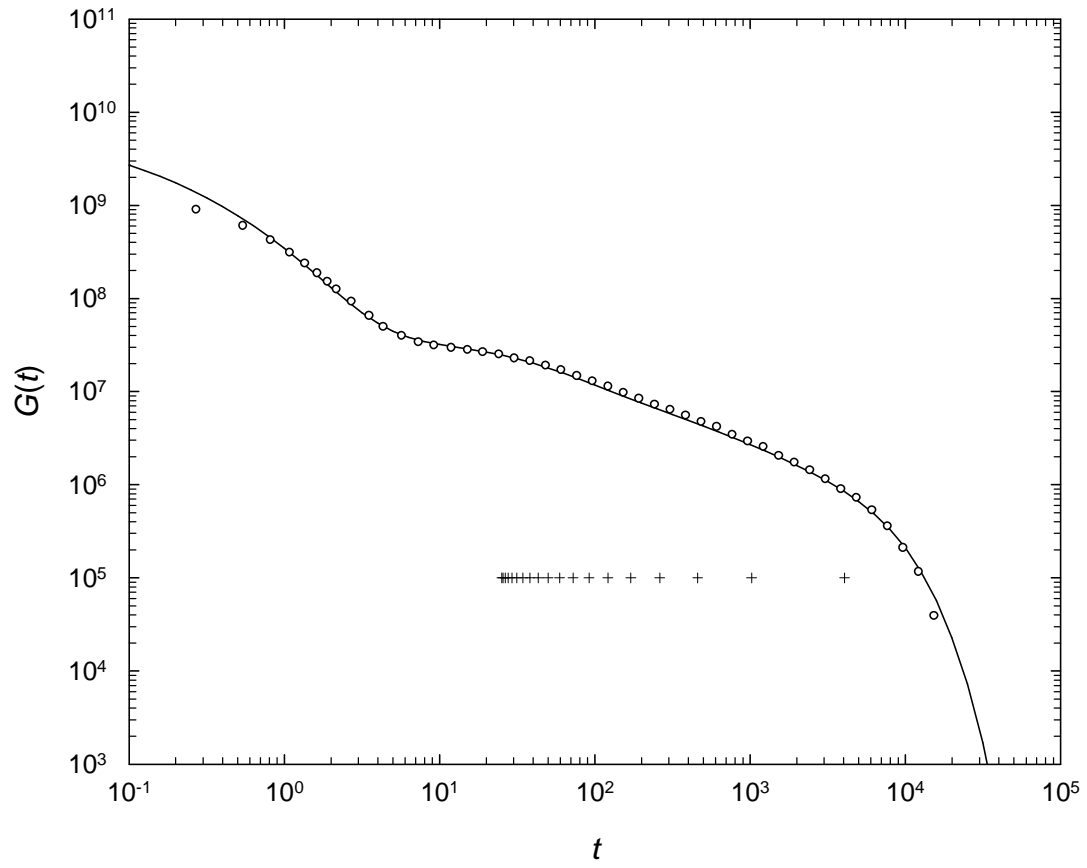
Figure 11

Monte Carlo Simulations

of Stress Relaxations of Entanglement-Free Fraenkel Chains. 2:

Non-Linear Polymer Viscoelasticity

Y.-H. Lin and A. K. Das

Department of Applied Chemistry

National Chiao Tung University

Hsinchu, Taiwan

Abstract

The non-linear viscoelastic behavior of the Fraenkel-chain model is studied with respect to the constitutive equation of the Rouse model.   Distinctly different from the results of the Rouse model, the Fraenkel-chain model gives the following characteristic non-linear behavior: (a) The two modes of dynamics in the relaxation modulus $G_S(t, \lambda)$ — as observed in the linear region reported in paper 1 — or in the first normal-stress difference function $G_{\Psi 1}(t, \lambda)$ are shown to have different strain dependences: strain-hardening for the fast mode and strain-softening for the slow mode. (b) The Lodge−Meissner relation $G_S(t, \lambda) = G_{\Psi 1}(t, \lambda)$ is shown both analytically and by simulation to hold over the whole time of relaxation.   (c) The second normal-stress difference is nonzero, being positive in the fast-mode region and becoming negative in the slow-mode region.   Making detailed comparison between

orientation and stress for all tensor components, the strong correlation of the slow mode with the segmental-orientation anisotropy and its entropic nature are shown to be the same as in the linear region studied in paper 1. A consequence of this correlation is the expectation of the stress-optical rule in the slow-mode region. Another consequence is the expectation that the damping function $h(\lambda) = G_S(t,\lambda)/G_S(t,\lambda \to 0)$ and the ratio between the first and second normal-stress differences $- N_2(t,\lambda)/N_1(t,\lambda)$ are described by the orientation tensor which has the same form as that of Doi and Edwards with independent alignment approximation; the simulation results are in close agreement with the calculated in the former case while roughly in the latter case.

Monte Carlo Simulations

of Stress Relaxations of Entanglement-Free Fraenkel Chains. 2:

Non-Linear Polymer Viscoelasticity

Y.-H. Lin and A. K. Das

Department of Applied Chemistry

National Chiao Tung University

Hsinchu, Taiwan

1.   Introduction

In paper 1,[195] the linear viscoelastic behavior for Fraenkel chains[196] has been studied by Monte Carlo simulations, revealing two modes of motion in the relaxation modulus $G_S(t)$: The fast mode arises from the segment-tension fluctuations or reflects the relaxation of the segment tension arising from segments being stretched by the applied step deformation—an energetic interactions-derived dynamic process; the slow mode arises from the fluctuating segmental-orientation anisotropy or represents the randomization of the induced segmental-orientation anisotropy—an entropy-derived dynamic process.   Very significantly the slow mode is well described by the Rouse theory[197,198,199] in all aspects: the magnitude of modulus, the line shape and the

---

[195] Lin, Y.-H.; A. K. Das, the companison paper.

[196] Fraenkel, G. K. *J. Chem. Phys.* **1952**, *20*, 642.

[197] Rouse, P. E. Jr. *J. Chem. Phys.* **1953**, *21*, 1271.

number-of-beads dependence of the relaxation time.   This result means that as far as the slow mode is concerned, one Rouse segment may be replaced by one Fraenkel segment, even though the latter is much stiffer than the former.   Furthermore, the comparison of the simulated relaxation modulus with experimental $G(t)$ indicates that the Fraenekel-chain model has captured the key energetic interactions in a polymer melt, allowing the relative positions of the glassy-relaxation process (the fast mode) and the entropy-derived Rouse relaxation (the slow mode) properly described. This general agreement between simulation and experiment is consistent with the well-confirmed success of the Rouse theory in explaining the linear viscoelastic response of an entanglement-free polymer melt system in the long-time or entropic region.[5,200,201,202]   Since the Fraenkel-chain model provides improvements in linear viscoelasticity upon the Rouse model, its non-linear viscoelastic response obtained from the Monte Carlo simulations may be profitably analyzed in comparison with the constitutive equation of the Rouse model.

2.   Constitutive Equation of the Rouse Model

[198]   Bird, R. B.; Curtiss, C. F.; Armstrong, R. C.; Hassager, O. *Dynamics of Polymeric Liquids, Vol.* 2, *Kinetic Theory,* 2nd ed.; Wiley: New York, 1987.

[199]   Lin, Y.-H. *Polymer Viscoelasticity: Basics, Molecular Theories, and Experiments*; World Scientific: Singapore, 2003.

[200]   Lin, Y.-H. *Macromolecules* **1987**, *20*, 885.

[201]   Lin, Y.-H.; Juang, J.-H. *Macromolecules* **1999**, *32*, 181

[202]   Lin, Y.-H. *J. Phys. Chem. B*

The constitutive equation of the Rouse model with each chain having N beads (corresponding to molecular weight M) is given by[4,5]

$$\boldsymbol{\sigma}(t) = ckT \int_{-\infty}^{t} \left(\frac{1}{\tau_p} \right) \sum_{p=1}^{N-1} \exp\left[-\frac{(t-t')}{\tau_p} \right] \boldsymbol{\gamma}_{[0]}(t,t') dt' \tag{1}$$

where $\boldsymbol{\gamma}_{[0]}(t,t') = \boldsymbol{\delta} - \mathbf{E}(t,t') \cdot \mathbf{E}(t,t')$ with $\mathbf{E}(t,t')$ being the deformation gradient tensor between the present time t and a past time t'; c is the number of polymer chains per unit volume; and τ_p, the relaxation time of the p-th mode, is given by eq 11 of the companion paper.[1] For comparison with the Monte Carlo simulation of a single chain in the mean field, both c and kT are set to be 1; and τ_p is expressed in terms of the time-steps as given by eq 12 of the companion paper.

Following a step shear deformation $\mathbf{E}$ at time $t=0$ (eq 4 of the companion paper), the relaxation modulus $G_S(t)$ and the first normal-stress difference function $G_{\Psi 1}(t)$ of the Rouse model, both normalized to that corresponding to a single segment, are given, respectively, as

$$G_S(t) = -\frac{\sigma_{xy}}{\lambda(N-1)} = \frac{1}{(N-1)} \sum_{p=1}^{N-1} \exp\left[-\frac{t}{\tau_p} \right] \tag{2}$$

and

$$G_{\Psi 1}(t) = -\frac{\sigma_{xx}(t,\lambda) - \sigma_{yy}(t,\lambda)}{\lambda^2 (N-1)} = \frac{1}{(N-1)} \sum_{p=1}^{N-1} \exp\left[-\frac{t}{\tau_p}\right] \tag{3}$$

The key results expected from the constitutive equation of the Rouse model may be summarized as in the following:

(1) No non-linear effect in the shear stress relaxation; in other words, $G_S(t)$ as given by eq 2 is independent of strain λ.

(2) The observation of the Lodge–Meissner relation;[203] namely, as indicated by eqs 2 and 3, $G_S(t) = G_{\Psi 1}(t)$.

(3) The second normal-stress difference as defined by $-\left(\sigma_{yy}(t,\lambda) - \sigma_{zz}(t,\lambda)\right)$ is zero.

These results of the Rouse model are exactly confirmed by our simulations; in Figure 1, the strain independence of $G_S(t)$ and $G_{\Psi 1}(t)$ for a five-bead Rouse chain and the agreements of the simulation results with the theoretical Rouse curve are shown.

3. Nonlinear Viscoelastic Behavior of the Fraenkel Chain

For the Fraenkel chain, the simulations of stress components as a function of time-step following a step shear deformation are done in the same way as for obtaining the relaxation modulus $G_S(t) = -\sigma_{xy}(t)/\lambda$ in the companion paper. As shown in Figure 2, the $G_S(t,\lambda)$ curves obtained for a five-bead chain at different strains from $\lambda = 0.5$ to 4 indicate that the relaxation modulus of the Fraenkel-chain model is strain-dependent as opposed to $G_S(t)$ being independent of the strain in the

---

[203] Lodge, A. S.; Meissner, J. *Rheol. Acta* **1972**, *11*, 351.

Rouse model. However, as also shown in Figure 2, the Lodge–Meissner relation is followed even though nonlinear effect occurs to both $G_S(t,\lambda)$ and $G_{\Psi 1}(t,\lambda)$.   As shown in Figure 3, unlike in the Rouse model, the second normal-stress difference $N_2(t,\lambda)$ in the Fraenkel-chain model is not zero. Thus, the Fraenkel-chain model exhibits significant deviations in the nonlinear viscoelastic behavior from the Rouse model, even though its linear relaxation modulus in the long-time region is well described by the Rouse theory.   Below, we analyze these deviations as caused by the particular form of the Fraenkel potential.

4.   Effects of the Nonlinear Tensile Force on the Fraenkel Segment

A large tensile force on the Fraenkel segment is created when it is significantly stretched, which leads to the stress level showing up in the fast mode region. The strain-hardening of the fast mode as shown in Figure 2 can be understood by examining the tensile force $\mathbf{F}_F$ on a Fraenkel segment denoted by $\mathbf{b}$:

$$\mathbf{F}_F = -\frac{H_F}{b_0^2}\mathbf{b} + \frac{H_F}{b_0}\left[\frac{\mathbf{b}}{|\mathbf{b}|}\right] = -H_F\frac{\delta(t)}{b_0^3}\mathbf{b} \tag{4}$$

where $\delta(t)$ is defined by eq 16 of the companion paper.   As shown in Figure 4, right after the application of a step shear to the Fraenkel chain at equilibrium, a $\left|\mathbf{b}(t=0)\right|$ value larger than b_0 (set equal to 1) in average is created; as a result, the second term of eq 4 becomes smaller than the first term, leading to a tensile force that would pull the two separated beads back to the equilibrium distance−a recoiling effect.   In the

182

equilibrium simulation as studied in paper 1, $\delta(t)$ is used to represent approximately the deviation of the bond length $|\mathbf{b}|$ from the b_0 value. For the present study in the nonlinear region, $\delta(t)$ is treated more as a parameter, characterizing the nonlinear enhancement of the tensile force on the segment as the segment is significantly stretched.

As will be shown below (Figure 6), when the applied shear strain λ is greater than ~0.005, the average tensile force starts to increase in a nonlinear way, causing the stress level of the fast mode region to increase nonlinearly as well.   Besides this obvious expectation, this effect leads to the emergence of the second normal-stress difference. The second normal-stress difference is of significant magnitude in the fast-mode region; as the time enters the slow-mode region, it declines towards the zero line and beyond; and finally relaxes as a negative tail.   This effect can be understood from the following analysis:

The use of the Langevin equation has implied that our studied system is ergodic.[5,204,205] Thus, we shall simply use the language of the ensemble averaging to discuss the results obtained from averaging the behavior of a single chain over time in the equilibrium state or over the repeating cycles following the step deformation. As obtained from the equilibrium simulation the mean squared bond length $\left\langle \mathbf{b}^2 \right\rangle_0$ is only

[204] Doi, M.; Edwards, S. F. *The Theory of Polymer Dynamics*; Oxford Univ. Press: New York, 1986.

[205] McQuarrie, D. A. *Statistical Mechanics*; Harper & Row: New York, 1976.

larger than $b_0^2 = 1$ by 1.3%; the ensemble-averaged components of $\langle \mathbf{b}^2 \rangle_0$ are identical:

$\langle b_x^2 \rangle_0 = \langle b_y^2 \rangle_0 = \langle b_z^2 \rangle_0 = 0.3377$. However, in the ensemble different segments have

different b_x^2, b_y^2 and b_z^2 values. Among the segments with the same b_x^2, those with

larger b_y^2 are expected to have a smaller b_z^2. Following the step shear deformation,

those segments with a larger b_y^2 and a smaller b_z^2 will be stretched more, leading to

nonlinear enhancements in their tensile forces as characterized by the parameter $\delta(t)$,

than those with a smaller b_y^2 and a larger b_z^2. Since the contribution of a segment to

the normal stress in the y direction is proportional $\delta(t)b_y(t)^2$ at time t, the average of

the initial value $\delta(0)b_y(0)^2$ (right after the application of the step strain) is much

more weighted by those segments with larger b_y^2; the opposite can be said about the

normal stress in the z direction. As a result, the effect leads to a positive second

normal-stress difference, $N_2(t) > 0$, in the short-time or fast-mode region, as shown in

Figure 3. Such an effect will not occur to a Rouse segment, whose tensile force

increases with bond length linearly.

As explained above, the segmental tensile force created by the step deformation

will shrink the segmental length back to its equilibrium value. Those segments with a

larger y component initially having larger tensile forces will be most affected by the

recoiling effect. Right after the step shear deformation, the average

$\langle b_x(0)^2 \rangle, \langle b_y(0)^2 \rangle$, and $\langle b_z(0)^2 \rangle$ values in accordance with the affine deformation are

expected to be given, respectively, by $\langle b_x^2(t=0) \rangle = \langle b_x^2 \rangle_0 + \lambda^2 \langle b_y^2 \rangle_0 = 0.3377(1+\lambda^2)$;

$\left\langle b_y^2(t=0) \right\rangle = \left\langle b_y^2 \right\rangle_0 = 0.3377$; and $\left\langle b_z^2(t=0) \right\rangle = \left\langle b_z^2 \right\rangle_0 = 0.3377$. The average values

of $\left\langle b_x(0)^2 \right\rangle, \left\langle b_y(0)^2 \right\rangle$, and $\left\langle b_z(0)^2 \right\rangle$ obtained right after the step deformation from the

simulations are in close agreement with the expected values at different strains. As the

chain configuration evolves according to the Langevin equation, the recoiling effect

causes all the $\left\langle b_x(t)^2 \right\rangle, \left\langle b_y(t)^2 \right\rangle$, and $\left\langle b_z(t)^2 \right\rangle$ values to decline, as shown in Figure 5.

Due to the nonlinearly enhanced tensile force associated with segments with

larger b_y^2 initially, $\left\langle b_y(t)^2 \right\rangle$ decreases faster than $\left\langle b_z(t)^2 \right\rangle$ before $\left\langle \mathbf{b}(t)^2 \right\rangle$ reaches

its equilibrium value at a time which is about the end of the fast mode, as shown in

Figure 4.   As $\left\langle \mathbf{b}(t)^2 \right\rangle$ reaches its equilibrium value, $\left\langle b_y(t)^2 \right\rangle$ and $\left\langle b_z(t)^2 \right\rangle$ also

reach their respective minimum points, meaning no more recoiling effect.   Due to its

fast declining rate from the very beginning, $\left\langle b_y(t)^2 \right\rangle$ is smaller than $\left\langle b_z(t)^2 \right\rangle$ at the

end of the recoiling effect.   At about this point the second normal-stress difference

crosses the zero line and becomes negative.   In this region of time, even though there

is still a significant degree of segmental orientation anisotropy, the tensile force on the

segment is of the value in an equilibrium state.   As a result the negative values of the

second normal stress difference in the region are of small magnitude as shown in

Figure 3.   The above described mechanism of the chain dynamics as revealed in the

results shown in Figures 2 to 5 becomes more prominently visible as the applied strain

λ increases.

5.   The Lodge−Meissner Relation for The Fraenkel Chain

The relation $G_S(t, \lambda) = G_{\Psi 1}(t, \lambda)$ first proposed by Lodge and Meissner was based on a phenomenological argument. However, the Lodge–Meissner relation observed for the Fraenkel-chain model from the simulation as shown in Figure 2 can be proved analytically. This is done from considering the configurations of all the chains in a finite volume V as changed by the applied step deformation and their subsequent evolution.

Consider a volume containing c Fraenkel chains, each with N beads. Right after the application of a step shear deformation $\mathbf{E}$ (eq 4 of the companion paper) to a system at equilibrium, the shear stress, $-\sigma_{xy}(0_+)$, is given by (setting $kT = 1$)

$$
-\sigma_{xy}(0_+) = \frac{c(N-1)}{V} \left\langle T_x(0_+) b_y(0_+) \right\rangle
$$

$$
= \frac{H_F}{V b_0^3} \sum_k^c \sum_s^{N-1} \delta_s^k(\lambda) \left(b_{s,x}^{o,k} + \lambda b_{s,y}^{o,k} \right) \left(b_{s,y}^{o,k} \right)
$$

(5)

where T_x denotes the x component of the tensile force $\mathbf{F}_F$ on a representative Fraenkel segment in the ensemble; $b_{s,\alpha}^{o,k}$ ($\alpha = x, y$) denotes specifically the α component of the s-th segment on the k-th chain of the system in an equilibrium state right before the application of the deformation $\mathbf{E}$. Because of the presence of $\delta_s^k(\lambda)$, which depends on the applied strain and the orientation of the segment, the summation of the terms containing the products of $b_{s,x}^{o,k}$ and $b_{s,y}^{o,k}$ over all segments is not zero. In the Rouse model, as $\delta_s^k(\lambda)$ is a constant, the sum equals to zero. Because at equilibrium $\left\langle \mathbf{b}^2 \right\rangle = 1.013 b_0^2$, we may conveniently regard each segment as having a

unit length before the initial step deformation is applied (the unit length is not a required assumption to prove the Lodge–Meissner relation as given below for the Fraenkel-chain model; see the note at ref 12)[206] and the stress component as given by eq 5 but normalized to that for a single segment (denoted by $-s_{xy}(0_+)$) can be expressed by

$$-s_{xy}(0_+) = H_F \left\langle \delta(\lambda) \left(u_x^o u_y^o + \lambda u_y^o u_y^o \right) \right\rangle_{\mathbf{u}^o} \tag{6}$$

where

$$\delta(\lambda) = 1 - \frac{1}{\sqrt{\left(u_x^o + \lambda u_y^o \right)^2 + \left(u_y^o \right)^2 + \left(u_z^o \right)^2}} \tag{7}$$

with u_x^o, u_y^o and u_z^o denoting the x, y and z components of a unit vector $\mathbf{u}^o$ representing the orientation of a segment in the system at equilibrium right before the step shear deformation is applied; and $\left\langle f \right\rangle_{\mathbf{u}^o}$ denotes averaging f over all orientations of $\mathbf{u}^o$.

Similarly the first normal-stress difference $-\left(\sigma_{xx}(0_+) - \sigma_{yy}(0_+) \right)$ can be expressed by

---

[206] Note: In the ensemble, segments with a certain bond length are oriented in all directions with equal probability; this is true with any bond length that can occur in an equilibrium state.   Each "group" of segments with the same bond length can be normalized the same way and averaged over all orientations as described in the text.

$$-\left(\sigma_{xx}(0_+) - \sigma_{yy}(0_+)\right) = \frac{c(N-1)}{V}\left(\left\langle T_x(0_+)b_x(0_+)\right\rangle - \left\langle T_y(0_+)b_y(0_+)\right\rangle\right)$$

$$(8)$$

$$= \frac{H_F}{Vb_0^3}\sum_k^c\sum_s^{N-1}\left[\delta_s^k(\lambda)\left(b_{s,x}^{o,k} + \lambda b_{s,y}^{o,k}\right)\left(b_{s,x}^{o,k} + \lambda b_{s,y}^{o,k}\right) - \delta_s^k(\lambda)\left(b_{s,y}^{o,k}\right)^2\right]$$

In the same way as obtaining eq 6, the first normal-stress difference normalized to that for a single segment can be expressed by

$$N_1(0_+) = -\left(s_{xx}(0_+) - s_{yy}(0_+)\right)$$
$$= H_F\left\langle \delta(\lambda)\left(u_x^o + \lambda u_y^o\right)\left(u_x^o + \lambda u_y^o\right) - \delta(\lambda)\left(u_y^o\right)^2\right\rangle_{\mathbf{u}^o}$$

$$(9)$$

which, as shown in the Appendix, can be rewritten as

$$N_1(0_+) = H_F\lambda\left\langle \delta(\lambda)\left(u_x^o u_y^o + \lambda u_y^o u_y^o\right)\right\rangle_{\mathbf{u}^o} = -\lambda s_{xy}(0_+)$$

$$(10)$$

As there is one-to-one correspondence between the orientation representation and the segmental (molecular) representation—i.e. between eqs 5 and 6 and between eqs 8 and 9, the contribution of $\sum_k^c\sum_s^{N-1}\delta_s^k(\lambda)\left[\left(b_{s,x}^{o,k}\right)^2 - \left(b_{s,y}^{o,k}\right)^2 + \lambda b_{s,x}^{o,k} b_{s,y}^{o,k}\right]$, corresponding to eq A1, has to be zero; in other words, as corresponding to eq 10, eq 8 may be rewritten as

$$-\left(\sigma_{xx}(0_+) - \sigma_{yy}(0_+)\right) = \frac{H_F}{Vb_0^3}\lambda\sum_k^c\sum_s^{N-1}\delta_s^k(\lambda)\left(b_{s,x}^{o,k} + \lambda b_{s,y}^{o,k}\right)\left(b_{s,y}^{o,k}\right)$$

$$(11)$$

The comparison of eqs 5 and 11 indicates that both the shear stress and the first normal stress difference arise from the same molecular source $\sum_{k}^{c}\sum_{s}^{N-1}\delta_s^k(\lambda)(b_{s,x}^{o,k}+\lambda b_{s,y}^{o,k})(b_{s,y}^{o,k})$; therefore, the same evolutions of the corresponding configurations are responsible for their relaxations. As $N_1(0_+) = -\lambda s_{xy}(0_+)$ (eq 10), the Lodge–Meissner relation is followed. The above analysis can be more easily applied to the Rouse model, in which $N_1(0_+) = \lambda^2 G_S(0_+)$ and $-s_{xy}(0_+) = \lambda G_S(0_+)$. As opposed to $G_S(t)$ and $G_{\Psi1}(t)$ being independent of strain as given by eqs 2 and 3 for the Rouse chain model, $G_S(t,\lambda)$ and $G_{\Psi1}(t,\lambda)$ as defined by

$$G_S(t,\lambda) = -\frac{s_{xy}(t)}{\lambda} \tag{12}$$

$$G_{\Psi1}(t,\lambda) = \frac{N_1(t)}{\lambda^2} \tag{13}$$

have the same strain dependence as shown in Figure 2. The initial values: $G_S(t=0,\lambda)$ or $G_{\Psi1}(t=0,\lambda)$ at different λ may be calculated numerically using eq 6 or eq 10 for comparison with the values obtained from the simulations as shown in Figure 6. As also shown in the figure, the calculated curve may be further improved by the multiplication of the correction factor $\langle\mathbf{b}^2\rangle_0/b_0^2 = 1.013$. The close agreement between simulations and numerical calculations as shown in Figure 6 and the agreement between the simulation results of $G_S(t,\lambda)$ and $G_{\Psi1}(t,\lambda)$ as shown in

Figure 2 confirm the above theoretical analysis.

Only after an averaging so complete that

$$\sum_{k}^{c}\sum_{s}^{N-1}\delta_s^k(\lambda)\left[\left(b_{s,x}^{o,k}\right)^2 - \left(b_{s,y}^{o,k}\right)^2 + \lambda b_{s,x}^{o,k}b_{s,y}^{o,k}\right] \to 0 \;,\; \text{eq 8 becomes the same as eq 11.}$$

Before this is fully realized, $G_{\Psi 1}(t,\lambda)$ shows a higher noise level than $G_{S}(t,\lambda)$ as indeed observed in the simulation. Thus, the Lodge–Meissner relation is shown only followed within some noise by the Monte Carlo simulations.

The second normal stress difference as a function of time obtained from the simulation of the Fraenkel chain is nonzero as shown in Figure 3. It is also shown analytically in the Appendix that the initial value of the second normal stress difference

$$N_2(0_+) = -\left(s_{yy}(0_+) - s_{zz}(0_+)\right) = H_F\left\langle \delta(\lambda)\left(\left(u_y^o\right)^2 - \left(u_z^o\right)^2\right)\right\rangle_{\mathbf{u}^o}, \tag{14}$$

is nonzero. In Figure 7, magnitudes of the initial first and second normal stress differences at different strains: $N_1(0_+)$ and $N_2(0_+)$ are compared and each are shown to be in close agreement with the numerical calculations based on averaging over all orientations.

6. Stress and Segmental Orientation

It was pointed out in the companion paper studying the linear viscoelastic response of the Fraenkel chain that the slow mode reflects the fluctuation or randomization of the segmental orientation anisotropy, with the bond length being the

same as in an equilibrium state—therefore, the slow mode is an entropy-derived

dynamic process. Here we show that, at the nonlinear strains studied

(from $\lambda = 0.5$ to 4), the strong correlation between the stress and the segmental

orientation, responsible for the entropic nature, is well maintained in the slow mode

region. In Figure 8 we show the comparison of the time dependences of $-s_{xy}(t)$,

$\langle b_x(t)b_y(t) \rangle$ and $\langle u_x(t)u_y(t) \rangle$; in Figure 9, the comparison of $N_1(t)$,

$\langle b_x(t)^2 \rangle - \langle b_y(t)^2 \rangle$ and $\langle u_x(t)^2 \rangle - \langle u_y(t)^2 \rangle$; and in Figure 10, the comparison of

$|N_2(t)|$, $\langle b_y(t)^2 \rangle - \langle b_z(t)^2 \rangle$ and $\langle u_y(t)^2 \rangle - \langle u_z(t)^2 \rangle$. The most important feature of

these results is that in the slow-mode region, the stress components are proportional to

the corresponding orientation components by about the same factor 4 in all cases,

which can be concisely denoted by

$$\mathbf{s}(t,\lambda) = 4\langle \mathbf{b}(t,\lambda)\mathbf{b}(t,\lambda) \rangle \qquad (15)$$

or

$$\mathbf{s}(t,\lambda) = 4\langle \mathbf{u}(t,\lambda)\mathbf{u}(t,\lambda) \rangle \qquad (16)$$

with the difference between $\langle \mathbf{b}(t)\mathbf{b}(t) \rangle$ and $\langle \mathbf{u}(t)\mathbf{u}(t) \rangle$ being negligibly small. In the

case of the Rouse theory, it is expected to have

$$\mathbf{s}(t,\lambda) = 3\langle \mathbf{b}(t,\lambda)\mathbf{b}(t,\lambda) \rangle \qquad (17)$$

Note that $s_{xz}(t) = s_{yz}(t) = 0$ in both eqs 15 (or 16) and 17; and $s_{yy}(t) \neq s_{zz}(t)$ in eq 15 (or 16), while $s_{yy}(t) = s_{zz}(t)$ in eq 17. The factor 4 in eq 15 being so close to the value 3 expected from the entropic force constant of the Rouse segment as shown in eq 17 strongly indicates the entropic nature of the slow mode. The difference between 4 and 3 (eq 15 versus eq 17) here may be caused by the same reason as that responsible for the best value of δ_0, viz. $\delta_F = 0.01$, being about 33% higher than the value obtained from the virial theorem, $\delta_V = 0.0075$, as shown in the analysis presented in section 3.2 of the companion paper. As an approximation is involved in expressing eq 19 by eq 20 in the companion paper, a discrepancy should be expected. The important point is the closeness of the two values: 0.01 versus 0.0075 for δ_0 in the companion paper and 4 versus 3 here.

The entropic nature of the slow mode as revealed in this study is very significant considering that the Fraenkel segment is much stiffer than the Rouse segment and that the segment has been *greatly* stretched by the application of a strain in the nonlinear region.   Of course, this is made possible by the fast relaxation of the segment tension allowing the segment length to reach its equilibrium value while the segmental orientation anisotropy is still at a high level.   In addition to providing an explanation resolving the paradox between the Rouse segment size *m* being of the same order of magnitude as that of the Rouse segment and the definition of the Rouse segment based on the Gaussian probability distribution as pointed out in paper 1, the strong correlation of the slow mode to the segmental orientation anisotropy strongly suggests that the entropic viscoelastic behavior, as may be described by the Rouse theory, may

exist or appear under a condition less restrictive than that previously thought–i.e., limited to a region that the applied strain is not too large (weakly nonlinear).

With the unit vector $\mathbf{u}$ representing the bonding direction, we may denote the polarizability of a Fraenkel segment at *equilibrium length* in the direction parallel to $\mathbf{u}$ by $\alpha_{\parallel}$ and in the perpendicular direction by $\alpha_{\perp}$. Then the anisotropic part of the polarizability tensor of each Fraenkel segment may be expressed as[10,207,208]

$$\alpha_{\alpha\beta} = \left(\alpha_{\parallel} - \alpha_{\perp}\right)\left(u_{\alpha}u_{\beta} - \frac{1}{3}\delta_{\alpha\beta}\right) \qquad (18)$$

With the polarizability anisotropy being given by eq 18, the relation as given by eq 16 means that the stress-optical law holds in the entropic region. The widely observed stress-optical law in the entropic region has been explained by assuming that the distribution of the distance between any two beads in a chain is Gaussian.[10,13] The Gaussian statistics applied to the segment is also the source of the entropic force constant. Here, we show that both the existence of an entropic region in the viscoelastic response and its associated stress-optical law can be satisfied by the Fraenkel chain model without invoking the Gaussian statistics for both the segment and chain conformation. In fact, the Gaussian statistics for the chain should not hold in the nonlinear region of strain as covered in this study, even in the entropic

[207] Kuhn, W. *Kolloid Z.* **1934**, *68*, 2; Kuhn, W.; Grun, F. *Kolloid Z.* **1942**, *101*, 248; Kuhn, W. *J. Polym. Sci.* **1946**, *1*, 360.

[208] Berne, B. J.; Pecora, R. *Dynamic Light Scattering*; John Wileys: New York, 1976.

(long-time) region of $G_S(t,\lambda)$.

In the entropic region where the stress-optical law is valid, the orientation angle χ' of the stress ellipsoid is identical to the extinction angle χ of the birefringence; the stress relaxation corresponds to the reduction of the birefringence Δn with time.[209] Because the Lodge–Meissner relation holds over the whole time range of the stress relaxation, the orientation angle χ' remains the same in both the fast-mode and slow-mode regions. While $\chi = \chi'$ in the slow-mode region, it is not clear from the present simulation, whether the same is true in the fast-mode region, as this would require the knowledge of how the polarizability changes with the elongation of the segment. However, it is very likely that the stress-optical coefficient will be quite different if another stress-optical rule holds in the fast-mode region. Inoue et al[210,211] have analyzed the results of *linear* dynamic viscoelasticity and birefringence measurements on different polymers by using a sum of two stress-optical rules, one for the high-frequency region (glassy component as denoted by Inoue et al, occurring in the energetic-interactions region) and the other for the low-frequency region (rubbery component as denoted by Inoue et al, which occurs in the entropic region and is equivalent to the kind ordinarily encountered). The two stress-optical coefficients obtained by Inoue et al are in general of very different magnitude and

[209] Janeschitz-Kriegl, H. *Adv. Polym. Sci.* **1969**, *6*, 170.

[210] Inoue T.; Okamoto, H.; Osaki, K. *Macromolecules* **1991**, *24*, 5670.

[211] Inoue, T.; Hayashihara,H.; Okamoto, H.; Osaki, K. *J. Polym. Sci. Polym. Phys. Ed.* **1992**, *30*, 409.

some with opposite signs; for instance $C_{\mathrm{R}} = -5 \times 10^{-9}$ versus $C_{\mathrm{G}} = 3 \times 10^{-11}$ for polystyrene melts.

7. Comparison of Nonlinear Relaxation Modulus between Entangled Polymer System and Entanglement-Free Fraenkel-Chain System

a. Overall Line Shapes of $G_{\mathrm{S}}(t, \lambda)$

One may recall the two consecutive processes: the chain-tension relaxation[5,10,212,213,214] (theoretically denoted by $\mu_{\mathrm{B}}^*(t, \mathbf{E})$ in ref 20) and the terminal mode (theoretically denoted by $\mu_{\mathrm{C}}(t)$ in refs 19 and 20) occurring in the non-linear relaxation modulus $G(t, \lambda)$ of an entanglement system (see Figures 4‒7 of ref 20 or Figures 12.4‒12.7 of ref 5); there are some interesting similarities in these two processes to the two relaxation modes in $G_{\mathrm{S}}(t,\lambda)$ of the entanglement-free Fraenkel chain as revealed in the present study.   To draw an analogy between the two, we regard each Fraenkel segment as corresponding to an entanglement strand and each bead as corresponding to a slip-link (as in the Doi-Edwards model[215]).   As what we intend to discuss is mainly an analogy, there are significant differences between the counterparts: For instance, a particularly strong chain tension on an entanglement strand will draw segments from neighboring entanglement strands, slipping through

[212] Doi, M. *J. Polym. Sci., Polym. Phys. Ed.* **1980**, *18*, 1005.

[213] Lin, Y.-H. *J. Rheol.* **1985**, *29*, 605.

[214] Lin, Y.-H. *J. Non-Newtonian Fluid Mech.* **1987**, *23*, 163.

[215] Doi, M.; Edwards, S. F., *J. Chem. Soc., Faraday Trans. 2* **1978**, *74,* 1789; **1978**, *74*, 1802.

the entanglement links, while the segment tension in the Fraenkel chain is localized in

each segment. The tensile force on the Fraenkel segment is quite large—proportional

to H_F (see eq 4), which is much greater than $3kT$; while the tensile force on an

entanglement strand is typically of the order $\approx 3kT/a$ with a being the entanglement

distance.[5,10,21]   Thus, in applying the models to an experiment, the segment-tension

relaxation of the Fraenkel chain would occur in the short-time region of $G(t,\lambda)$ (in

the short-time region, $G(t,\lambda \to 0)$ has modulus values—$4\times10^7 \sim 10^{10}$dynes/cm^2 for

polystyrene, much larger than the plateau modulus, $10^6 \sim 10^7$ dynes/cm^2,[216] which is

related to the entanglement molecular weight: $G_N = 4\rho RT/5M_e$), while the

chain-tension relaxation $\mu_B^*(t,\mathbf{E})$ with a modulus similar in magnitude to that of G_N

occurs in the time region corresponding to the plateau region of the linear $G(t)$ (see

Figure 9 of ref 20 or Figure 12.8 of ref 5).   In spite of these differences, there are

important similarities between these two different kinds of tension relaxation and their

respective following processes.   As both occur in viscoelastic responses of chain

molecules, a discussion of the analogy between them may shed light on the basic

nature of the physics affecting polymer viscoelasticity.   An important common effect

following both the segment-tension relaxation and chain-tension relaxation process is

the randomization of orientation anisotropy, which is responsible for the relaxation of

the remaining stress.   In the entanglement-free Fraenkel-chain case, the

randomization of the segmental orientation anisotropy is done directly by the

Brownian motion of the beads in the chain; while in the entangled polymer system,

---

[216] See chapter 13 of ref 5.

the orientation associated with the entanglement strand (namely, orientation associated with the primitive chain) is randomized by the reptation mechanism moving the primitive chain back and forth and eventually out of the deformed (or oriented) tube (of the Doi–Edwards model), with assistance from the chain contour-length fluctuation process.[5,19,20,217,218] Either of the two different processes, which randomizes orientation anisotropy, is an entropy-derived process: In the Fraenkel-chain case, the process is well described by the Rouse model as shown above, while in the case of an entangled system, the process is well described by the $\mu_C(t)$ process in the extended reptation model,[5,19,20,23,24] with the strain dependence of the modulus quantitatively described by the damping function of the Doi-Edwards theory.[5,19–21,219,220] As it turns out, the strain dependence of $G_S(t,\lambda)$ in the entropic region of the Fraenkel chain also closely follows the Doi-Edwards damping function for a different physical reason as analyzed in the following:

b.Damping Function in the Entropic Region of $G_S(t,\lambda)$

As shown in Figure 11, the entropic region of the Fraenkel-chain $G_S(t,\lambda)$ curves at different λ values can be superposed on one another very well by a vertical shift, allowing the damping factors $h(\lambda)$ defined and determined from the simulation results. That is,

---

[217] Lin, Y.-H. *Macromolecules* **1984**, *17*, 2846.

[218] Lin, Y.-H. *Macromolecules* **1986**, *19*, 159; **1987**, *20*, 885.

[219] Osaki, K.; Kurata, M. *Macromolecules* **1980**,*13*, 671.

[220] Osaki, K.; Nishizawa, K.; Kurata, M. *Macromolecules* **1982**, *15*, 1068.

$$h(\lambda) = \left[\frac{G_\mathrm{S}(t,\lambda)}{G_\mathrm{S}(t,\lambda \to 0)} \right] \tag{19}$$

with t spanning only the slow-mode region. At the same time, the damping function is closely related to the strain-dependence of the orientation tensor $\langle \mathbf{u}(t,\lambda)\mathbf{u}(t,\lambda) \rangle$ in the entropic region as indicated by eq 16. As shown in Figures 8, 9 and 10, $\langle \mathbf{u}(t,\lambda)\mathbf{u}(t,\lambda) \rangle$ in the very early part of the entropic region remains basically the same as it is initially at time zero (i.e., right after the application of the step strain); in other words, the randomization of the segmental orientation has hardly taken place as the fast mode completes its relaxation. Thus the obtained damping factors $h(\lambda)$ should be closely correlated with the function $h_\mathrm{o}(\lambda)$ calculated from the initial orientation caused by the step strain via affine deformation:

$$h_\mathrm{o}(\lambda) = \frac{g(\lambda)}{g(\lambda \to 0)} \tag{20}$$

with

$$g(\lambda) = \left\langle \frac{\left(u_x^\mathrm{o} + \lambda u_y^\mathrm{o} \right) u_y^\mathrm{o}}{\lambda \left(\left(u_x^\mathrm{o} + \lambda u_y^\mathrm{o} \right)^2 + \left(u_y^\mathrm{o} \right)^2 + \left(u_z^\mathrm{o} \right)^2 \right)} \right\rangle_{\mathbf{u}^\mathrm{o}} \tag{21}$$

From eq 21, one obtains $g(\lambda \to 0) = 0.2$. One can notice that eqs 20 and 21 is simply the damping function of the Doi–Edwards theory with the independent alignment approximation, which is close to the exact one over the whole range of strain λ, both explaining very well the experimental results obtained in the terminal

198

region of $G(t,\lambda)$ of a well-entangled nearly monodisperse system.[5,10,19-21,25,26] Note that the unit vector **u** here represents the orientation of a Fraenkel segment as opposed to representing the orientation associated with an entanglement strand in the Doi‒Edwards theory. While eqs 20 and 21 is an approximation to the exact expression in the Doi‒Edwards theory,[5,10,19-21,25,26] using them here is based on the observation (Figures 8, 9 and 10) that the relaxation strength of the slow-mode is basically directly related to the initial orientation. In Figure 12, we compare the $h_o(\lambda)$ curve calculated numerically from eqs 20 and 21 and the $h(\lambda)$ values‒as defined by eq 19‒determined from the superposition of the $G(t,\lambda)$ curves as shown in Figure 11. As there is virtually no difference between $h(\lambda = 0.2)$ and $h(\lambda = 0.5)$; and the numerically calculated results indicate that $h_o(\lambda = 0.2)$ is only smaller than $h_o(\lambda \rightarrow 0)$ by one percent, we have substituted $h(\lambda = 0.2)$ for the role of $h(\lambda \rightarrow 0)$ in determining $h(\lambda)$ at different values of λ. As shown, $h_o(\lambda)$ has basically described the trend of change in $h(\lambda)$ with increasing strain.

It is interesting and important to note that, as opposed to the similarity between their relationships to orientation as both can be characterized by the damping function given by eqs 20 and 21, the functional forms of the relaxation modulus in the entanglement-free Fraenkel-chain case and in the entangled system are very different. The relaxation strength in the former case receives equal contributions from all normal modes (see eq 2) while in the latter case dominated by the lowest normal mode (see eq 13 of ref 20 or eq 9.11 of ref 5).

In Figure 12, we also show the comparison of $h_o(\lambda)$ with the damping factor associated directly with the unit vector **u** in the entropy region, $h_u(\lambda)$, defined by

$$h_u(\lambda) = \frac{\left\langle u_x(t,\lambda)u_y(t,\lambda)\right\rangle\Big/\lambda}{\left[\left\langle u_x(t,\lambda)u_y(t,\lambda)\right\rangle\Big/\lambda\right]_{\lambda\to 0}} \qquad (22)$$

More directly representing the orientation, the $h_u(\lambda)$ values appear to have a closer agreement with $h_o(\lambda)$ than $h(\lambda)$. The small differences between $h_u(\lambda)$ and $h(\lambda)$, less than 10%, merely reflect the small deviations from being an exact constant as given in eq 16 for all strains. These small differences, which may arise from the fluctuations in simulations or hidden approximation that may be involved in the interpretation, does not affect the basic picture that the slow mode is closely related to segmental orientation and is of entropic nature.

8. Second Normal-Stress Difference versus First Normal-Stress Difference

Experimentally the second normal-stress difference is, in general, much smaller than the first normal-stress difference; so indicated by the comparison of the two obtained from the present simulation as shown in Figure 13. As pointed out above, as opposed to the first normal-stress difference $N_1(t,\lambda)$ being positive over the whole time range, the second normal-stress difference $N_2(t,\lambda)$ is negative in the entropic region. If a polymer system can be described by the Fraenkel-chain model, one may use birefringence measurements to determine the hard-to-obtain second normal-stress differences in the entropic region experimentally, as the stress-optical law is applicable in this region as shown in the analysis given in section 6. Interestingly,

this is very much the way in which Osaki et al[221] have carried out a study on an entangled system. By showing that the stress-optical law is followed in the terminal region(an entropic region), Osaki et al have studied the first and second normal-stress differences of an entangled nearly monodisperse polystyrene solution ($M_w = 6.7 \times 10^5$; 32.6% in Aroclor 1248) in the region by measuring the birefringence as a function of time following a step shear deformation. The second normal-stress difference in the terminal region as determined by them in comparison with the first normal-stress difference are similar to the simulation results shown in Figure 13 in several aspects. This may not be surprising as both the terminal relaxation of an entangled system and the slow mode of an entanglement-free Fraenkel-chain system reflect the randomization of orientation—of the primitive chain in the former case and of the segment in the latter case; and the orientations in both cases can be described well by the same shear damping function calculated from eqs 20 and 21. Thus, even though the relaxation functional forms are very different as pointed out above, their first and second normal-stress differences are of opposite sign in the same way and their $-N_2(t,\lambda)/N_1(t,\lambda)$ ratios have nearly the same values and λ dependence. Just as the shear damping function $h_o(\lambda)$ can be calculated from eqs 20 and 21, the ratio $-N_2(t,\lambda)/N_1(t,\lambda)$ can be calculated from the Doi–Edwards expression with the independent-alignment approximation for comparing with the values determined from the present simulations and the experimental values of the entangled system studied by Osaki et al, as shown in Figure 14. The close agreement between the present

---

[221] Osaki, K.; Kimura, S.; Kurata, M. *J. Polym. Sci.*: *Polym. Phys. Ed.* **1981**, *19*, 517.

simulation results and Osaki's results remains to be tested by experimental studies. Nevertheless, this agreement together with the agreement in the damping function further supports that the close relationship of the entropic nature in the long-time region of stress relaxation with orientation anisotropy as revealed in this study is a generally valid physical concept, whether entangled or not.

9. Summary

As shown in the companion paper, the relaxation of the slow mode of the Fraenkel chain in both the linear and nonlinear regions of strain is well described by the relaxation functional form of the Rouse theory with the same number of beads. However, in reference to the constitutive equation, the Fraenkel chain behaves very differently from the Rouse chain in several important aspects. While the Lodge–Meissner relation holds in the Fraenkel chain over the whole course of relaxation as shown both analytically and by simulation, both $G_S(t,\lambda)$ and $G_{\Psi 1}(t,\lambda)$ are strain-dependent. Furthermore, unlike being zero in the Rouse theory, the second normal-stress difference of the Fraenkel chain has the same sign as the first normal-stress difference in the fast-mode region and changes sign as the time entering the slow-mode region.

That the strain dependence of $G_S(t,\lambda)$ and $G_{\Psi 1}(t,\lambda)$ in the slow-mode region of the Fraenkel chain basically follows the damping function of Doi and Edwards with the independent-alignment approximation is explained and illustrated. As the stress tensor in the slow-mode region is directly proportional to the orientation as expressed

by $\langle \mathbf{u}(t)\mathbf{u}(t) \rangle$, the validity of the stress-optical law in this region of time is indicated. In the slow-mode region the obtained ratio $-N_2(t,\lambda)/N_1(t,\lambda)$ and its strain dependence are similar to those observed in an entangled system, which are roughly explained by the Doi–Edwards expression with the independent-alignment approximation.

In addition to the important nonlinear features summarized above, the Fraenkel chain as a molecular model for the polymer viscoelastic behavior, while keeping the entropic viscoelastic behavior of the Rouse model, in a natural way gives rise to a fast energetic interactions-derived mode, which, as also shown in the companion paper, properly accounts for the well-known existence of the energetic interactions-derived dynamic process, unexplainable by the Rouse theory.

Acknowledgement

Appendix

The Proof of the Lodge–Meissner Relation and Nonzero Second Normal-Stress Difference

If we can prove

$$\left\langle \delta(\lambda)\left(\left(u_x^{\circ}\right)^2 - \left(u_y^{\circ}\right)^2 + \lambda u_x^{\circ} u_y^{\circ}\right) \right\rangle_{\mathbf{u}^{\circ}} = 0 \tag{A1}$$

then, eq 9 becomes eq 10. Considering the symmetry, we

have $\left\langle \left((u_x^o)^2 - (u_y^o)^2 + \lambda u_x^o u_y^o \right) \right\rangle_{\mathbf{u}^o} = 0$; thus, eq A1 is true if

$$A(\lambda) = \left\langle \frac{(u_x^o)^2 - (u_y^o)^2 + \lambda u_x^o u_y^o}{\sqrt{(u_x^o + \lambda u_y^o)^2 - (u_y^o)^2 + (u_z^o)^2}} \right\rangle_{\mathbf{u}^o} \tag{A2}$$

is zero for all values of λ. Both the numerator and denominator of eq A2 contain

even and odd terms with respect to the transformation $u_x^o \rightarrow -u_x^o$ or $u_y^o \rightarrow -u_y^o$. The

averaging over all orientations of $\mathbf{u}^o$ is invariant to a rotation of the coordinate system.

The way to show $A(\lambda)=0$ is to do an orthogonal transformation to eq A2 make its

denominator contain only even terms. This can be done by finding the principal axes

for the quadratic form inside the square root of the denominator, which is simply

$\mathbf{u}^o \cdot \mathbf{C} \cdot \mathbf{u}^o$ with $\mathbf{C}$ being the Cauchy tensor. With $\mathbf{C}$ represented by a matrix C:

$$C = \begin{pmatrix} 1 & \lambda & 0 \\ \lambda & 1+\lambda^2 & 0 \\ 0 & 0 & 1 \end{pmatrix} \tag{A3}$$

and the unit vector $\mathbf{u}^o$ represented by a column U:

$$U = \begin{pmatrix} u_x^o \\ u_y^o \\ u_z^o \end{pmatrix} \tag{A4}$$

we may write

$$\mathbf{u}^\circ \cdot \mathbf{C} \cdot \mathbf{u}^\circ = U^T C U \qquad \text{(A5)}$$

Expressing the unit vector $\mathbf{u}^\circ$ with respects to the principal axes as

$$U' = \begin{pmatrix} u'_x \\ u'_y \\ u'_z \end{pmatrix} \qquad \text{(A6)}$$

the orthogonal transformation is given by

$$U = SU' \qquad \text{(A7)}$$

with

$$S = \begin{pmatrix} \dfrac{\sqrt{2}}{\sqrt{\mu + \lambda\sqrt{\mu}}} & \dfrac{-\lambda - \sqrt{\mu}}{\sqrt{2}\sqrt{\mu - \lambda\sqrt{\mu}}} & 0 \\[4mm] \dfrac{\lambda + \sqrt{\mu}}{\sqrt{2}\sqrt{\mu + \lambda\sqrt{\mu}}} & \dfrac{\sqrt{2}}{\sqrt{\mu - \lambda\sqrt{\mu}}} & 0 \\[4mm] 0 & 0 & 1 \end{pmatrix} \qquad \text{(A8)}$$

where $\mu = \lambda^2 + 4$. In terms of u'_x, u'_y and u'_z, eq A2 is expressed by

$$A(\lambda) = \left\langle \frac{-\sqrt{\mu}\, u'_x u'_y}{\sqrt{q_1\left(u'_x\right)^2 + q_2\left(u'_y\right)^2 + q_3\left(u'_z\right)^2}} \right\rangle_{\mathbf{u}^\circ} \qquad \text{(A9)}$$

205

where q_1, q_2 and q_3 are the three eigenvalues of C:

$$q_1 = \frac{\mu - 2 + \lambda\sqrt{\mu}}{2} \tag{A10}$$

$$q_2 = \frac{\mu - 2 - \lambda\sqrt{\mu}}{2} \tag{A11}$$

$$q_3 = 1 \tag{A12}$$

While the denominator of eq A9 contains only even terms, the numerator is an odd term. Thus, $A(\lambda) = 0$ for all λ; this leads to the result that the Lodge–Meissner relation $G_S(t, \lambda) = G_{\Psi 1}(t, \lambda)$ holds even though $G_S(t, \lambda)$ and $G_{\Psi 1}(t, \lambda)$ are not independent of strain and the second normal stress difference is not zero as shown below.

For the second normal stress difference to be nonzero, we need to show

$$B(\lambda) = \left\langle \frac{\left(u_y^o\right)^2 - \left(u_z^o\right)^2}{\sqrt{(u_x^o + \lambda u_y^o)^2 - \left(u_y^o\right)^2 + \left(u_z^o\right)^2}} \right\rangle_{\mathbf{u}^o} \neq 0 \tag{A13}$$

Carrying out the orthogonal transformation, one obtains

$$B(\lambda) = \left\langle \frac{1 - a\left(u_x^{'}\right)^2 - b\left(u_y^{'}\right)^2 + c u_x^{'} u_y^{'}}{\sqrt{q_1\left(u_x^{'}\right)^2 + q_2\left(u_y^{'}\right)^2 + q_3\left(u_z^{'}\right)^2}} \right\rangle_{\mathbf{u}^\circ} \qquad (A14)$$

with $a = \left(\mu - \lambda\sqrt{\mu}\right)/2\mu$, $b = \left(\mu + \lambda\sqrt{\mu}\right)/2\mu$ and $c = 2/\sqrt{\mu}$. The even terms present

in the numerator make $B(\lambda) \neq 0$.

Figure Captions:

Figure 1

Comparison of the Rouse theory (——) and the results of $G_S(t)$ ($\bigcirc$at λ=1; $\triangle$at λ=2) and $G_{\Psi_1}(t)$ ($\bullet$ at λ=1; $\blacktriangle$at λ=2) obtained from simulations on the 5-bead Rouse chain following the application of a step shear strain.

Figure 2

Comparison of the results of $G_S(t,\lambda)$ (—— at λ=0.5; —— at λ=1; −− at λ=2; and − − −at λ=4) and $G_{\Psi_1}(t,\lambda)$ ($\bigcirc$at λ=0.5; $\diamond$at λ=1; $\triangle$at λ=2; and $\triangledown$atλ=4) obtained from simulations on the 5-bead Fraenkel chain following the application of a step shear strain.

Figure 3

Second normal stress $N_2(t,\lambda)$ obtained from simulations on the 5-bead Fraenkel chain following the application of a step shear strain $\bigcirc$ at λ=0.5; $\diamond$ at λ=1; $\triangle$ at λ=2; and $\triangledown$ at λ=4).

Figure 4

$\langle \mathbf{b}(t)^2 \rangle$ (top) and $\langle \|\mathbf{b}(t)\| \rangle$ (bottom) as a function of time following the application of a step shear strain (λ=0.5, 1, 2 and 4) obtained from simulations on the 5-bead Fraenkel chain.

Figure 5

$\langle b_x(t)^2 \rangle$ (——); $\langle b_y(t)^2 \rangle$ (— —); $\langle b_z(t)^2 \rangle$ (-- -) and $\langle u_x(t)^2 \rangle$ (○); $\langle u_y(t)^2 \rangle$ (△);

$\langle u_z(t)^2 \rangle$ (▽) as a function of time following the application of a step shear strain

(λ=0.5, 1, 2 and 4) obtained from simulations on the 5-bead Fraenkel chain.

Figure 6

Comparison of the initial values $G_S(t = 0, \lambda)$ (○) and $G_{\Psi 1}(t = 0, \lambda)$ (▲) obtained from

simulations on the 5-bead Fraenkel chain with the λ-dependent curve calculated

numerically using eq 6 or eq 10 (——); the (— —) line indicating the λ-dependent curve

corrected for the ratio $\langle \mathbf{b}^2 \rangle_0 / b_0^2 = 1.013$.

Figure 7

Comparison of the initial first and second normal stress differences $N_1(0_+)$ (●)

and $N_2(0_+)$ (○) obtained from simulations on the 5-bead Fraenkel chain at different

strains with the λ-dependent curves (—— for the former; — — for the latter) numerically

calculated based on averaging over all orientations.

Figure 8

Comparison of the time dependences of $- s_{xy}(t, \lambda)$ (○); $4 \times \langle b_x(t)b_y(t) \rangle$ (——); and

$4 \times \langle u_x(t)u_y(t) \rangle$ (-- -) obtained from simulations on the 5-bead Fraenkel chain at

different λ (0.5, 1, 2 and 4).

Figure 9

Comparison of the time dependences of $N_1(t, \lambda)$ ($\circ$); $4 \times \left(\left\langle b_x(t)^2 \right\rangle - \left\langle b_y(t)^2 \right\rangle \right)$ (——);

and $4 \times \left(\left\langle u_x(t)^2 \right\rangle - \left\langle u_y(t)^2 \right\rangle \right)$ (- - -) obtained from simulations on the 5-bead Fraenkel

chain at different λ (0.5, 1, 2 and 4).

Figure 10

Comparison of the time dependences of $\left| N_2(t, \lambda) \right|$ ($\circ$); $4 \times \left(\left\langle b_y(t)^2 \right\rangle - \left\langle b_z(t)^2 \right\rangle \right)$ (——);

and $4 \times \left(\left\langle u_y(t)^2 \right\rangle - \left\langle u_z(t)^2 \right\rangle \right)$ (- - -) obtained from simulations on the 5-bead Fraenkel

chain at different λ (0.5, 1, 2 and 4); the vertical lines indicate the points

where $N_2(t, \lambda)$ changes sign.

Figure 11

Superposition of the $G_S(t, \lambda)$ curves at different strains obtained from simulations on

the 5-bead Fraenkel chain as shown in Figure 2 by an upward vertical shift (multiplied

by 1 at λ=0.2 and 0.5; 1.1 at λ=1; 1.5 at λ=2; and 3.5 at λ=4)

Figure 12

Comparison of the damping factors $h(\lambda)$ ($\bullet$) determined using eq 19 from simulations

on the 5-bead Fraenkel chain at different λ with the $h_o(\lambda)$ curve calculated

numerically from eqs 20 and 21; also shown are the values of $h_u(\lambda)$ ($\blacktriangle$) as defined by

eq 22 obtained from the simulations.

Figure 13

Comparison of the $N_1(t,\lambda)$ (——) and $|N_2(t,\lambda)|$ (– –) results obtained from simulations on the 5-bead Fraenkel chain at different strains (λ=0.5, 1, 2 and 4); the vertical lines indicate the points where $N_2(t,\lambda)$ changes sign.

Figure 14

Comparison of the simulation values (●) of $-N_2(t,\lambda)/N_1(t,\lambda)$ in the slow-mode region obtained from the present study and the experimental values (○) in the terminal region of the entangled system studied by Osaki et al with the numerically calculated curve (——) equivalent to the Doi-Edwards expression with the independent-alignment approximation.

Figure 1
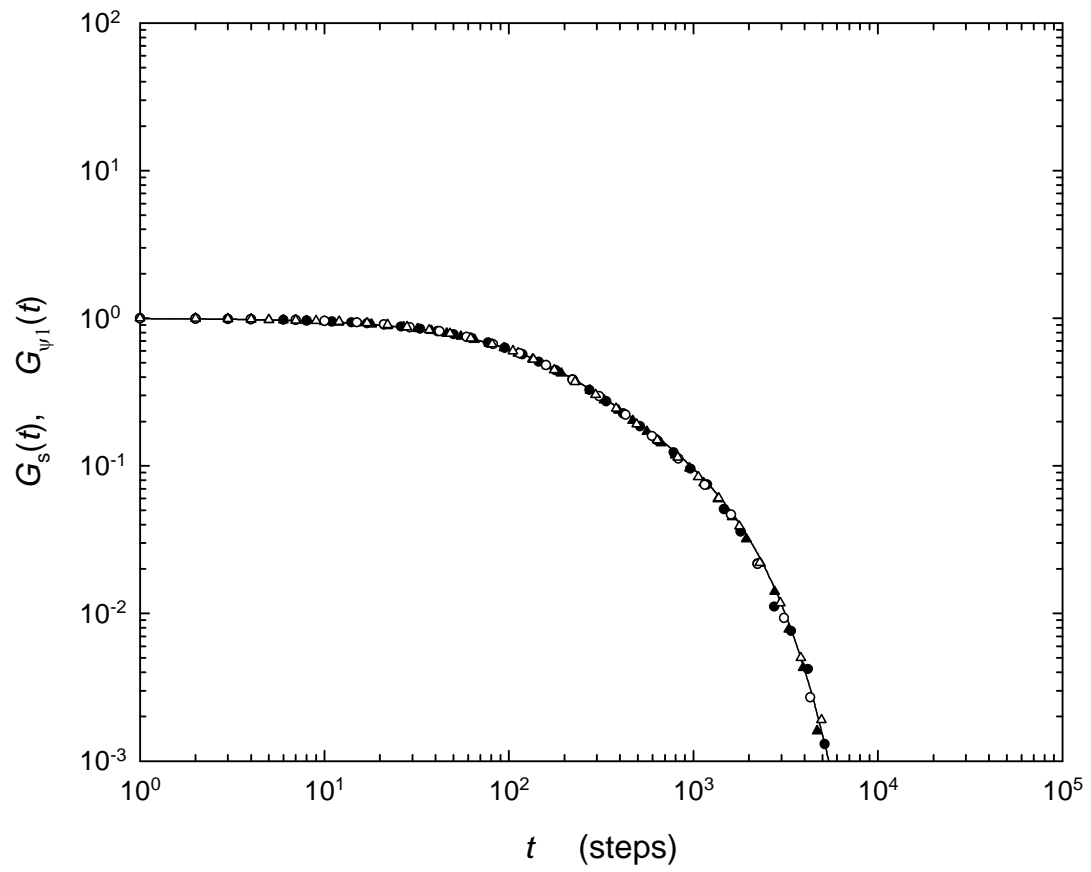
The plot shows $G_s(t)$, $G_{\psi 1}(t)$ on the vertical axis versus t (steps) on the horizontal axis, both on logarithmic scales.

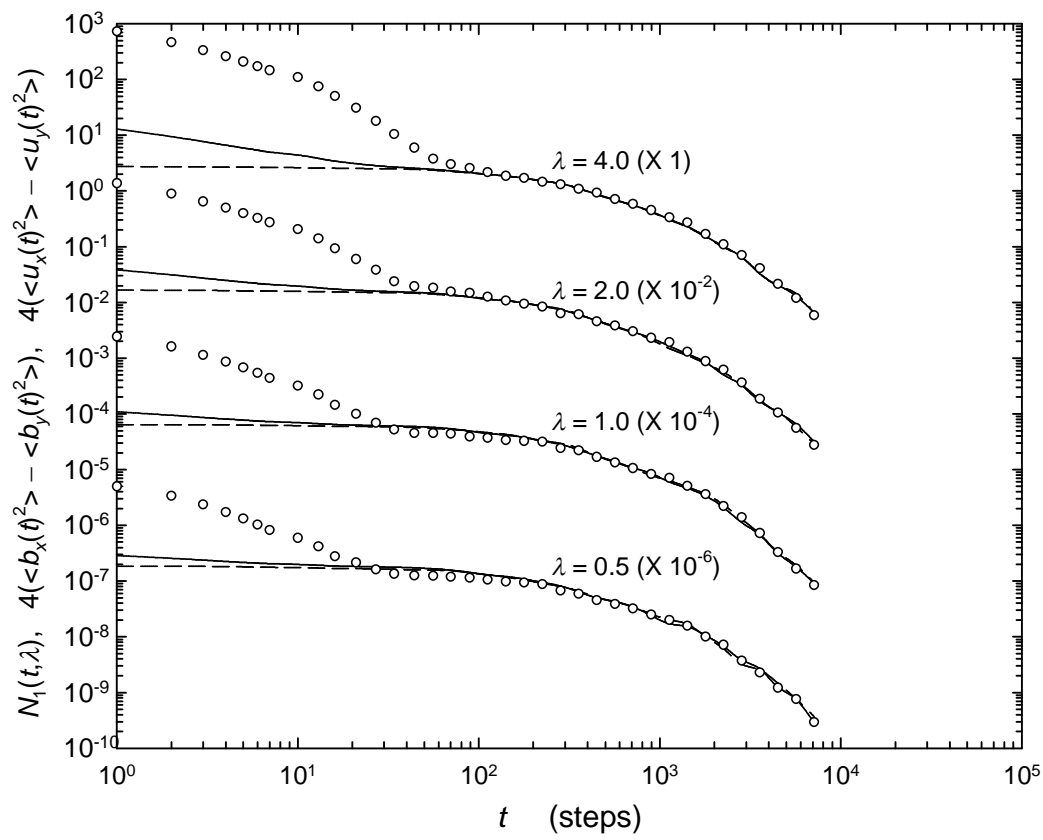Figure 2
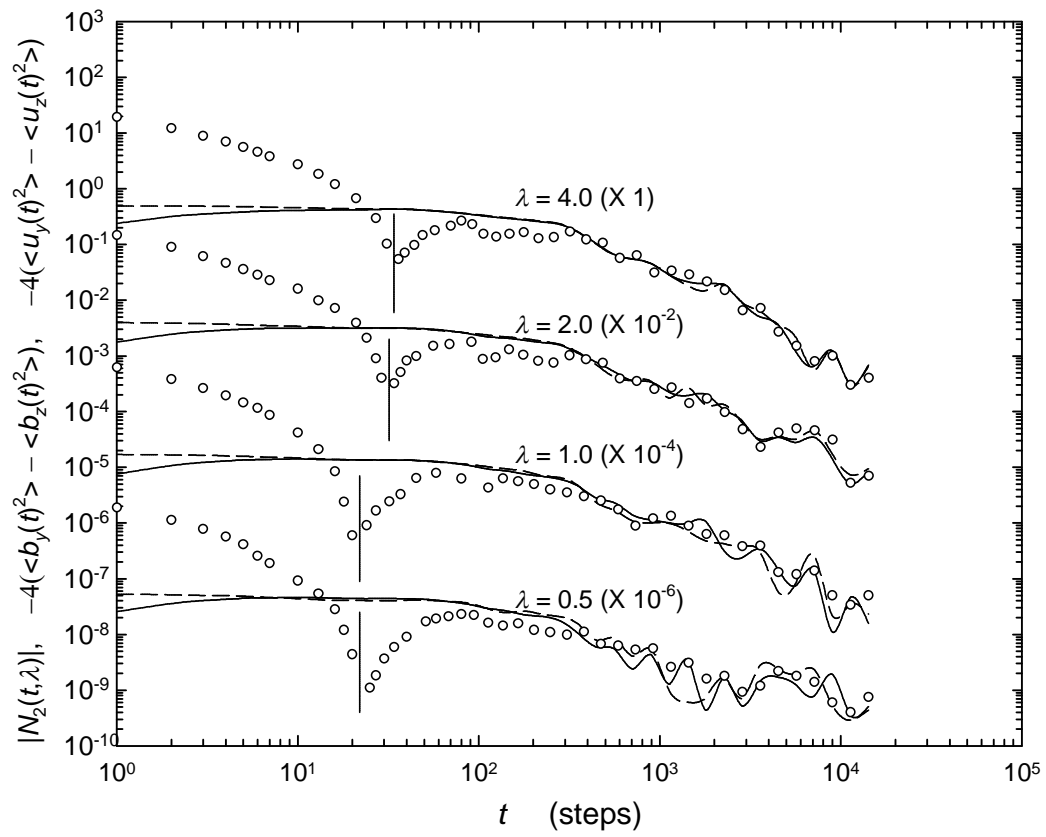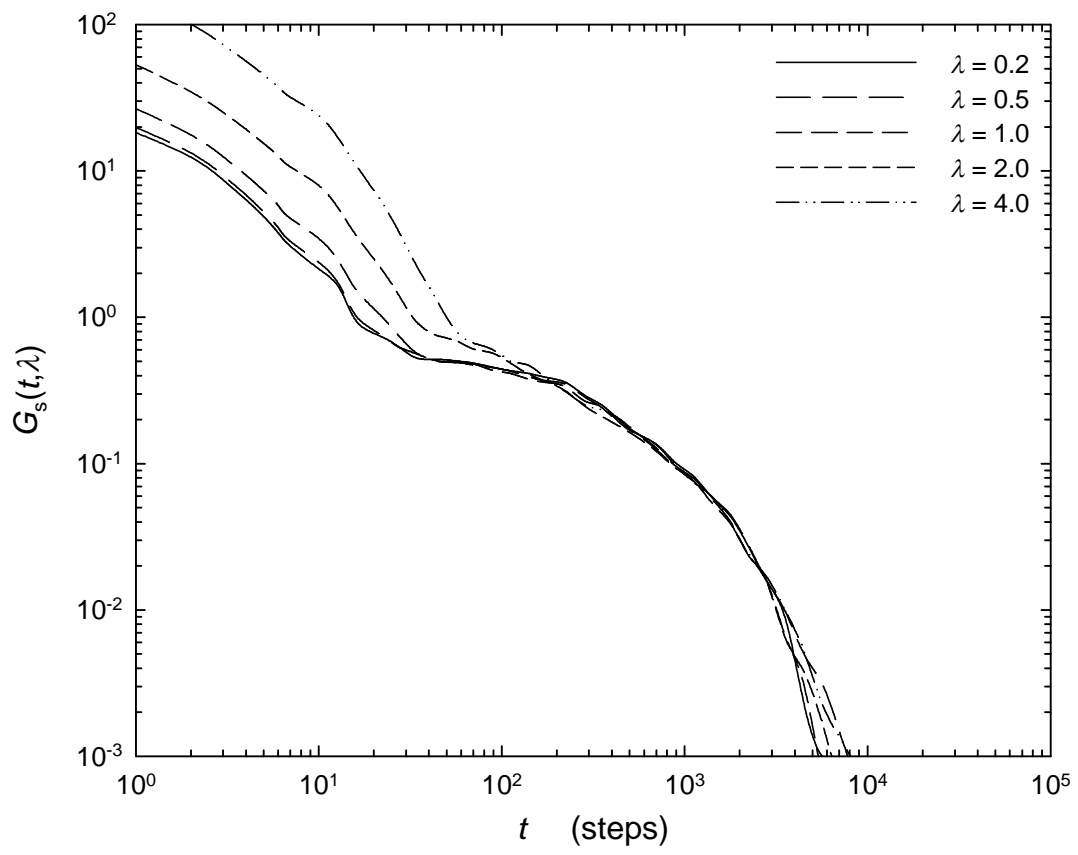
Figure 3

Figure 4

Figure 5

Figure 6

Figure 7

Figure 8

Figure 9

Figure 10

221
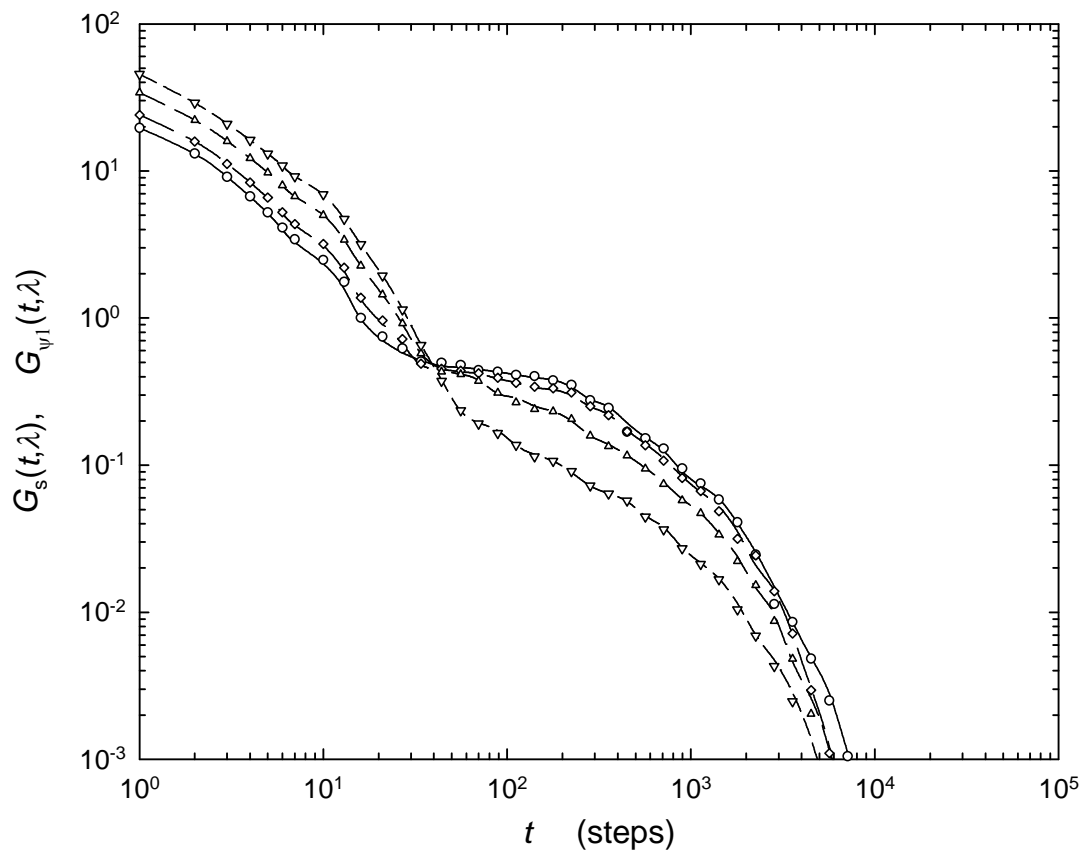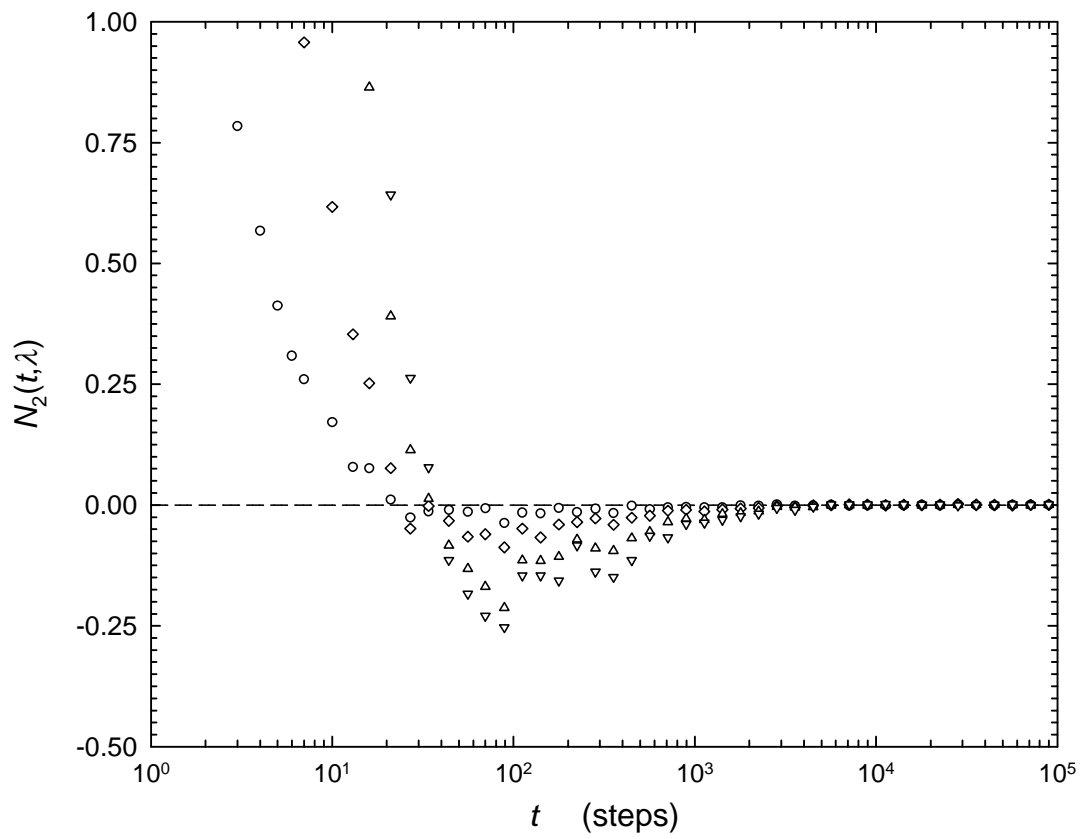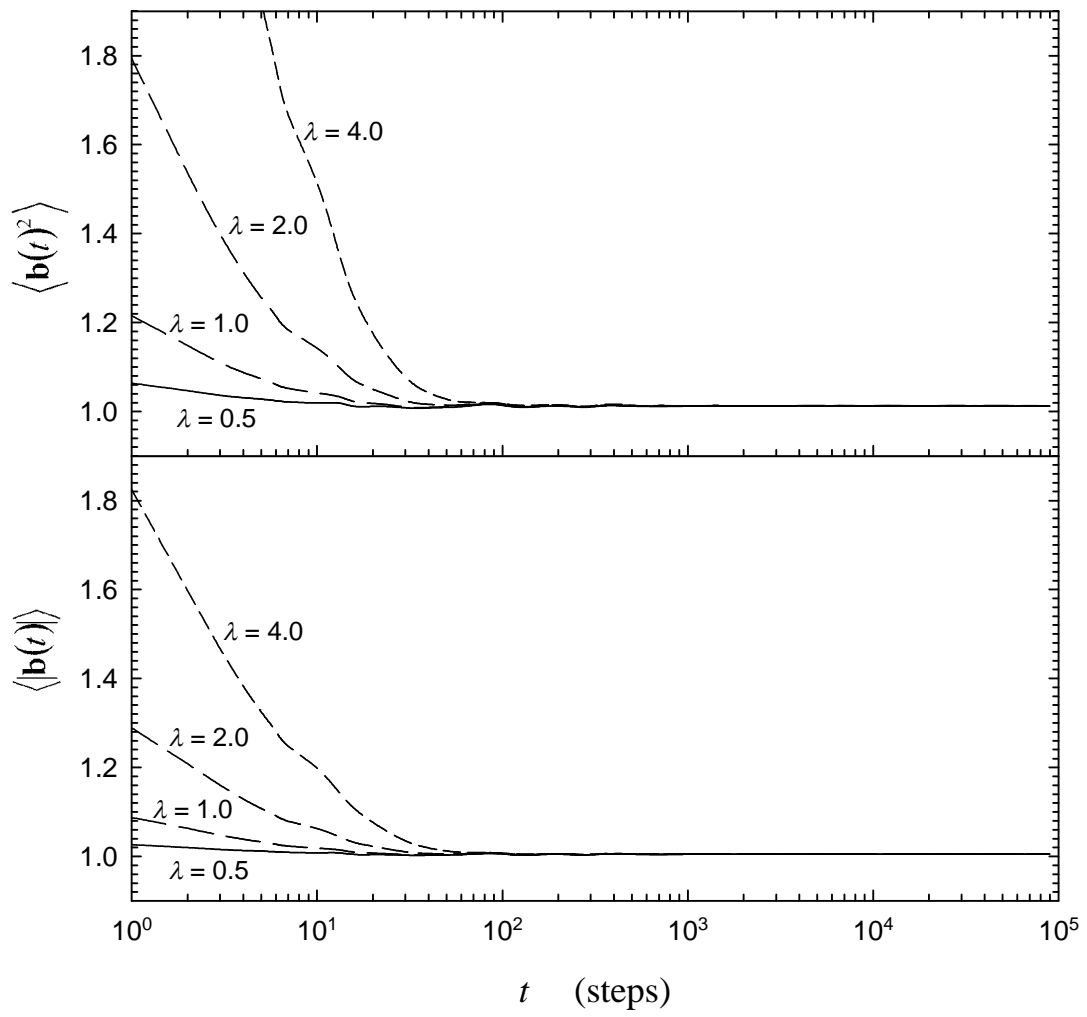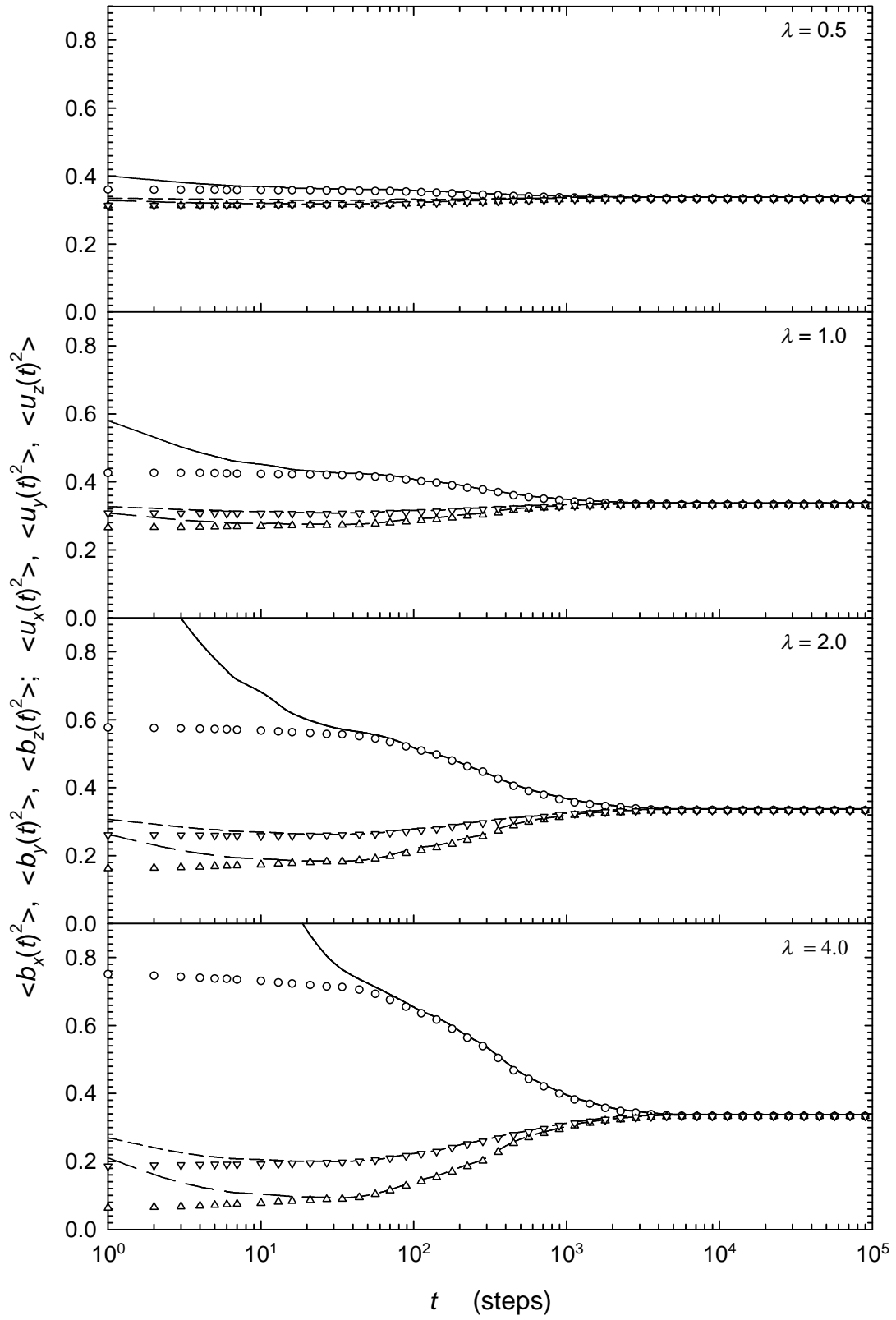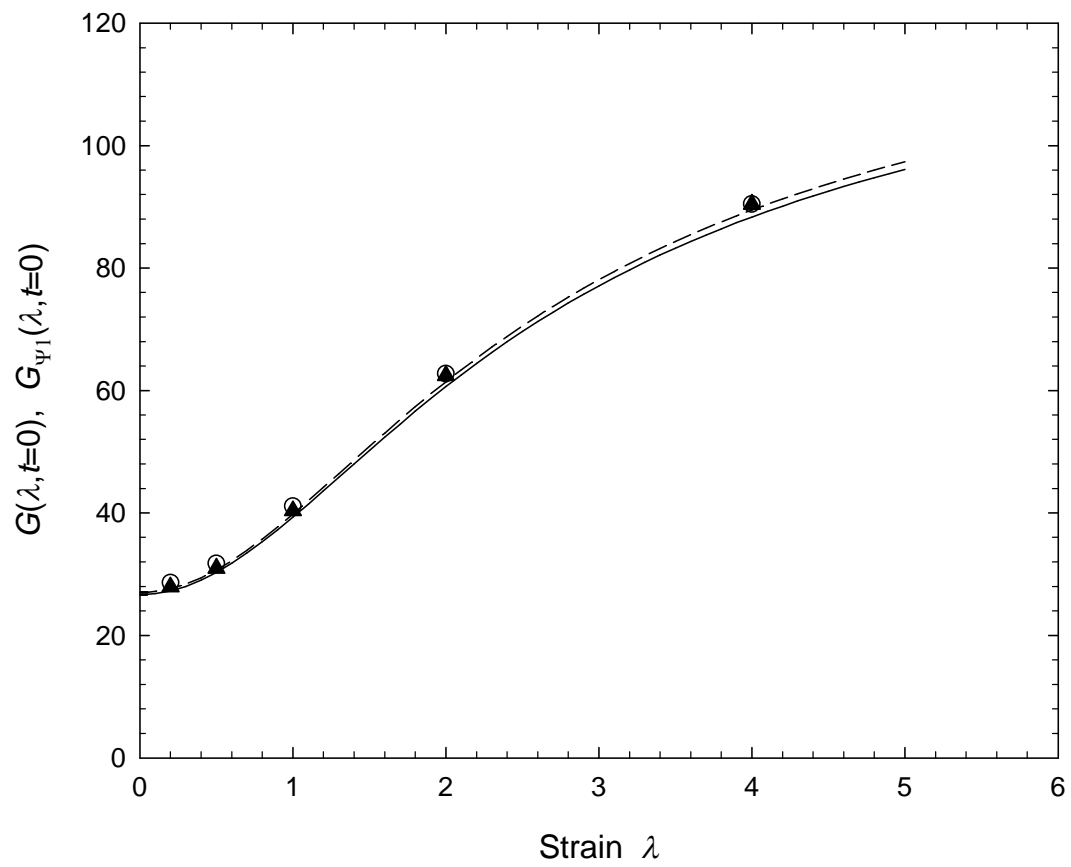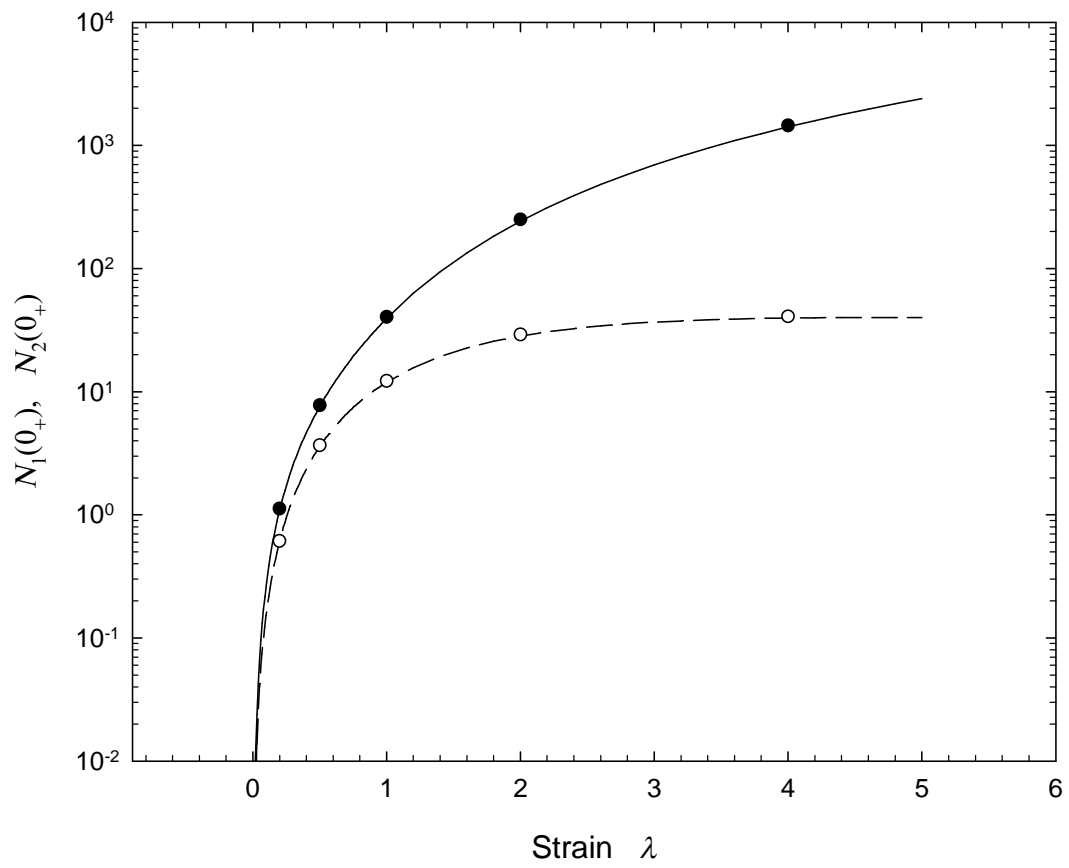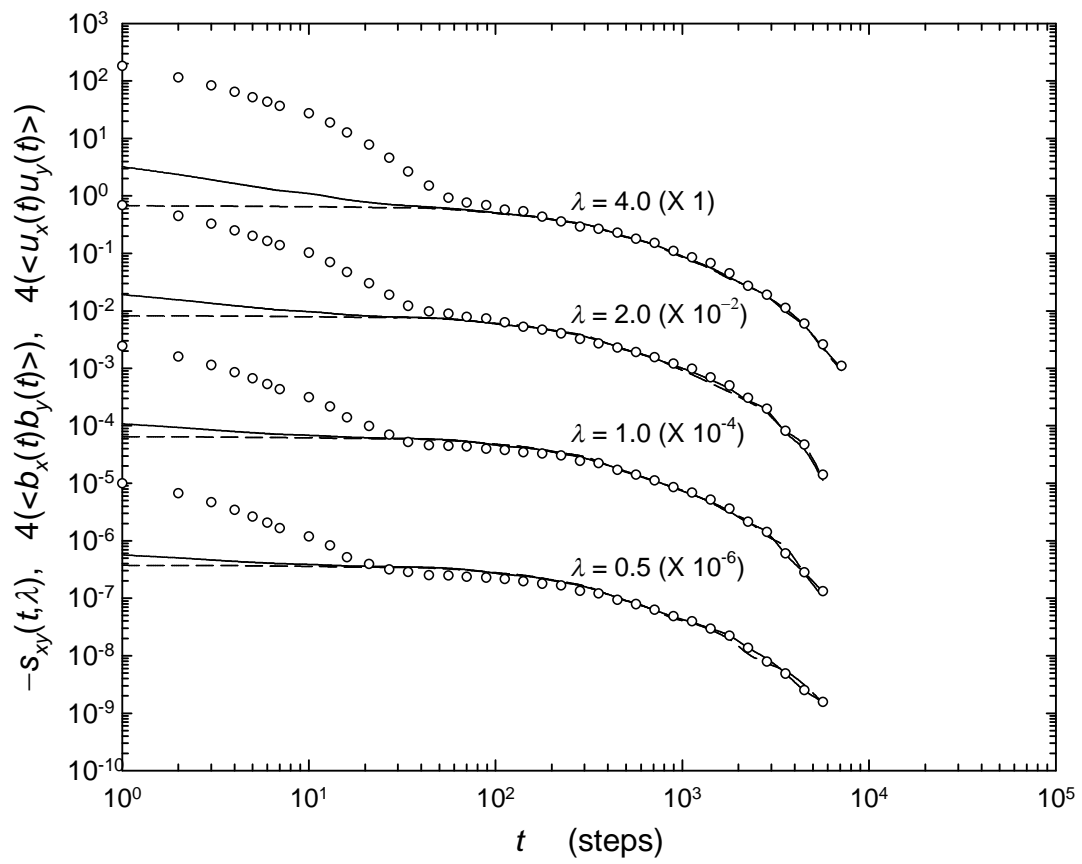
Figure 11

Figure 12

Figure 13

Figure 14